STUDY OF LIQUID AND MOISTURE MANAGEMENT PROPERTIES OF FABRICS BY USING A NOVEL SWEATING SIMULATOR

SHAHZAD AMIR

PhD

THE HONG KONG POLYTECHNIC UNIVERSITY

2023

The Hong Kong Polytechnic University

School of Fashion and Textiles

Study of Liquid and Moisture Management Properties of Fabrics by Using a Novel Sweating Simulator

SHAHZAD Amir

A thesis submitted in partial fulfilment of the requirements for the degree of Doctor of Philosophy

December 2022

CERTIFICATE OF ORIGINALITY

I hereby declare that this thesis is my own work and that, to the best of my knowledge and belief, it reproduces no material previously published or written, nor material that has been accepted for the award of any other degree or diploma, except where due acknowledgement has been made in the text.

__________________________(Signed)

SHAHZAD Amir (Name of student)

Abstract

This research is aimed at investigating the liquid and moisture management properties of fabrics under profuse sweating conditions. The research consists of two parts: (i) the development of a sweating simulator to determine the amount of sweat accumulated in as well as evaporated and dripped from the fabric when subjected to continuous sweating, and (ii) the development of fibrovascular capillary bed moisture management fabrics for use under profuse sweating conditions.

The fabric function of real-time personal sweat management may involve liquid absorption, spreading, evaporation, dripping, and drying occurring simultaneously. However, the concurrent and real-time measurements of these fabric properties under the conditions representing the actual end-use conditions have been a great challenge. The commonly used bench-scale instruments generally lack the true replication of fabric-perspiring skin interaction, simulated skin and sweat temperatures as well as changing body posture. This research presented an advanced instrument, a novel sweating simulator (NSS), for concurrent and real-time assessment of fabric liquid and moisture management at a simulated skin and sweat temperature, in an inclined upright orientation, and under continuous sweating. NSS comprises a sweating plane with a regional sweating zone located in the upper middle region to simulate a person's upper-back sweating zone. The temperatures of the sweating plane and sweat were adjustable to simulate the skin and sweat temperature of a sweating human body.

Eight different kinds of knitted fabrics were tested on NSS to validate the accuracy, reproducibility, and capability of NSS in differentiating the fabrics. On the NSS, liquid and moisture management properties were evaluated by the simultaneous and real-time measurement of liquid accumulation, evaporation, dripping, and drying with three calibrated measuring balances. The tests consisted of a sweating phase followed by a drying phase, each lasting one hour. The fabrics were tested on NSS twice; first, the temperature of the sweating plane and sweat was set to room temperature, and then it was regulated to a body's simulated skin and sweat temperature. NSS demonstrated excellent reproducibility and measurement accuracy in evaluating and differentiating the fabrics under different testing conditions. The measurement accuracy ranged from 98% to 100%, with most tests exceeded 99%.

In addition, using the temperature sensors embedded on the sweating plane, NSS measured the upward, lateral, and downward flow rates of liquid through the fabrics at the constant rate of liquid supplied. Experiments revealed that some fabrics showing excellent

capillary flow could not sustain the downflow rate of liquid through fabric against the increasing liquid content under continuous sweating. A stage is arrived when the liquid flow is accelerated through fabric in downward direction under the prevailing influence of gravitation force in upright orientation of NSS. While some fabrics demonstrated superior potential for sustaining the downflow rate throughout the entire sweating phase.

Because evaluating fabric liquid and moisture management in terms of liquid accumulation, evaporation, dripping, drying, and variation of capillary flow rate along the gravitational direction at increasing liquid content has practical implications, NSS's comprehensive testing capability can be extremely useful in the design and development of next-generation liquid and moisture management fabrics for clothing and various industrial applications.

Furthermore, the interrelationships between NSS test results of liquid mass distribution for both non-temperature-controlled NSS and temperature-controlled NSS and conventional wicking tests were investigated. During the sweating phase, the liquid evaporation, accumulation and discharge were found to be negligibly correlated with the rate of vertical wicking. However, the rate of horizontal wicking was found to be strongly positively and significantly correlated with the liquid evaporation during sweating phase, only at temperature-controlled NSS.

The quick absorption, wicking and evaporation of sweat by the next-to-skin fabrics play an indispensable role in personal wet-thermal management. However, when subjected to the bulk of sweat from profuse sweating, conventional moisture management fabrics that focus on liquid quick absorption, fast spreading, and evaporation may become heavier, sticky, odorous, and uncomfortable. In cases of extreme sweating, sweat dripping from fabric may also occur. Therefore, effective liquid sweat management by conventional textiles has been challenging in extreme sweating conditions. Herein, to address the limitations of conventional moisture management fabrics in profuse sweating, we report a cardiovascular capillary bed-inspired fibrovascular capillary bed design to regulate the bulk flow of sweat accumulated in the fabric from sweating skin. We designed and fabricated fibrovascular capillary bed (FVCB) networks by laser cutting a conventional moisture management fabric. The FVCB networks demonstrated a significant reduction in liquid accumulation, an increase in liquid transmission and discharge, and an improvement in area-specific liquid evaporation and drying efficiencies when compared to a plain specimen of the same fabric. Additionally, the feasibility of creating a FVCB network on a conventional moisture management fabric was also investigated using the spray finishing method. When compared to the conventional fabric substrate, the FVCB-treated fabric showed a 42% reduction in liquid accumulation, a 20% increase in liquid discharge, about 50% increase in area-specific liquid evaporation but only a slight decrease of about 6.0% in the absolute mass of liquid evaporation. Besides, sweat drained, instead of dripping inappropriately on the floor, was able to be collected at the end of sideways branches of FVCB network. Because of the promising liquid moisture management potential of FVCB networks, this work offers insight into the design and development of futuristic garments for enhanced personal comfort in sweaty conditions.

Contributions and Achievements

Publications

1. S. Amir and J. Fan, "Concurrent and real-time measurement of fabric liquid moisture management properties using a novel sweating simulator," Textile Research Journal, vol. 93, no. 3-4, pp. 774-794, 2022. (Published)

2. Amir Shahzad, Jintu Fan, Evaluation of fabric liquid and moisture management properties at simulated skin and sweat temperatures using an advanced Novel Sweating Simulator, Textile Research Journal (Under review)

3. Amir Shahzad, Jintu Fan, Experimental investigation of nature-inspired fibrovascular capillary bed patterns for efficient profuse sweat management (To be submitted)

4. Zhanxiao Kang, Amir Shahzad, Yiying Zhou, Jintu Fan, Fibrovascular Capillary Structures for Personal Evaporative Cooling (To be submitted)

Patents

1. J. Fan, A. Shahzad, An Evaporative Cooling Garment with a Fibrovascular Capillary Bed Liquid and Sweat Management System. Application no. PCT/CN2021/078643, (Patent pending)

2. J. Fan, A. Shahzad, A sweating simulator. China invention patent application, EM/P23956CN00 PAT-1417-CN-NP, (Patent pending)

Acknowledgements

First and foremost, I'd like to express my heartfelt gratitude to Prof. Jintu Fan, my Chief supervisor, for providing me with the opportunity to work on this novel and rewarding research. Prof. Jintu Fan has been an ideal advisor, mentor, and role model to me in all his professional, ethical, and moral traits. His novelty of ideas, clarity of advice, depth of understanding, passion for impactful innovations and commitment to research studies have always impressed me. Also, I am thankful for his patience, kindness, and uninterrupted support to me in achieving my goals. The knowledge, skills, and values I gained while working under his dynamic leadership will be a great asset to me in my life.

I wish to send my sincere gratitude to Dr. Zhou and Dr. Qing CHEN, for their support in the preparation of fabrics.

My warm and sincere thanks to Dr. Kang, Dr. Lawrence and Ms. Yiying, who always have been very helpful and friendly to me.

Special thanks to Dr. Jiang for his technical support in electrical and coding works involved in this research.

Also, special gratitude to Mr. Yang for his warm cooperation and special assistance in printing 3D components for me.

I would also like to extend my thanks to all family members of our research group including Dr. Annie, Dr. Yi Shu, Dr. Jiayin, Dr, Jiale, Dr. Hanchao, Mr. Pu Yi, and Ms. Juddy for all their cooperation and friendly attitude.

Gratitude and thanks are also extended to technical staff Dr. Kevin Hui, Mr. Ng Shui-wing, Mr. Kwan. and Ms. Rise for all their technical advice.

My heartiest thanks are due to my family, for their everlasting love and sacrifice. During this journey, I have been deeply missing them.

I am also grateful to my brotherly seniors Dr. Adeel Zulfiqar, Muhammad Waseem and my friends Mr. Awais Akhtar and Mr. Hassan Raza for all their love, care, kindness, respect, and selfless support.

Table of Contents

List of Figures

List of Tables

Chapter 1

Introduction

1.1 Research background

Clothing, as the human body's second skin, must meet the essential aesthetic, mechanical, and functional requirements in order to provide the necessary protection, performance, and comfort. The functional requirements of clothing are determined by the human body's response to various environmental conditions. As a result, research on the interaction of the body, clothing, and environment is critical to the development of wearable textile materials and products.

Clothing materials, construction, and design are all closely related to the human body's thermos-physiological comfort. Among the physical and mechanical properties of clothing, the heat and mass transfer, moisture, and sweat management properties of fabrics are the most important in addressing the body's fundamental need for thermos-physiological comfort. To address the critical need for personal thermal comfort, research has been primarily focused on two areas: 1) the development of various methods and instruments for measuring the thermal and moisture management properties of fabrics, and 2) the development of materials, finishes, and technologies to design and develop fabrics and garments with improved thermal and moisture management properties. Consequently, many instruments and methods have been developed, and various innovative materials and products have been introduced over time. However, due to the tremendous breadth and depth of research in this area, progress in exploring advanced evaluation techniques and new types of functional materials, novel fabric construction, finishing, and clothing design is continued.

Sweating is the skin's natural cooling mechanism for regulating body temperature. As a result, effective sweat management through clothing is critical for improved thermo-physiological comfort and performance efficiency. Excessive sweating, on the other hand, is a problem, especially when the sweat produced by the body exceeds the sweat evaporated from the clothes. Sweat accumulating in the shirt may cause discomfort, build wet stress on the body, and even drip on the floor inappropriately, making the floor slippery during indoor games or exercises. Hence, the cloth is an important medium for managing liquid sweat as well as transmitting heat and moisture from the body to the environment. As a result, optimal clothing is critical when dealing with excessive sweating conditions. Furthermore, real-time sweat management by moisture management clothing may include sweat absorption, spreading, evaporation, dripping, and drying functions to relieve the body's heat and wet stress effectively. Therefore, concurrent and real-time measurement of these parameters would be extremely beneficial for deep insight into fabric liquid moisture management and the development of next-generation moisture management clothing for use under profuse sweating.

1.2 Research gap and challenges

Fabrics' liquid and moisture management behaviour have primarily been assessed in terms of wicking, spreading, permeability, and drying properties. The most commonly used tests involved vertical wicking[1-9], horizontal wicking [10-12], downward wicking[13], transplanar wicking [14, 15], air permeability [16-19], moisture vapours permeability [19-22], overall moisture management capabilities [23, 24], and drying of fabrics [25-30]. Concurrent liquid moisture transportation and evaporation must also be evaluated in high-performance moisture management fabrics, especially when they become saturated because fabric saturation can be felt in a variety of situations, including hot and humid environments, outdoor construction work, athletics, training, and industrial working conditions [31-39]. As a result, understanding the liquid management behaviour of fabrics under profuse sweating conditions is critical for designing an evaporative cooling garment with superior sweat management potential. Under excessive sweating of the human body, an oversaturating shirt panel may lead to sweat dripping from the shirt. In the case of a clothed body, the amount of sweat produced by the body as well as accumulated evaporated, and dripped by cloths, if measured, can help define the fabric requirements for profuse sweating conditions. However, current test methods for measuring liquid and moisture management properties of textiles are not capable to perform such measurements. Wearer trials, on the other hand, may be useful for assessing the real-time performance of fabric liquid sweat management, but human-based trials are often more complicated, expensive, and difficult to standardise. The deficiency necessitates the exploration of advanced solutions to replicate the human body’s sweating skin- fabric-environment interaction so that the relationship between the human body, clothing, and environment can be better investigated in order to accelerate the research and development of high-performance personal sweat management textiles.

In addition, from a fabric point of view, moisture management cooling fabrics for profuse sweating must fulfil the following essential requirements.

- Protection of the body from direct exposure to sun rays or heating waves

- To have a UPF value of 50, particularly in the case of outdoor applications
- Excellent thermal conductivity (to regulate body heat)
- Excellent moisture management property enabling it to wick away and quick-dry. However, it should not dry too quickly to overheat again in a hot climate. It must hold the right amount of moisture near the skin for some prolonged evaporative cooling effect under hot and dry weather. While in the case of a cold climate, it should release the liquid sweat quickly in the resting phase to avoid a subsequent chilling effect.
- Transplanar wicking, i.e., directing sweat away from the skin to the outer surface of the fabric for quick spreading and evaporation to keep the wearer cool and dry.
- Breathable: Maximum airflow through fabric can increase moisture vapour transmission from skin to the atmosphere to minimize the heat and humid stress on the skin.
- To prevent the dripping of sweat off the body since the sweat dripped off cannot contribute to the evaporative cooling effect and may cause slippery floors in some sports.
- To be smooth and textured to minimize the clinging and friction on the skin.
- Effective transmission of the evaporative cooling effect from the fabric's top surface to the underneath skin.
- Lightweight in both dry as well as wet conditions.
- It should not retain too much sweat to avoid wetness and clingy sensation.

Fabrics with less moisture regain and higher wicking properties have been found to improve the evaporation and drying properties of fabrics [25, 29, 40]. The traditional and evolving fabrics for liquid sweat management primarily focus on improving the liquid absorption, spreading, and transplanar wicking properties of fabrics for enhanced evaporation [28, 41-44]. In a low to moderate sweating intensity, such fabrics are supposed to provide efficient personal sweat management by moving sweat away from the skin to the outer surface of the fabric for faster evaporation and drying. However, excessive sweating can cause the outer surface to become saturated and the transplanar wicking rate may decrease, leaving the fabric to be heavy and clingy. In addition, once the whole panel of a shirt gets wet, the rate of evaporation is limited by the fixed size of the shirt panel. Because, during high-intensity exercise, the human body's average sweat rate could reach about 1000 $gm^{-2}h^{-1}$ [45, 46], which is far greater than the possible rate of evaporation from a shirt fabric surface [36, 47, 48]. Sweat buildup in the fabric can also affect body vapour transmission through the fabric. Furthermore, as the fabric absorbs more sweat, its ability to dry quickly suffers, raising serious concerns about the post-exercise chilling effect in cold climates. Apart from that, inappropriate sweat dripping from a sweaty fabric may also be undesirable.

To address the limitations of conventional moisture management fabrics for profuse sweating, it is necessary to study liquid absorption, accumulation, dripping, and drying properties of moisture management fabrics under profuse sweating, and on that basis to develop innovative solutions for more efficient liquid and moisture management fabrics for sweat management.

1.3 Objectives of research

To address the research gap and challenges, this study aims to develop a new instrument called a “novel sweating simulator (NSS)” to evaluate the liquid and moisture management properties of fabrics and to investigate the potential of a nature-inspired Fibrovascular capillary bed (FVCB) networks in improving the liquid moisture management properties of fabrics subjected to profuse sweating.

More specifically, the study has the following major goals and objectives.

1. To develop a sweating simulator simulating the upper middle back of the human body in an upright orientation and capable of concurrent and real-time measurement of fabric’s rates of liquid accumulation, evaporation, dripping and drying in a simulated sweating and drying processes.
2. To equip the sweating simulator with temperature control functions needed to study the fabric dynamic liquid and moisture management properties at the simulated sweating skin and sweat temperatures.
3. To further equip the sweating simulator to measure the upward, lateral, and downward liquid flow rates in the fabric at a predetermined rate of continuous sweating.
4. To evaluate the capability, repeatability, and accuracy of NSS measurements by recurring testing of numerous kinds of fabrics.
5. To design and fabricate the nature-inspired CBFV networks and evaluate their potential for profuse sweat management in terms of liquid accumulation, evaporation, dripping and drying properties.

1.4 Research significance

For functional apparel, especially sportswear and active wear, the moisture management properties of the fabrics, namely their ability in sweat absorption, distribution, evaporation, draining and drying, are critical to wear comfort and performance. Such properties should be measured for quality evaluation and product development. The research topics of NSS being within an active and important industry sector is believed to have a potential significant impact as for the first time it would be possible to measure the real-time sweat evaporation, dripping, accumulation and spreading in different directions from/in the fabric concurrently, as occurs in real-life. The higher evaporation rates, lower sweat accumulation and faster drying rates of fabrics as determined by NSS can be useful in fabric design, choice of appropriate materials, fabric engineering, and garment comfort evaluation. Furthermore, the idea of fibrovascular capillary bed moisture management fabric can introduce a new class of moisture management evaporative cooling fabrics for body efficient sweat management.

Besides, liquid and moisture management properties of fabrics are important because of:

- Global warming results in prolonged hot summer seasons
- Heat stress management during severe heatwaves, exercise, sports, and workwear.
- Increasing awareness of moisture management materials and technologies in clothing
- Hot and humid workplace environments

Moisture management fabrics growth is projected to reach USD 13.26 Billion by 2024 at a CAGR of over 12%, owing to the increasingly health-conscious population globally. Increasing demand for sports apparel and protective wear are the main factors that have led to the growth of the moisture management fabric market. Initial investment and high manufacturing costs of moisture management fabrics are restraining the growth of the moisture management fabrics market [49].

Since the market for moisture management fabric is growing globally every year, any value addition in this field will contribute to the technology-driven knowledge economy by fulfilling the needs of consumers in national and international markets. The increasing demand has opened a new window for researchers in their quest to create a real impact on society by providing innovative solutions to the thermo-physiological needs of people under various environmental conditions.

1.5 Research outline

Chapter 01 consists of the research background, research gap, challenges, objectives, and significance.

Chapter 02 is the literature review of various instruments, techniques and studies related to the development and evaluation of liquid and moisture management properties of fabrics.

Chapter 03 describes the NSS's design, principles, and operation. Furthermore, it explains the concurrent and real-time measurement of fabric liquid and moisture management properties using NSS under no temperature control of simulated sweating planes and sweats as well as the validation of its reproducibility and accuracy. In addition, the effect of adjustable inclination and sweating rates on the measurements is reported.

Chapter 04 reports on the further instrumentation of NSS for the temperature control of the simulated sweating plane and sweat as well as the measurements of liquid flow rates by temperature change. The reproducibility and accuracy of the improved instrument with simulated skin and sweat temperature control are validated through testing commercial moisture management fabrics. In addition, NSS results are also compared with the results from existing test methods such as standard vertical and horizontal wicking tests and standard moisture management test using MMT (moisture management tester).

Chapter 05 discusses the design, fabrication, and evaluation of liquid and moisture management properties of nature-inspired fibrovascular capillary bed design for potential application in next-generation garments for used under profuse sweating conditions.

Chapter 06 summarizes the conclusion and recommendations for future work.

Chapter 2

Literature Review

The literature review covers past research in two parts, viz. the instrumental techniques for the evaluation of liquid and moisture management properties of fabrics and the strategies employed in the development of moisture management fabrics.

2.1 Measurement of liquid and moisture management properties of fabrics

Human comfort and the purpose of clothing. Comfort is a pleasant state of physiological, psychological, and physical harmony between a human being and the environment. While clothing being an integral part of human beings plays a vital role in bringing this harmony. Overall human thermal comfort is a complex interaction, of various attributes of human body, clothing, and environment [50, 51]. It is reported that human body, starts sweating as the body core temperature rises above 37 degrees Celsius, during some heat exposures or physical activities, and clothing, can play an efficient role in body sweat management through sweat accumulation, spreading, draining, evaporation and quick drying to keep the wearer feel cool and dry.

However, in case of profuse sweating, any increasing sweat accumulation in fabrics can make it heavier, sagging, sticky, sweaty, and uncomfortable, resulting in sweat dripping from saturated clothing, and causing performance and productivity losses. Therefore, it is critical to evaluate the fabrics real-time sweat management properties in terms of sweat accumulation, evaporation, discharge and drying to ensure the enhance comfort, performance, and productivity of wearer in extreme conditions.

Since, fabrics are important conduits of liquid and moisture transmission from the skin to the outer atmosphere by various mechanisms, like wetting and wicking, absorption and releasing, spreading, and draining, evaporation and vapors transmission. Hence, various test methods and instruments have been developed to investigate the liquid and moisture management properties of fabrics. Here related methods and instruments in context to the objectives of current research are reviewed.

2.1.1 Liquid absorbency test

The liquid absorbency properties of fabrics are generally characterized by the following methods.

1. AATCC 79: Test method for absorbency of textiles

A drop of water is allowed to fall from a fixed height of about 1cm onto the surface of a taught fabric and the time required for the specular reflection of the water drop to disappear is measured and recorded as wetting time. In general, five seconds or less is considered to reflect the adequate absorbency of fabrics [52].

2. Sinking time test

In a sinking time test, a specimen is put on the surface of water and the time taken by it to be completely wetted by water is determined. A sinking time of five seconds or less is generally considered satisfactory. The test can be performed according to the test methods including JIS L1907 clause 7.1.3, EN 14697 Annex B, GB/T 21655.1 clause 8.1, and KS K 0434. Whereas details of various other methods to measure the absorbency of textiles can be found in the following references [53, 54].

2.1.2 Siphon test

This method used a rectangular strip of the test fabric to act as a siphon. The amount of water transferred in the collecting beaker is measured over time. It is found that the siphon test works well only for hydrophilic fabric, while hydrophobic fabrics couldn't start the siphon of water [55].

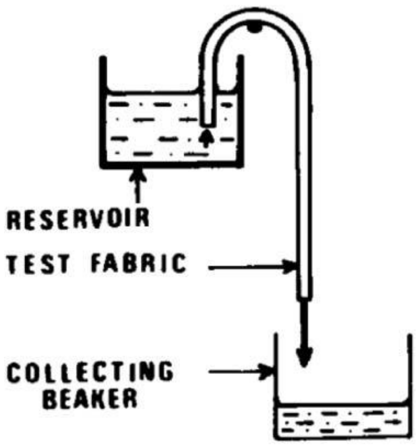

Figure 2.1. Apparatus for siphon test [56]

The siphon test is simple and easy to conduct since it requires no complicated setup. Yet, it doesn't simulate sweat absorption and transportation in actual wear conditions. Moreover, the longer time interval of the test with simultaneous evaporation from the fabric could be the major concern in the precise quantitative assessment of water transferred through the fabric.

2.1.3 Vertical wicking tests

Different setups for measuring the vertical wicking in a rectangular piece of fabric are shown in Figure 2.2. In its simplest form, the wicking in a strip of fabric can be tested by immersing its bottom end in a reservoir of water while hanging it straight. The water column's height in the fabric is recorded with time, or the time for a fixed height of the water column rise can be recorded (Figure 2.2a). The results can be reported as the height achieved in a fixed time or time to reach a fixed height and the rate of wicking. In other setups, an electronic balance can be used to measure the amount of water wicked with time by placing the water reservoir on balance (Figure 2.2c) or by connecting the hanging strip of fabric with an upper head balance (Figure 2.2b).

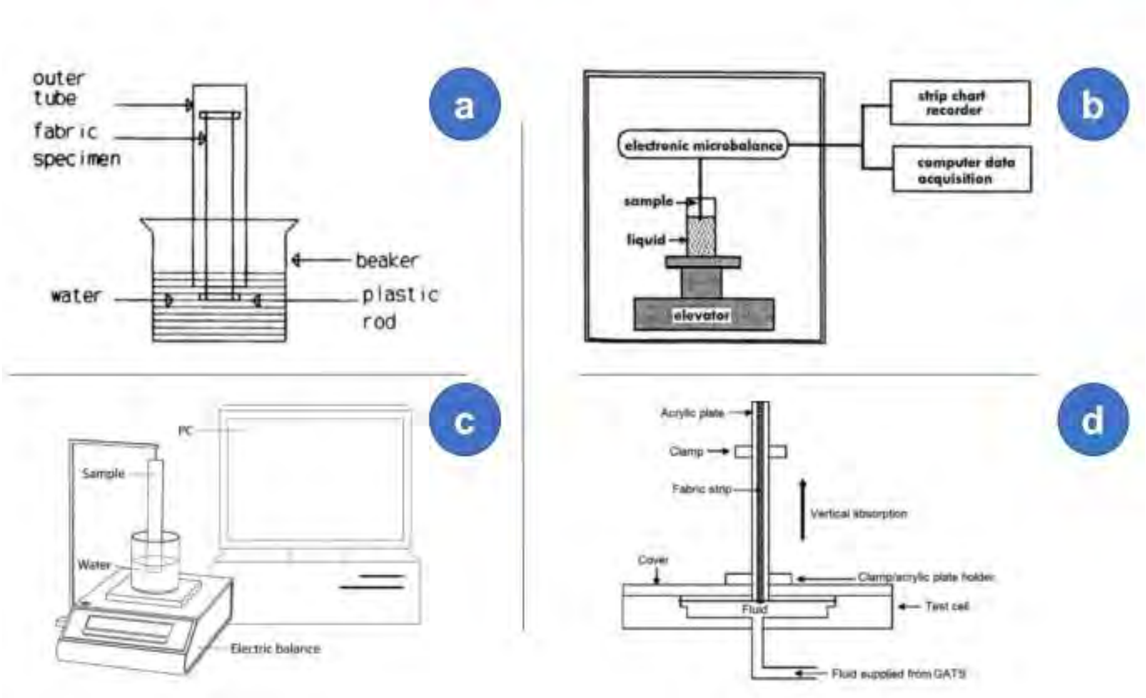

Figure 2.2. Setups for vertical wicking testing. (a) Apparatus for vertical strip wicking test [55]; (b) Tensiometer setup for vertical wicking test [57]; (c) Schematic illustration for measurement of dynamic water absorption [58] ; (d) Vertical wicking measurement using a test cell in gravimetric absorption testing system (GATS)[59].

The gravimetric system of vertical wicking is further employed in the simultaneous measurement of water wicking-evaporating behaviour of fabric, as shown in Figure 2.3 [60]. However, upward wicking is the opposite of gravity, the wicking rate gradually decreases with height, and the fabric strip does not get saturated equally from bottom to top [55]. Since in a longitudinal upward wicking strip test, the saturation varies along with the height of the fabric, the evaporation can also be different at different saturation sites. To overcome the problem of evaporation from a vertical wicking fabric strip, Hong and King introduced a modified method of the Gravimetric Absorption Testing System (GATS) (Figure 2.2d) [59]. They clamped the fabric strip in between two transparent acrylic plates under controlled pressure, with a 1mm bottom end of the fabric immersed in a liquid reservoir placed on a load cell. Nevertheless, though the evaporation from the fabric is minimized in this method, the probability of potential wicking between the acrylic-fabric interface could lead to the overestimation of the wicking-ability of the fabric.

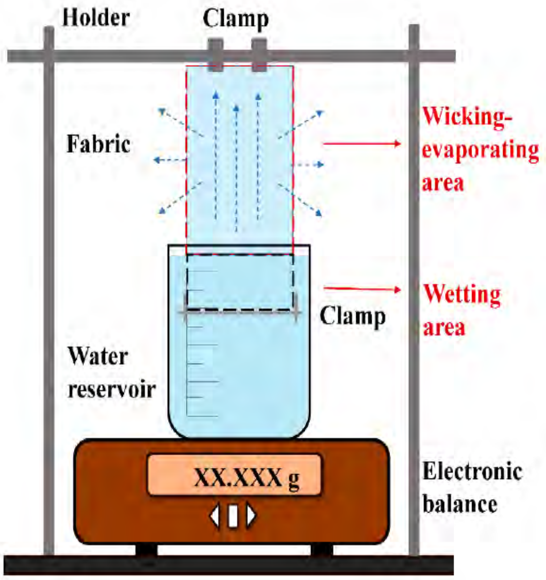

Figure 2.3. Setup for simultaneous measuring of wicking-evaporation in a longitudinal strip of fabric[60]

In summary, both the gravimetric and volumetric vertical wicking tests are useful to characterize the wicking ability of the fabrics. The gravimetric approach, irrelevant to the position of the liquid front, provided better accuracy, especially in the cases of irregular, indistinct liquid front or dark colour of the fabrics. Another advantage of the gravimetric vertical wicking test is that it does not need to add dye to the liquid, as any additive added to the liquid could change its surface tension and viscosity, which may affect the accuracy of the results. Similarly, in the experiments where the fabrics under wicking testing are directly exposed to ambient conditions, the issue of evaporative mass loss from the fabric can be resolved by immersing the fabric end into the liquid inside a volumetric flask instead of a beaker.

Besides, the gravimetric vertical wicking tests can't determine the equilibrium height of the liquid column in the fabric as well as the amount of liquid absorbed at different altitudes of wicking unless the fabrics are cut into pieces and weighed. Furthermore, starting from an infinite liquid reservoir, the vertical wicking tests don't replicate the directional flow of liquid in the actual fabric scenario in contact with a sweating skin, wherein the in-plane wicking and transplanar wicking both take place simultaneously. That is why the vertical wicking tests have limited implications for clothing comfort evaluation. Besides, detailed information about vertical wicking systems and advanced techniques of wicking measurement can be found in the literature [53].

2.1.4 Transverse wicking test

A transverse wicking test can be applied to measure the liquid absorption and spreading behaviour of fabrics. With some modifications, the transverse wicking test can also be used to measure through-the-plane transfer of liquid. Preferably water is supplied from underneath the fabric, and the wetted area and the mass absorbed are recorded with time. A few illustrations of transverse wicking test methods are presented here for reference in Figure 2.4. Whereas, detailed information about the old and modern techniques of transverse wicking measurement can be found in the references [12, 53, 61].

The transverse wicking tests are probably most relevant to liquid sweat absorption and wicking during wear. Because, in profuse sweating conditions, the sweat brought up to the cloths may be wicked across as well as along the thickness of the fabric. Therefore, the fabrics are preferred to be tested under conditions simulating the direction of liquid flow and profuse sweating conditions experienced in practice. The sweat may be wicked faster in one direction than the other due to the construction of the fabric and the perspiring body's posture. Thus, one sample used in the transverse wicking test represents both the lengthwise and width-wise directions, which in the case of longitudinal wicking tests need to be tested separately.

Moreover, transverse wicking tests need a shorter sample size and test duration compared to vertical wicking tests. However, precise determination of transplanar wicking is highly critical due to the limited thickness of the fabric, resulting in the typically small distance and a shorter time to transport the liquid across the fabric thickness. Any variations while placing the fabric sample on the sample podium or displacement of the liquid reservoir to maintain a constant pressure head beneath the fabric can change the initial absorption values of the fabric. Besides, in the case of a high initial absorption rate of fabrics and the continuous supply of the liquid, it is again difficult to characterize the transplanar wicking properties accurately. Additionally, existing transverse wicking instruments could test the specimen in one and only horizontal flat position, therefore lacking in simulating the different body postures in practice, whereby commonly occurring gravity-inclined sweat distribution in the clothes cannot be determined by the existing transverse wicking instruments.

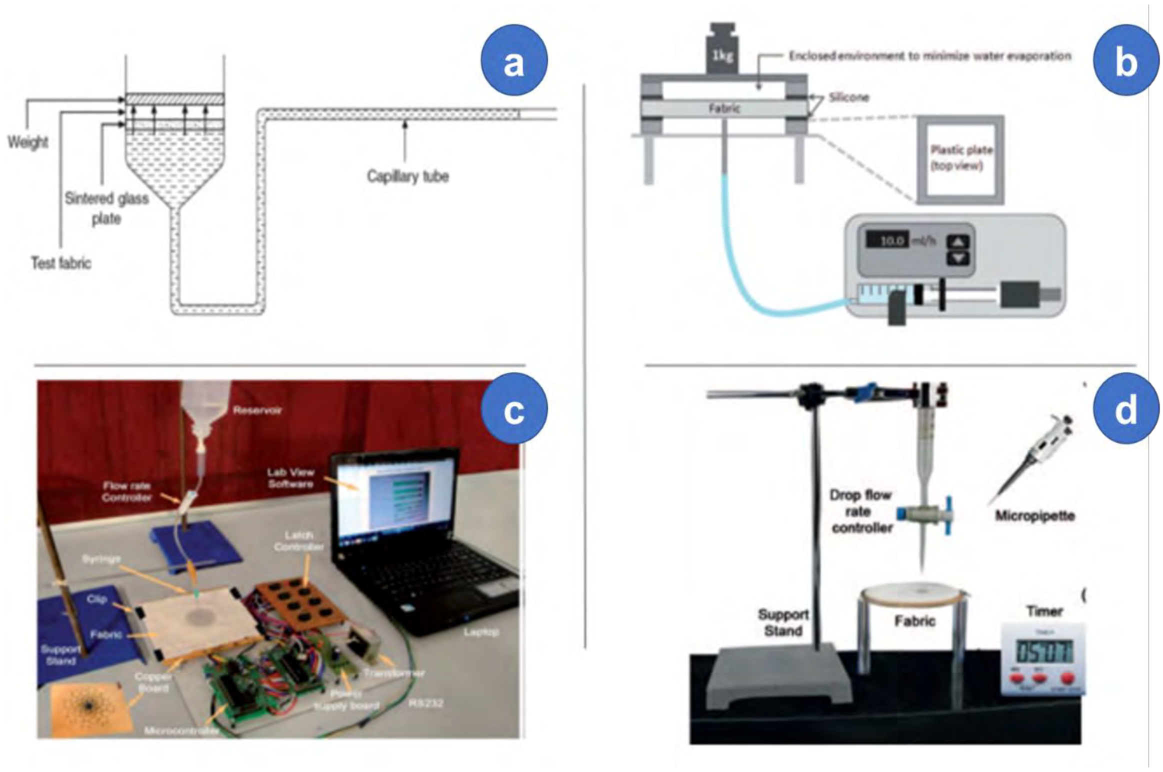

Figure 2.4. Transverse wicking test setups. (a) Transverse wicking by porous plate test [56]; (b)Horizontal wicking test [62]; (c) Dynamic sweat transfer test [63]; (d) Instrument for transverse liquid spreading [12].

2.1.5 WickView moisture management tester

Recently WickView moisture management tester (Figure 2.5) has been introduced by James Heel as a new technology for dynamic measurement of both vertical and horizontal wicking testing of fabrics with the same instrument by employing an image analysis technique. The measurements are rather accurate and insightful being examined in terms of direction, shape, speed, and actual wet area of fabric. However, it doesn't evaluate the rate of one-way liquid transport property of the fabric [64].

Figure 2.5 VickView moisture management tester [65]

2.1.6 Moisture management tester (MMT)

Moisture management tester (MMT) is the most widely used transverse wicking test that measures the moisture absorption, spreading, and transporting behaviour of fabric by recording a change in its electrical resistance. The schematic illustration of the sensing head of MMT is shown in Figure 2.6. The instrument can measure the following parameters.

- Overall Moisture Management Capacity
- Accumulative One-Way Transport Capacity
- Wetting Time for top and bottom surfaces
- Absorption Rate for top and bottom surfaces
- Max Wetted Radius for top and bottom surfaces
- Spreading Speed on top and bottom surfaces

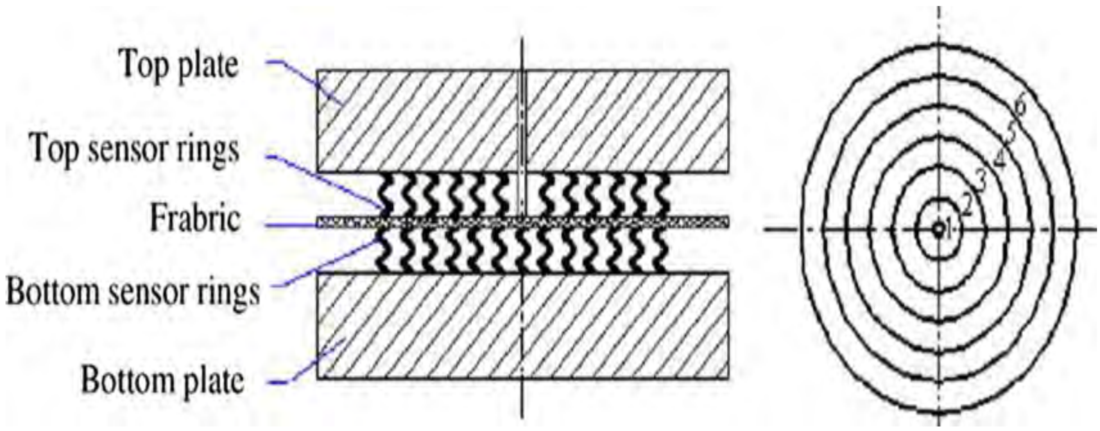

Figure 2.6 Schematic of MMT [66]

Unlike various convectional transverse wicking setups, the MMT is a relatively simple instrument in characterizing the transplanar wicking properties of fabrics with a limited amount of water supply, thereby allowing the measurement of water absorption through thickness transportation and spreading on the top and bottom surface of the fabric in a short time interval. However, the instrument has some limitations in simulating profuse sweating due to the limited liquid content and single point of liquid supply. Besides, during testing of fabrics with irregular surfaces and mesh type construction (widely used in lining and sportswear applications), all the sensing electrodes may not come in good contact with the fabric's surface, which may affect the accuracy of results.

2.1.7 Single pore wicking evaluation of yarns in fabrics

Recently, the use of continuous microfluidic flow mimicking a single sweat gland is reported to investigate the liquid wicking behaviour of individual yarns in the fabric as well as the transfer of liquid between the consecutive yarns in the fabrics. The schematic setup microfluidic device is shown in Figure 2.7. The system has an advantage in concurrently measuring the mechanics of liquid transportation within and among the yarns inside a fabric. However, in actual wear conditions, the threads in a piece of cloth don’t come to contact with a single sweat gland from sweating skin in real wearing conditions. Therefore, the implications of the test method to evaluate the overall moisture management properties of clothing are limited.

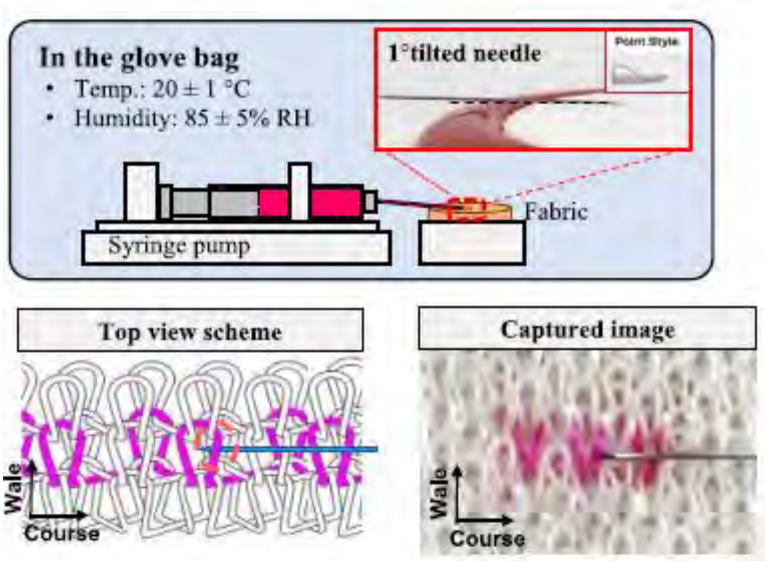

Figure 2.7. Single pore wicking evaluation sweat test for textiles [67]

2.1.8 Transplanar water transport tester

The transplanar water transport tester (Figure 2.8) can measure the initial absorption and evaporation from a fully saturated fabric surface lying flat on the sample podium under its own weight. The temperature of water supply can also be controlled to simulate any end-user conditions.

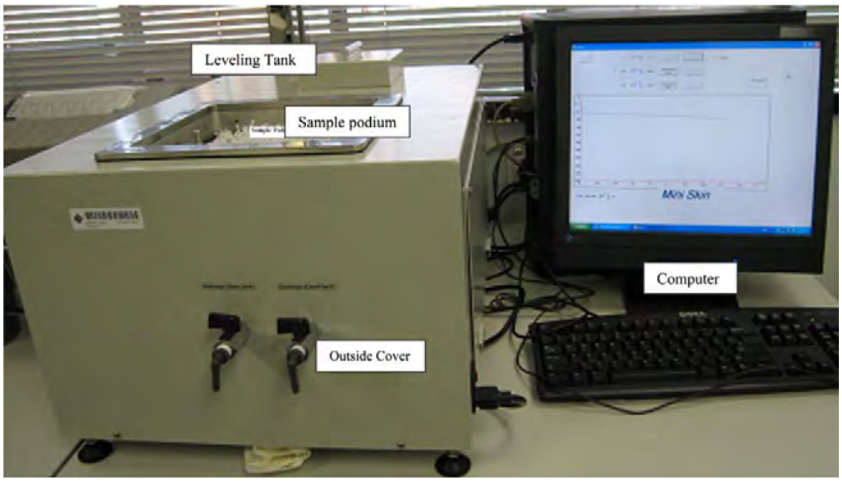

Figure 2.8. Transplanar water transport tester [15]

Although the instrument is novel in simulating the various end-user applications, yet it doesn't emulate the real-time wearing posture, spatial distribution of sweat into the fabric from a sweating skin as well as the sweating mechanism of the skin. Further, with a continuous supply of water beneath the fabric and higher absorption rates of fabrics, it is difficult to characterize the transplanar wicking ability of the fabric in the real sense.

2.1.9 Spontaneous uptake water transport tester (SUTWTT)

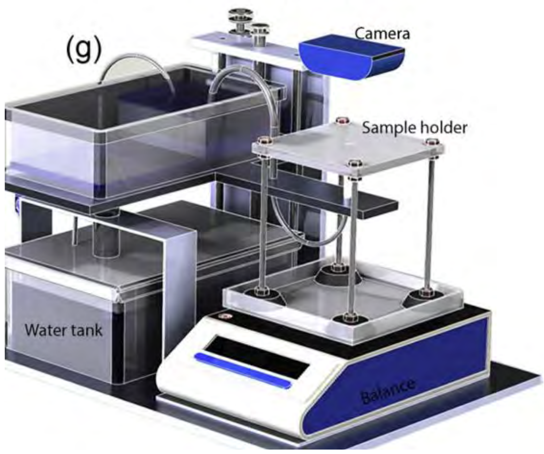

Figure 2.9. Spontaneous uptake water transport tester [68]

A spontaneous uptake water transport tester (SUTWTT) developed by Tang et al. is used to determine the in-plane and transplanar wicking properties of fabrics [68]. The instrument employs gravimetric and image analysis techniques to measure the amount of liquid absorbed and spread into the fabric over time. The water is supplied to the fabric underneath using a siphon tube so that a constant pressure head is maintained. The amount of water uptake is governed by the demand wettability of fabric. Over a test period, the amount of water absorbed by fabric i.e., water content and the area of spreading is measured directly over a single layer of fabric. Whereas, for evaluating the transplanar wicking ability of fabric, the sample is sandwiched between two layers of filter paper i.e., bottom, and top filter paper. The water supplied to the bottom filter paper is sucked by the sample and transported to the top filter paper. The relative amount of water absorbed in the top filter paper to that of the bottom filter paper determines the transplanar wicking ability of the fabric. The instrument possesses advantages of being simple, versatile, and accurate in measurement. However, the application is limited only to the fundamental liquid absorption and transport properties of the fabrics against a constant level of liquid supplied by a siphon tube. The phenomenon may not correspond closely with the real-time interaction of clothing and sweating skin.

2.1.10 Forced flow water transport tester (FFWTT)

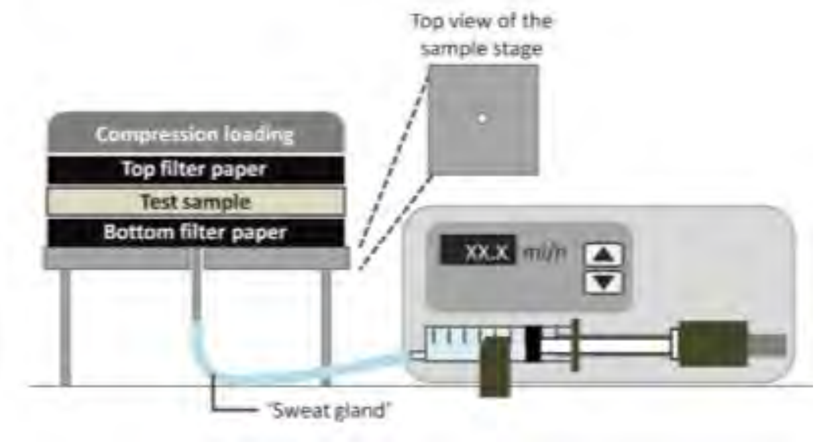

Figure 2.10. Force flow water transport tester. (a) 3D diagram (b) schematic description [69]

Force flow water transport tester (FFWTT) reported by Tang et al. is a dedicated instrument to measure transplanar water transport properties of fabrics subjected to a simulated sweat gland [69]. The fabric to be tested is sandwiched between two filter papers under slight pressure. The liquid is supplied continuously at a constant rate using a syringe pump, simulating a sweat gland, to the bottom filter paper. The sweat rate is recommended to switch between 10 ml/h to 40 ml/h corresponding to the high-speed running and the maximum possible sweat rate of the human body, respectively. By the end of the test period, from the amount of water absorbed in the layer, as measured by a weighing balance, the water content of the fabric and transplanar ratio are measured. The instrument is simple, accurate and versatile in its use. However, in this technique, the filter papers pose a strong hydrophilic potential on both sides of the fabric sample, which may alter the true water content of the fabric. Similarly, the transplanar ratio of fabric will also depend somehow on the absorption and release properties of the bottom filter paper. In other words, the transplanar ratio of fabric will be a function of the hydrophilic and liquid concentration gradient of filter papers. Furthermore, in relation to true wearing conditions, the fabric-filter paper interaction does not exactly simulate the fabric sweating skin interaction as the fabric is contacting directly with the sweating liquid of sweating skin. Additionally, the bottom filer paper is quick absorbent and super hydrophilic in nature, whereas the skin is typically hydrophobic in nature and the fabric facing the sweating skin contact directly with the sweating liquid.

2.1.11 Sweating torso

Measurement of coupled heat and mass transfer with the sweating torso (heated sweating cylinder) as shown in Figure 2.11.

Figure 2.11. Sweating torso for measurement of dry and thermal resistance, absorption, evaporation, and drying properties of the fabrics [70, 71]

Sweating TORSO is an upright standing cylinder simulating the human trunk with 54 sweating nozzles on its surface and upper and lower thermal guard, developed for ISO 18640 Part 1 in collaboration with the EMPA research institute [71]. The cylinder can be heated to the desired temperature for testing, and a sweating rate between $0.01Lh^{-1}m^{-2}$ and $1.5\ Lh^{-1}m^{-2}$ can be achieved to assess the heat and moisture transfer properties of fabric samples. The device can measure the thermal insulation, cooling power, absorption, evaporation, and drying properties of the fabrics [72].

However, the system has some following limitations.

- Although the sweating torso is supposed to simulate the sweating trunk of the human body, however, it may not adapt to the different inclinations of the trunk postures in practice.
- Moreover, due to the equal distribution of sweating nozzles on its surface, it is difficult to characterize the wicking ability of fabrics with continuous sweating applied in testing.
- In addition, with equal distribution of sweating nozzles and continuous sweating therefrom, the whole fabric will become equally saturated after some time, which doesn't replicate the spatial and temporal distribution of sweat from perspiring skin to the clothing in actual wearing conditions [73].
- Likewise, the equal distribution of sweating nozzles on a cylindrical surface does not better simulate the varying sweat densities among different sweating regions of the body.
- Furthermore, due to the cylindrical shape of the sweating torso, the uniform effect of wind velocity on evaporation around the cylinder is difficult to realize as the wind gusts from the fans of an environmental chamber could not move around the cylindrical surface equally. There is a possibility of different evaporation behaviours from the fan facing opposite and lateral sides. Therefore, it is difficult to accurately measure the effect of wind velocity on evaporation from the fabric's surface surrounding the sweating torso.

2.1.12 Sweating thermal manikins

Sweating thermal manikins are essential tools to measure the thermal insulation and evaporative resistance of clothing ensembles. In garment manufacturing and retailing, the enhancement of clothing thermal comfort is in great demand. The thermal manikins provide a relatively cost-effective, accurate, adoptable, repeatable, and reproducible response for the evaluation of clothing thermal comfort [74]. In a hot humid environment or high-intensity sweating exercise, the lower evaporative resistance to promote sweat evaporation and diffusion loss is highly desirable. While in extremely cold conditions, the clothing's thermal insulation is decisively associated with human survival. There have been developed many kinds of thermal manikins ranging from stational, standing and non-perspiring, non-sweating but wetted skin sweat simulating, walking but non-perspiring, walking, and perspiring such as Taro and Ken (Japan), Walter (Hong Kong) and Sam (Switzerland) and Coppelius (Finland). Overall, Holmer concluded that thermal manikins can be used to evaluate thermal factors realistically [74, 75]. However, due to extremely high development cost and installation costs, complex operations, and skilled operator requirements, the use of manikins in garment manufacturing and retailing has not been widely accepted. According to Holmer, since the world's first thermal manikin developed by US Army in early 1940, to date worldwide presence of thermal manikins is approximately over 100 so far. Moreover, the use of thermal manikins is mainly useful on a whole garment. The results represent the performance of clothing as a whole system of clothing-manikin interaction including air layers, gaps between clothing and sweating skin, and resistance of air trapped between clothing layer and manikin. Given that, the clothing is in direct contact with the liquid sweating from manikin, the true contribution of fabric intrinsic features such as materials, composition, construction, sweat transportation, evaporation, dripping, and drying properties are hard to evaluate accurately and simultaneously on thermal manikins.

On the other hand, due to the heavy weights of manikins, the evaporative weight loss resulting from sweat diffusion and evaporation from clothing is typically not measured by direct weighing of manikins on a weighing scale. Typically, the measurements are made indirectly by recording the change in heat loss and power supplied to the manikin. Any error caused by variations in temperature controlling and measuring system, or devices regulating and controlling the power is subjected to large variations in results affecting the accuracy of results.

2.1.13 Wearer trials

Apart from applications of thermal sweating manikins in the evaluation of clothing heat and mass transfer properties, human subject (wearer) trials are an alternative. Though the results from wearer trails are more realistic in nature, they are less reproducible. The variation in results could be high due to varying responses of human subjects and difficulty in experimental control depending on factors such as perceived comfort, experience, age difference, availability, the ability to decisions making and report etc. To address such variations, a large sample size of subjects is essential, thereby making the subjective trials complicated, time consuming and costly. The reproducibility and repeatability of physiological responses are also challenging in wearer trials.

2.1.14 Research gap of instruments measuring liquid and moisture management properties

Most of the bench scale instruments test the liquid and moisture management properties, lack adequate simulation of profuse liquid sweating, "fabric-sweating-skin" interaction and the sweating body posture. Although sweating thermal manikins can simulate sweating conditions but the reproducibility and accuracy for fabric testing are generally low. Walter, a sweating fabric manikin is accurate, but it doesn't simulate liquid sweating,

For the above-mentioned reasons, we feel the need for a relatively simple sweat simulator to facilitate the realistic, accurate, real-time, and simultaneous measurements of fabric liquid and moisture management properties including liquid accumulation, spreading, evaporation, dripping, and drying in a consecutive sweating and drying process.

2.2 Development of high-performance moisture management fabrics

Various techniques have been developed to improve the moisture management abilities of fabrics. The reported methods include an appropriate combination of hygroscopic and hydrophilic fibres in the yarns and/or fabrics, chemical and surface treatment of yarns and fabrics, as well as unique construction of the fabrics. Fibres with different deniers, cross-sections, moisture regain, and hydrophilicity are critical in deriving efficient moisture management abilities in such fabrics. Hydrophilic fibres like cotton are good in moisture absorption but slower in sweat release due to their polar sites making hydrogen bonding with water molecules. In contrast, non-hygroscopic fibres like polyester and polypropylene show lower absorption due to few bonding sites but can have better moisture transport if provided with some modified cross-section and hydrophilic treatment. The hydrophilic polyester produced through topical finishing, modified cross-section, co-polymerization, and alkalization exhibits faster moisture transport and release.

The creation of a wettability gradient and differential absorbency is another way of achieving faster transport of liquid within the yarns and the fabrics for better moisture management properties. US Patent 2003/0182922A1 disclosed that a sheath-core bicomponent yarn having a core of hydrophilic fibres surrounded by a sheath of hydrophobic fibres and used alone or in combination with other yarns could improve the moisture management properties of the knitted fabrics [76]. The Dri-release® technology claims an everlasting wicking feature in blended spun yarns being composed of 85-90% of synthetic hydrophobic fibres and 10-15% of natural hydrophilic fibres. Since the wicking-away function of moisture may not necessarily equate to the quick release and rapid drying of the fabrics. The fabrics produced from Dri-release® yarns demonstrate enhanced wicking, lower water retention, and a superior drying rate than cotton. The patented technology of Dri-release® yarn claimed that the fabric composed of synthetic-natural fibre blends is more comfortable than fabrics composed of only natural or synthetic fibres [77]. Similarly, the wool-bamboo and wool-polyester blended plaited single-jersey knitted fabrics have shown better moisture management properties than pure wool, polyester, and bamboo fabrics [24]. The moisture management properties of plaited single jersey fabrics produced with various combinations of yarns in the face and back of the fabrics were compared. A face/back polypropylene/cotton fabric showed the best overall moisture management and one-way transport capacity, followed by polyester/cotton and polyamide/cotton fabric [78]. The use of alternate filament and spun yarns in the construction of knitted fabrics such that the courses alternate with filamentary and spun yarns are also found beneficial in improving the moisture management properties of the fabrics [79].

The double-layer fabric construction has been found as a platform technique for improving the overall moisture management properties of knitted fabrics [53]. The one-way liquid transportation from the inner to the other surface of the fabric has been a centre of attention in such fabrics wherein a push-pull effect is generated through the differential absorbency, capillary pressure difference, wettability gradient, or different pore size combination between the two adjacent layers; thus, the moisture from the skin side is directed to the outer surface for spreading and evaporation. In such kind of double-layer fabrics, the next-to-the-skin layer remains relatively dry while the degree of sweat content in the outer layer depends upon the degree of evaporation and sweating intensity from the body. The inner layer usually consists of synthetic fibres like polyester, polypropylene, and polyamide, while the outer layer may contain cellulosic fibres like cotton, rayon, and lyocell. The moisture management properties of double-faced knitted fabrics produced with different combinations of cotton and polypropylene on the face side and backside revealed that the fabric with inner side polypropylene and outer side cotton could offer better comfort and moisture management [80]. But another approach, as disclosed in US Patent 20050282455A, showed that bi-layer knitted fabrics having an outer absorbent layer and the inner hydrophilic layer could provide a perpetual wicking action, resulting in better liquid moisture management. The wicking yarns in the inner layer may consist of profiled fibres, while yarns in the outer layer may be of several types, such as filament yarns combined through the knitting process, blended spun yarns with a chief value of synthetic fibres like polyester, and counterpart being water-absorbent fibres like cotton and rayon fibres. The fabric carries out an efficient one-way liquid transport function in contact with the skin whereby the inner layer draws the liquid moisture toward the outer layer for its rapid dispersion and evaporation [81].

On the other hand, bilayer knitted fabrics produced with different combinations of fibres and yarns denier in consecutive layers have proven an effective technique for improving the moisture management properties of fabrics. Nike Inc. produced a double-faced irregular pique knitted fabric with a differential denier support mechanism where the coarser yarns are used in the layer worn against the skin while the micro-denier fibres (0.6 to 0.8 denier) are used on the outer layer of the fabric. Sweat wicked by larger capillaries on the inner layer is diffused into a large number of smaller capillaries on the outer surface. The microfibres on the outer surface are supposed to provide a larger surface area for evaporation [82]. US patent 6427493B1 disclosed another irregular pique knit fabric in which the conventional non-microfilament yarns such as polyester, polyamide, or polypropylene are knitted on the inner side, and microfilament yarns are knit on the face side of the fabric. It is claimed that the fabrics can demonstrate superior wicking and maximum siphon of body moisture [83]. The bilayer plated knitted fabric produced with a combination of relatively finer yarn count, but coarser fibres hydrophilic synthetic filament yarns in the inner layer and a coarser yarn count but finer fibres hydrophilic filament or spun yarn in the outer layer have also shown superior performance in moving the moisture away from the skin. Due to fibre fineness difference, the sweat migration is improved towards the outer layer, where it spreads along the surface of the fibres without being absorbed due to the hydrophilic nature of synthetic fibres [84].

Inspired by the water transpiration of plants in nature, an earlier study on the directional flow of liquid through the thickness of fabrics has been reported by Fan and his team, simulating the plant structure in the construction of woven and knitted fabrics [41, 85-87], in which the branch size of the capillaries for liquid flow changed from coarser to finer from the back (next to the skin side) to the face of the fabric, promoting one-way transportation of liquid. Biomimetics of a branching network of plant structure in knitted double jersey fabric demonstrated better initial absorption and accumulative one-way transport properties [86]. The double-layer knitted structure was produced on a circular knitting machine with two or more yarns combined at the backside of the fabric and split up at the face side of the fabric to emulate the plant-like branches in the fabric. In contrast to the conventional knitted structured fabrics, these fabrics knitted with plant-like structures showed superior overall moisture management and comfort-related properties [87].

Treated cotton fabrics have also shown superior moisture management, drying rates, and cooling potential over untreated cotton fabrics. In the case of profuse sweating conditions, the shirt fabrics might be oversaturated with the liquid, which in case of poor evaporation and slow drying rates especially associated with untreated cotton fabrics, can cause increased friction, irritation, clammy sensation, and chilling effect in the cold environment. The water absorbency of pure cotton fabrics can be reduced by some finishing treatment with silicones, waxes, and fluoropolymers while rendering the natural breathability unaffected. The wicking channels produced by screen printing of cotton fabrics with fluorocarbon in four different designs of star, circle, square, and line revealed the improved moisture management performance without scarifying the breathability [17].

The concept of Wicking Windows™ introduced by Cotton Incorporated is also based on printing the backside of cotton fabric with fluorochemicals in a sporadic stipple pattern such the treated areas act as water repellent while the untreated areas remain water-absorbent, as shown in Figure 2.12. Since the fabric is treated only at the backside, the face side remains totally hydrophilic, and sweat or liquid moisture coming in contact with treated regions is repelled away towards the untreated rejoins where it is readily wicked through the absorbent "windows" and spreads over the outer absorbent face. The creation of selective absorption rejoins through wicking windows™ treatment has helped to significantly reduce the water absorbency and drying times of cotton fabrics [88].

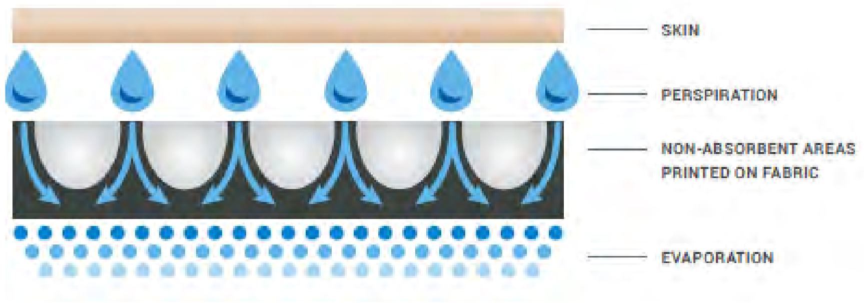

Figure 2.12. Moisture movement in Wicking Windows™ fabrics [88]

Similarly, TransDRY® is another patented technology for creating high-performance moisture management cotton fabrics by improving the sweat transfer and drying properties of cotton fabrics, as the name implies. Trans DRY® technology starts at the yarn stage, where cotton yarns are rendered water-repellent with some special treatment process. During the construction of knitted fabrics, the right amount of water-repellent yarns are combined with the water-absorbent yarns such that the plurality of water-transporting channels is created. The unique construction of TransDRY® doubled layer knitted fabrics coupled with the natural breathability of cotton can move the sweat away from the skin to spread over a larger surface area for faster evaporation so that it can dry as well as, or even faster than most competitors' synthetic fabrics, thus preventing oversaturation of garment during exercise [89]. The pictorial description of moisture movement in TransDRY® is shown in Figure 2.13.

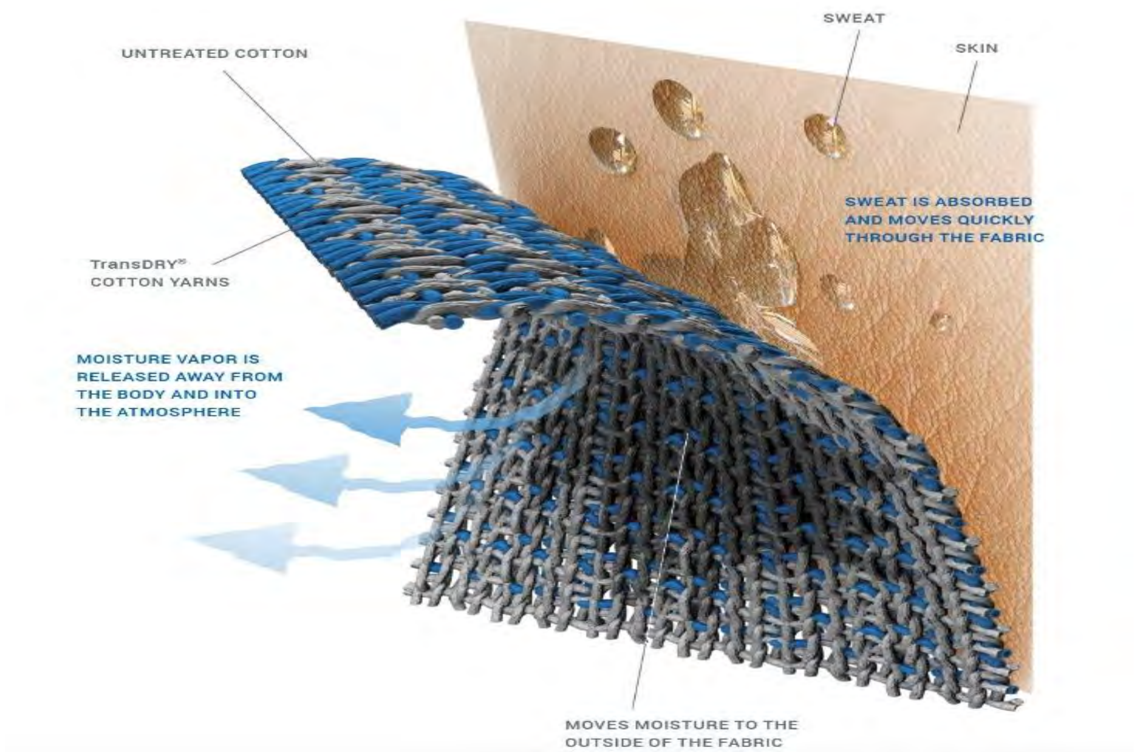

Figure 2.13. Moisture movement with TransDRY® technology [90]

Liquid moisture management by directional transportation of liquid via manipulating the biomimetic structures has become a very promising research direction. Directional liquid transportation has triggered technological advancements in many promising applications ranging from fog collection, lubrication, emulsification, microfluidic operations, agriculture irrigation, oil-water separation, and moisture management functional textiles [91-94]. Liquid directional transport phenomena exist naturally in many biological organisms, including plants, spider silk, the peristome of the pitcher plants, and cactus spines, among others [95-98]. Inspired by these living organisms, scientists have successfully fabricated materials with the artificial directional flow of liquid. While promoting research on this hot topic, the researchers have tried to design and fabricate structures controlling the directional flow of fluid by various combinations of surface roughness and gradients. The application of energy gradient, wettability gradient, curvature effect, Laplace pressure, ratchet mechanism, and energy conversion using condensation and static electricity has been reported as underlying mechanisms of directional liquid transport [99]. Lao et al. fabricated a skin-like fabric employing a wettability gradient at spatially distributed porous channels acting like sweating glands, enabling a continuous directional flow of liquid through them yet repelling the external water. They achieved the effect in a piece of hydrophilic pristine cotton fabric by rendering it superhydrophobic via treating it with perfluorosilane-coated titanium dioxide (TiO_2) nanoparticles. Additionally, to create artificial localized porous sweating glands through the thickness of the fabric, the predominant hydrophobic cotton fabric was subjected to O_2 plasma etching process at selective spots by applying a predesigned patterned mask (Figure 2.14) [100]. The as-produced piece of cloth exhibited excellent water repellent characteristics with superior one-way liquid transport abilities through the artificial sweat glands. The treated fabric contact angle was 152^{o,} contrary to that 0^{o} of super hydrophilic pristine cotton fabric. However, at selected spots of plasma etching, the CA was dropped to 44^{o} after a time interval of 5 minutes. While the CA on the backside (unexposed to plasma treatment) of the treated spot was interestingly recorded zero. This is because when a droplet of water was placed on the backside of the treated spot, it quickly travels to the other side, exhibiting excellent out-of-plane directional water transportation acting like a sweating gland.

Since the directional transport of liquid is the most desirable function of performance apparel, managing excessive sweat released from the body under conditions, mostly confronted by athletes, construction workers, soldiers, and outdoor occupants of hot and humid weather. For continuous uptake of sweat away from the skin with enhanced moisture-wicking functional textiles, a skin memetic tri-layer composite fibrous membrane was reported with one-way directional transport of liquid, yet preventing the penetration of water in the reverse direction. The membrane mimics the function of the skin in an aspect of directional sweat secretion. The composite membrane consisting of hydrophobic/transporting/super hydrophilic tri-layers was produced by hydrolysis of PU/(PU-PAN)/(PAN-SiO2) into PU/(PU-HPAN)/HPAN (PU:

Polyurethane, PAN: Polyacrylonitrile and HPAN: Hydrolyzed polyacrylonitrile) and demonstrated excellent directional transport index R of 1021% with a required outstanding pressure of 16.1 cm H_2O in reverse direction [101].

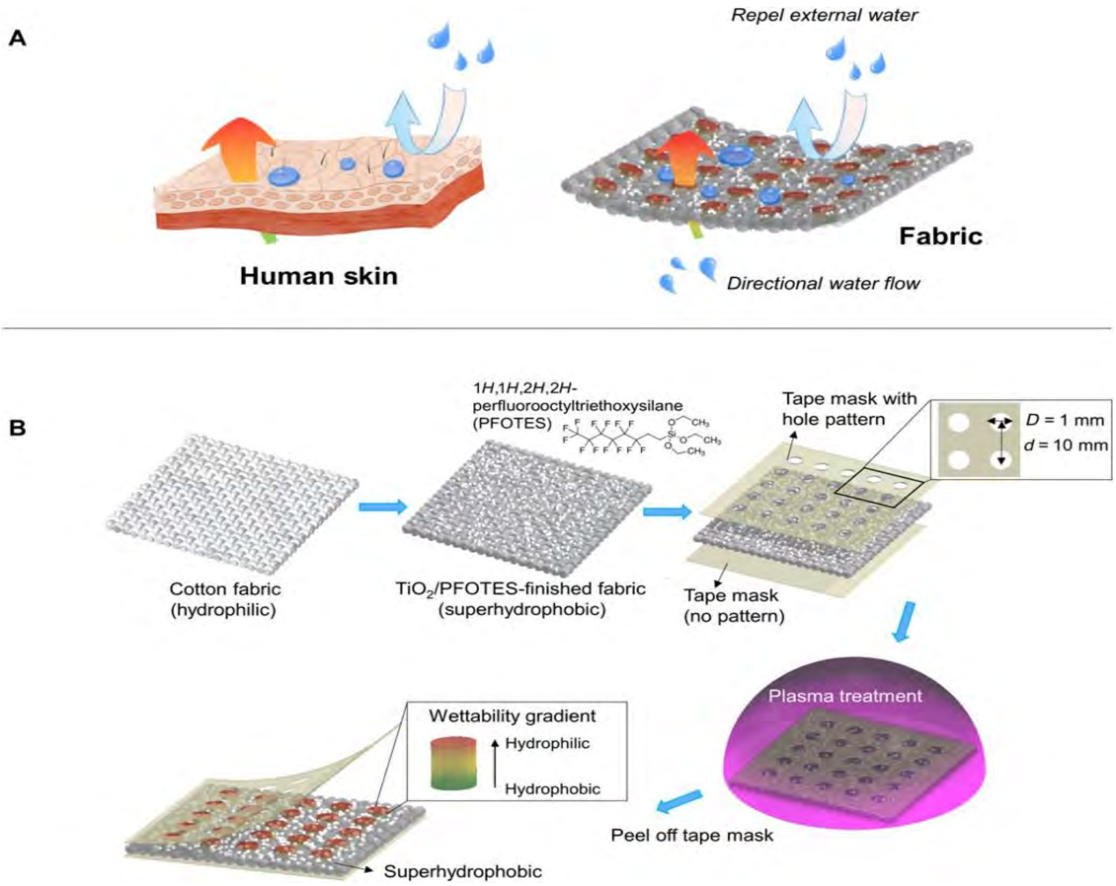

Figure 2.14. Schematic illustration of the process for the development of skin-like fabric [100]

Nature-designed Murray network is an essential element of a hierarchical distributed multi-branching fibrous system of vascular plants, imparting them the ultrafast antigravity transpiration and evaporation supported by Murray's Law [102, 103]. Wang et al. reported a biomimetic fibrous membrane endowed with the Murray network, enabling them with ultrafast liquid transport and evaporation properties, potentially applicable in moisture management fabrics [104]. Producing a hierarchically arranged micro-nano fibrous membrane mimicking the leaf vein network with an energy gradient provided ultrafast antigravity water transportation and quick-drying ability. The multilayer structure with pores size varying from micro to nano was obtained by depositing electro spun nanofibrous cellulose acetate on a nonwoven substrate of polylactic acids, subsequently dip-coated in a well-dispersed solution of micro fibrillated cellulose and TF-629C hydrophilic agent (Figure 2.15). The resulting structure exhibited an outstanding evaporation rate of 0.67 gh^{-1}, ultrafast one-way liquid transportation capability of 1245%, and a fascinating overall moisture management capability

(OMMC) of 0.94. The outstanding directional water transfer phenomena in nature is also emulated in designing a fiber assembly of one-dimensional (ID) structure. Mao et al. imitated a tree-like structure by coating a 1D cotton yarn with polycaprolactone nanofibers via electrospinning, thus creating a differential capillary effect with multiscale micro-nano channels, moving from the core to the surface. The yarns were woven into fabrics, which demonstrated an excellent OMMC of 0.88, and a unique one-way transportation index (R) of 1034.5%. In another study, the achievement of directional liquid transport was reported in a hydrophobic/super hydrophilic, Janus polyester/nitrocellulose (PE/NC) membrane with an array of conical hydrophilic micropores produced by CO_2 laser perforation process. Water, coming in contact with the hydrophobic PE layer, is pulled upward to the super hydrophilic NC layer through the asymmetric and conical hydrophilic pores by capillary action (Figure 2.16). The membrane exhibited an ultrafast directional water conveyance potential of 1246% [105]. The use of such membranes can provide efficient solutions in designing functional clothing with excellent water vapour permeability, water wicking, and evaporation properties.

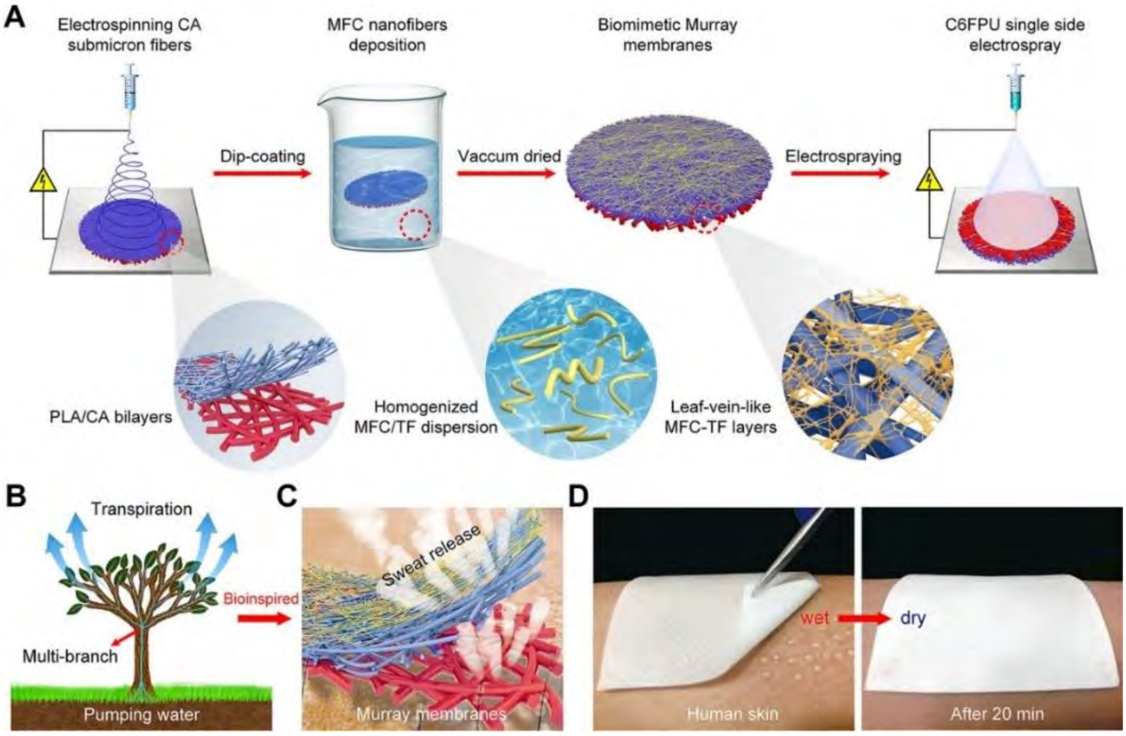

Figure 2.15. Biomimetic fibrous Murray membrane. (A) Fabrication process. (B) The antigravity transpiration. (C) Sweat transfers from the skin to the upper surface for evaporation. (D) Optical photographs displaying quick-drying performance [104]

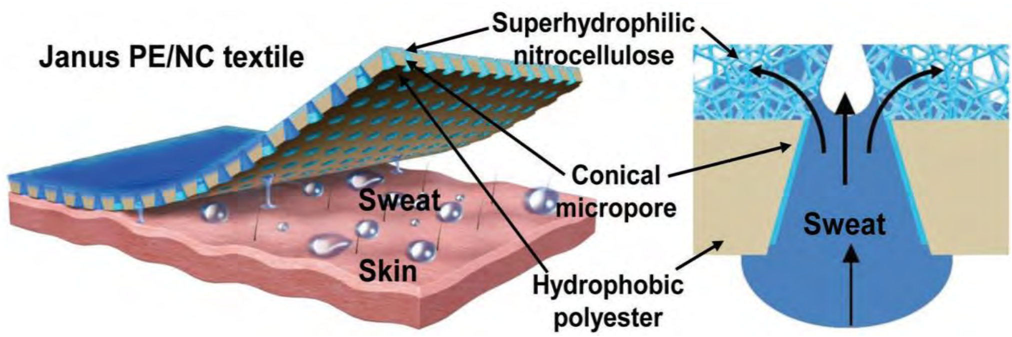

Figure 2.16. Schematic illustration of conical pores in Janus PE/NC composite textile [105]

Apart from this, most recently it has been reported a promising concept of integrated cooling (i-cool) textiles with distinct paths of sweat transportation and heat conduction for better thermoregulation of the human body. In preparation of i-cool textile, a copper matrix containing arrays of holes serves as the heat conducting matrix. Whereas a web of electro-spun polyamide 6 fibres, integrated into the holes and top surface of the copper matrix, wicks the sweat away from the body as presented in Figure 2.17. The synergetic effect of heat conducting matrix and selectively positioned wicking channels is claimed to provide fast wicking, improved evaporation along with efficient heat removal and cooling of the body [106].

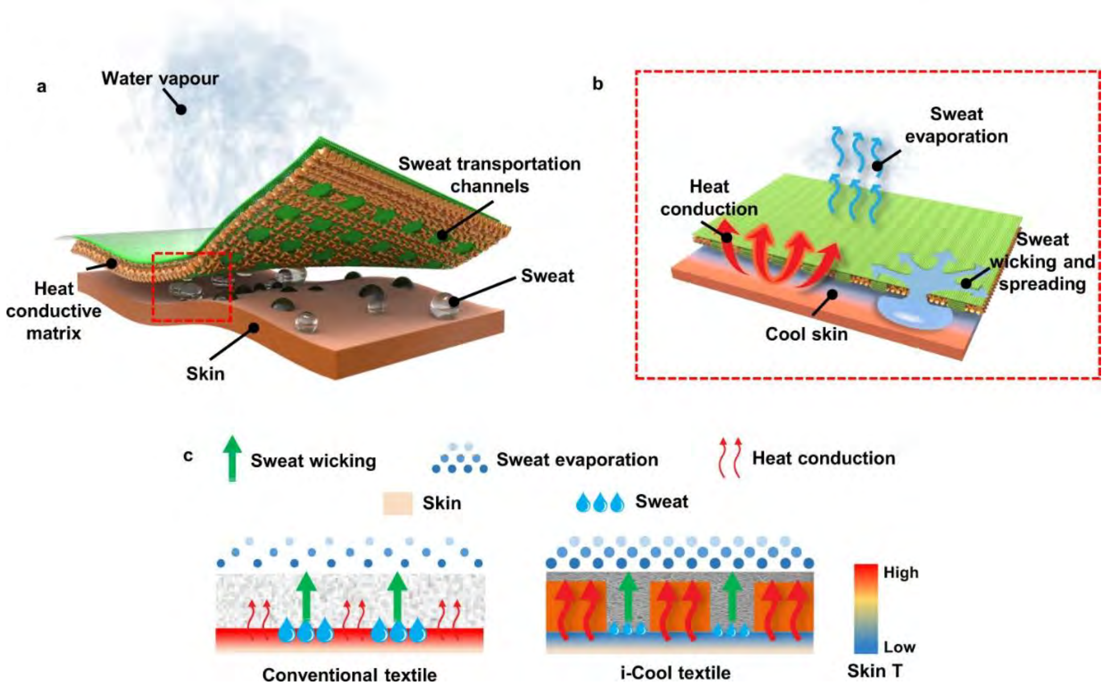

Figure 2.17. Integrated cooling (i-cool) textile for efficient heat conduction and sweat transportation [106]

On the other hand, for enhanced radiative cooling without perspiration, nano-porous polyethylene has been explored as a promising candidate for efficient thermal management. As illustrated in Figure 2.18, when imparted with an anisotropic wettability to the double-layer polyethylene membrane, it demonstrated the efficient evaporative cooling efficiency and sweat-draining ability [107].

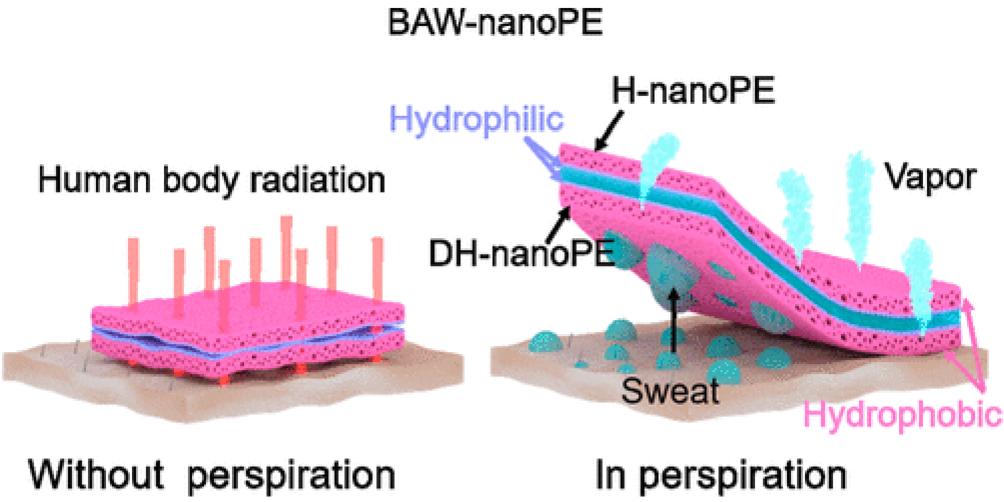

Figure 2.18. Double layer nano porous polyethylene membrane with anisotropic wettability [107]

2.2.1 Research gap of liquid and moisture management fabrics

Currently, many types of moisture management cooling fabrics have been developed to deal with body moisture and heat, but there is still a need for improvement to deal with profuse sweating conditions. Since, in profuse sweating, if the rate of evaporation is lower than the rate of sweating, the fast wicking, spreading along with reduced absorbency of fabric will result in quick saturation followed by sweat dripping. Sweat dripping on the floor is a problem in some sports and even at some workplaces. Therefore, further improvements are needed for

- Keeping the skin cool and dry in profuse sweating conditions
- Enhancement of sweat transmission and evaporation from fabric
- Reducing sweat weight gain and drying time of the fabric
- Collection of dripping sweat
- Minimize the post-exercise chilling effect due to excessive liquid accumulation and evaporation from fabric

2.3 Mechanisms of liquid transport through fibrous assemblies

Liquid transport through fibrous materials is the decisive factor in the processing and applications of fibrous assemblies. It is of vital role in the fields such as fluid filtration, lubrication, oil recovery, composite fabrication, wet processing, as well as dying, washing, and drying of fabrics. The thermos-physiological comfort of the body is also significantly associated with heat and moisture regulation through clothing [108]. Removal of skin perspiration by clothing is essential to eliminate the build of sweating fluid on the skin, causing discomfort and bad odor. Similarly, the quick evaporation of perspiration from clothing is also very important to cool the body and prevent liquid build-up in clothing potentially associated with degradation of clothing thermal insulation and evaporative resistance [107]. Moreover, the side of fabric touching the skin should remain dry to avoid unnecessary body heat dissipation, as well as discomfort of clinging and clumsiness[100]. The basic mechanism of liquid transport through the fibrous assemblies of clothing involves wetting and wicking [109]. Wetting and wicking are of great practical significance in determining the performance of products such as medical products, disposables, and moisture management clothing.

2.3.1 Wetting

Wetting is the condition that develops when a fibrous assembly is in contact with a specified liquid under certain conditions. There is another term called “wettability”, which is the potential of a solid surface to interact with the liquid of certain characteristics [57, 110]. A higher wettability of fabric indicates the quick absorption and spreading of liquid into the fabric. Wettability, in fact, is prior to wicking, the preliminary behaviour of liquid substrate interaction when a fabric or yarns comes in contact with a liquid [56]. Wetting is essential for wicking. If a liquid cannot wet fibres, it will not be wicked into the fabric. The degree of wettability of a fluid and wetting appearance of a solid is generally characterized by the surface tension of the liquid and contact angle and work of adhesion.

Surface Tension

The intermolecular forces of attraction in a bulk of liquid are balanced by equal and opposite forces in all directions. However, an imbalanced force of attraction is experienced by the molecules at the surface. The surface free energy present at the liquid's surface, which is commonly referred to as "surface tension," causes the liquid's surface area to be reduced to a bare minimum. For a liquid to wet a solid or a solid to be submerged in the liquid, the surface energy of the solid must be high enough to overcome the surface tension of the liquid.

Contact angle

For a given fluid, the contact angle is a basic parameter to test the wettability of a certain fluid. The contact angle is the angle between the tangent to the drop contour at the liquid-vapour (air) and liquid-solid interface [111].

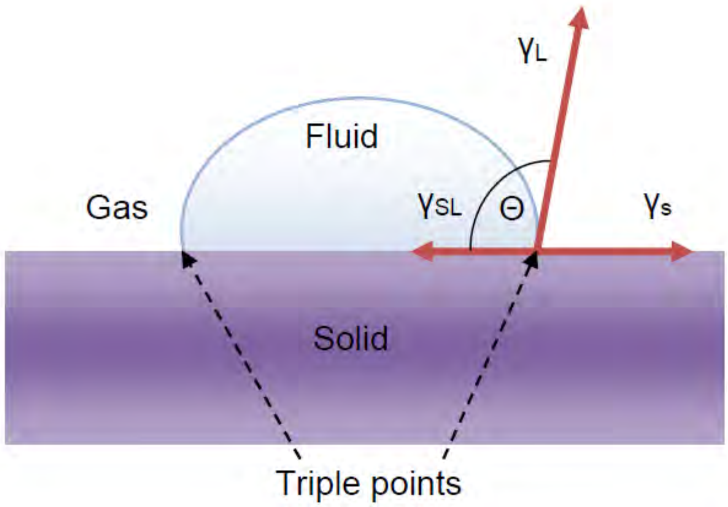

Figure 2.19. A liquid drop on a solid surface in the state of equilibrium [112]

The forces in equilibrium at the boundary of the solid-liquid interface are generally described by the Young-Dupree equation, as below.

$$\gamma_{S} - \gamma_{SL} = \gamma_{L} cos\theta \qquad (2.1)$$

Where γs represents the surface tension of a solid, γ_{SL} indicates the interfacial tension at the solid-liquid interface, γ_L is the surface tension of the given liquid and θ is the contact angle of liquid drop at equilibrium on the solid surface. The term $\gamma_L cos\theta$, is termed as 'adhesion tension' or 'specific wettability'. γ_S *and* γ_{SL} are difficult to measure directly, whereas the γ_L *and* $cos\theta$ can be measured easily. It is worth noting that Equation 2.1 is valid only when the solid surface is non-deformable, homogenous, smooth, and impermeable.

The contact angle defines wettability as "wetting" if $\theta < 90°$ and "non-wetting" if $\theta > 90°$. The $\cos\theta$ would be positive when $\gamma_{SV} > \gamma_{SL}$ such that the contact angle θ may be between 0° to 90°. On the other hand, if $\gamma_{SV} < \gamma_{SL}$, the θ would lie between 90° to 180°. The wettability is increased as the contact angle θ decreases, therefore the $\cos\theta$ increases. A zero-contact angel is associated with maximum wettability. It is worth noting that at zero contact angle, the equilibrium condition does not exist, so Equation 2.1 does not apply.

2.3.2 Wicking

Wicking is defined as the capillary-induced spontaneous flow of liquid into a porous medium. The liquid can transport through the yarn and fabrics only because of wicking or some external forces. As a liquid wet the fibrous assemblies of several capillaries, it triggers the necessary capillary action for wicking and spreading the liquid. As a result, an instantaneous displacement of a solid-air interface with a solid-liquid interface can be realized in the form of wicking within a porous system. Inside the capillary, when a liquid wet the capillary walls, a meniscus is formed at the liquid-vapour interface.

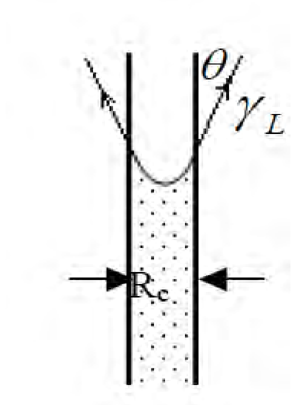

Figure 2.20. The capillary flow of liquid

A pressure difference, known as capillary pressure, is generated across the meniscus in relation to its radius of curvature and contact angle. The magnitude of capillary pressure is determined by the You-Laplace equation [113].

$$\Delta P = 2\gamma_L \cos\theta / r \text{ ....(2.2)}$$

Where ΔP is the capillary pressure, r is the capillary radius, γ_L is the surface tension of the liquid and θ is the contact angle. It should be noted that the capillary pressure is inversely proportional to the radius of the capillary. The difference in capillary pressure among consecutive pores in fabric causes the liquid to spread in the fabric [3, 53]. The volume flow rate of liquid through the capillary channel is proportional to the capillary pressure gradient. Wicking ability is the ability to sustain the capillary flow. The overall wicking ability of the fabric is determined by the combined effect of capillary pressure and permeability. The capillary pressure varies inversely with the saturation whereas the permeability tends to rise with saturation. At a low saturation level, the liquid first enters the small pores and then into the large pores. A network of small and uniformly distributed pores in the fibrous assemblies facilitates the fast spreading of the liquid [114]. Whereas, with the increase in the number of pores or total pore volume, as in the case of micro-denier fibres non-roundedness of fibres or profiled fibre surface, the amount of liquid retention in the fabric is increased [115].

Distance of capillary flow

In a capillary flow, the distance travelled by the liquid under capillary pressure is approximately determined by the Lucas-Washburn Equation.

$$L = \sqrt{\frac{R_c \gamma cos\theta}{2\eta}}\ t^{1/2} \ldots\ldots\ldots\ldots\ldots\ldots..(2.3)$$

Where, R_c is the capillary radius, L is the capillary rise in a time t, and η is the viscosity of the liquid. The Equation 2.3 may suggest that at a certain time the capillary rise would be higher with greater pore size. However, Miller found that the higher initial wicking rate at bigger pores is overtaken with time by the finer pores [110, 116]. This may be possible due to higher capillary pressure and consequently faster flow associated with the finer pores as described by the Laplace Equation 2.2. On the other hand, the distance of liquid advancement might be limited with increasing amounts of liquid accumulation in the larger pores.

Work of adhesion and cohesion

Adhesion is the force of attraction between two surfaces in contact. Due to adhesion between the solid and a liquid drop at equilibrium, the maximum possible contact angle of 180° is not possible to be realized in practice. During the immersion of a substrate in the liquid or capillary sorption process, the solid-vapour phase is replaced with the solid-liquid phase. The work of immersion or penetration is given by the Equation 2.4.

$$W_I = W_p = \gamma_S - \gamma_L \qquad (2.4)$$

For spontaneous penetration of liquid into solid i.e., positive capillary rise, the surface energy of solid should be higher than that of liquid, so that work of penetration Wp is positive. The W_p is the measure of energy needed for capillary penetration.

In the case of liquid-solid interaction, the work of adhesion as determined by the Equation 2.1 is given below,

$$W_A = \gamma_S + \gamma_L - \gamma_{SL} \ldots\ldots\ldots\ldots\ldots\ldots\ldots.(2.5)$$

Equation 2.3 can be further employed to liquid, to find the work of cohesion, which is the amount of work required to pull apart a liquid column into two surfaces, each having an interfacial tension of γ_L.

$$W_C = 2\gamma_L \text{.....................(2.6)}$$

In the process of wetting, as a fluid meets a solid, surface tensions of solid γ_S and liquid γ_L compete with the interfacial surface tension γ_{SL}.The relative magnitude of parameters from Equation 2.1 determines the form of the fluid drop. The fluid spreading coefficient is defined as:

$$S = \gamma_S - (\gamma_{SL} + \gamma_L) \text{ ....(2.7)}$$

For fluid to spread the value of S must be positive. The spreading will occur if the work of adhesion (attraction between the fluid and solid surface) is greater than the work of cohesion (attraction between two surfaces of a fluid).

$$S = W_{AD} - W_C > 0 \text{...............(2.8)}$$

In the case of complete wetting, a fluid film is formed at the solid surface, Whereas, in the case of incomplete wetting, a drop is formed with a defined contact angle at the solid surface. Any distinction between zero and non-zero contact angle differentiates between the spreading and non-spreading behaviour of a liquid on a solid surface.

2.4 Summary

The various methods of improving moisture management abilities of fabrics discussed above include the creation of wicking channels, wicking windows or one-way liquid transportation through surface treatment, fabric construction, a combination of yarns and fibre engineering. The different methods applied are unique in their nature, but they share some common functions like increasing wicking, spreading, evaporation and drying abilities of fabrics. Especially, the bilayer knitted fabrics with efficient one-way liquid transportation properties are proven to efficiently keep the wearer's skin dry. The moisture management fabrics produced by either double layer knit construction, showing one-way liquid transport because of differential wettability between two planes may be of in liquid moisture management under normal to moderate rate of sweating. However, in high physical activity and severe environmental conditions in summer, the sweat rates of the human body may surpass 1L/h-m^2

where an early saturation of such fabric is inevitable. Due to the limited rate of evaporation from the fabric surface, the increasing degree of saturation may reduce the moisture vapour transmission besides increasing the weight of fabrics. Consequently, under continuous profuse sweating, the sweat accumulated in the fabric can move downward through the fabric under gravity, where an inappropriate sweat dripping on floor may happen. Therefore, in the case of profuse sweating, there is still a need to improve the moisture management abilities of fabrics regarding sweat distribution, evaporation and drying to prevent early saturation and control the sweat dripping on the floor.

Chapter 3

Concurrent and real-time measurement of fabric liquid and moisture management properties using a novel sweating simulator

3.1 Introduction

The human body starts sweating under rising body temperature due to heat exposure and/or intense physical activities. The function of perspiration is to bring cooling to the body by heat dissipation through the evaporation of sweat. Clothing is a crucial pathway of heat and moisture transmission between the perspiring body and the environment. As a result, it is essential to assess the liquid moisture transmission properties of fabrics while designing clothing for efficient personal perspiration management and thermoregulation. The liquid moisture transport of textiles has been extensively studied in prior art by various methodologies. British Standards (BS) 4554, American Association of Textile Chemists and Colorists (AATCC) standards such as AATCC79, AATCC 195, AATCC 197, and AATCC 198 are the most commonly used standard test methods for assessing the wettability, absorbency, liquid moisture transport, vertical and horizontal wicking of fabrics, respectively [52, 117-119].

All existing methods of investigating the liquid transport of fabrics could be quite useful to readily compare the behaviour of fabrics, even quickly, repeatedly, and accurately [12, 56, 120, 121]. However, the evaluation of liquid transfer and distribution from the skin to the adjacent layer of clothing i.e., liquid and moisture management at the personal level, is out of their scope.

In the context of garments for personal perspiration management, several testing requirements come together as performance indicators. Considering a fabric in contact with an active perspiring body, the clothing perspiration management is not merely due to wetting and wicking, but many other factors such as multidirectional liquid transport (vertical wicking, transverse wicking, gravity-induced liquid flow), transplanar liquid transport, liquid accumulation and drainage, evaporation and drying, body posture, the relative distribution of sweating regional intensities, ambient conditions, air velocity, and last but not least the fabric construction, structure, treatments as well as weight of clothing become equally essential to be analyzed. Especially in moderate/profuse perspiration, the draining, evaporation, and drying properties of fabric become more crucial in relieving the wet stress of the perspiring body [25, 26, 30, 40, 122]. This wide range of testing requirements inspired us to investigate the liquid evaporation and transport properties in sample size approximate to a shirt panel in contact with a perspiring skin, under controlled ambient conditions. In this aspect, human-based subjective trials have been employed in previous reports [123, 124]. However, such trials are often much more complicated, expensive, and difficult to organize. Additionally, the accuracy, reliability, and reproducibility of results from subjective trials are undermined, subjected to the inconsistency among their metabolic rates, regional sweating intensities, ergonomics, and availability on demand. Alternatively, perspiring thermal mannequins and sweating cylinders, which are primarily designed to investigate heat and moisture transport through textiles, could be potential substitutes for human participants [37, 125-127]. Since tests on the entire garment are performed on mannequins, it is difficult to assess the inherent contribution of fabric properties to the overall results. Many additional elements, such as distribution of perspiration, the design feature of garment and instrument, as well as the fit of the garment, could also affect the overall results. Although the concept of a sweating cylinder has addressed this issue by allowing testing of fabric on it, it does not replicate the profile and relative distribution of regional sweating of the human torso. Moreover, the uniform influence of air velocity on convective evaporation through fabric cannot be realized on it due to the varied airflow along the lateral and back sides of the cylinder [72]. Additionally, due to the higher cost, heavyweight, complex operation, and repeatability error, such instruments are not widely in operation.

Under these constraints, the idea of the novel sweating simulator (NSS) emerged as a potential solution, simulating a clothed body, standing at a weighing scale, and perspiring profusely at its upper-middle back positions (Owing to the highest tendency of sweating in this region [31, 34, 46]). With this imagination, we set out to develop *NSS* enabling us to study the fabric liquid moisture distribution, including the sweat spatial and temporal migration, accumulation, evaporation, dripping and drying, all at once. The instrument consists of an upright sweating plane, where a regional sweating zone is established at the near upper-middle position simulating the highest sweating region at the human upper back. The fabric sample size that approximates a shirt panel can be fixed on the sweating plane. Sample pre-tension, the inclination of the sweating plane, and sweating intensity are adjustable to replicate the certain conditions under observation. This study concerns evaluating the influence of fabric material, structure, and construction properties on their liquid moisture distribution using *NSS* with no temperature control of the simulated sweating plane and sweat under the controlled testing and ambient conditions. The use of *NSS* to test the fabric dynamic liquid distribution and multidimensional transportation at the simulated skin and sweat temperature will be reported in next chapter.

3.2 Design and description of instrument

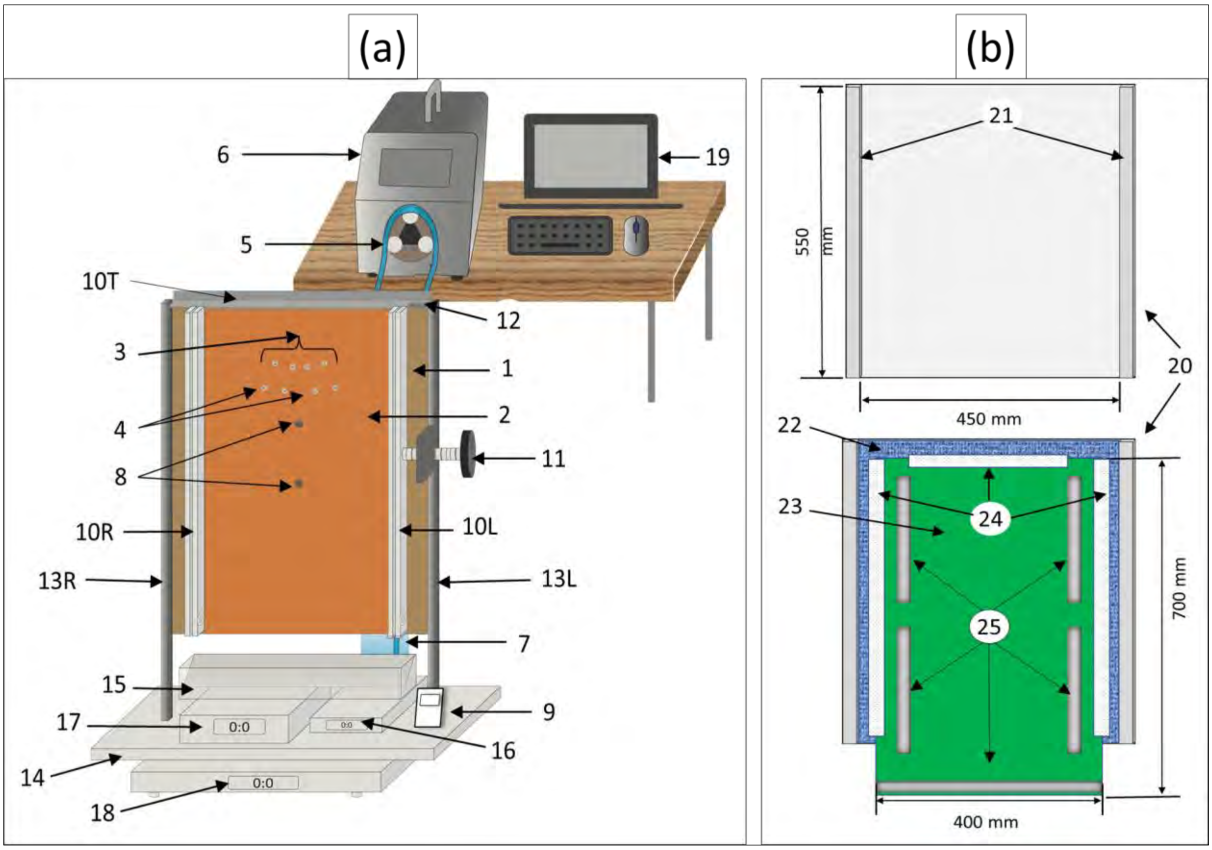

Figure 3.1. (a) Schematic illustration of NSS; (b) Apparatus used for transferring of the specimen on NSS.

1	Supporting panel	2	Silicone-based heating panel
3	Sweating zone	4	Sweating outlets
5	Silicone hose	6	Peristaltic pump
7	Liquid reservoir	8	Thermocouples
9	Temperature data logger	10L, 10R, 10T	Specimen holding clamps
11	Bolt for pre-tension adjustment	12	Scale bar
13R, 13L	Supporting columns	14	Baseplate
15	Container for dripping collection	16	Weighing balance
17	Weighing balance	18	Weighing balance
19	Computer	20	Board for specimen placement

21	Rubber strip	22	Specimen
23	Top loading plastic sheet	24	Paper tapes
25	Rubber strips as dead weights		

A schematic illustration of *NSS* is shown in Figure 3.1a. A PMMA (Polymethylene methacrylate) panel (1) (typical dimensions: 500 ×700 mm×3mm, to be wide and large enough to support the various attached components and their functions as well as potential testing of fabric for various shirt sizes such as medium, large, and extra-large.) is fixed on an aluminium bars frame. A panel (2) (about 400 ×700 mm×2mm) is placed on top of the panel (1) to constitute a sweating plane, awarded with akin to skin interface, wetting characteristics, and temperature. Panel (2) is composed of a silicone-based fibre reinforced composite with an integrated heating element and a temperature sensor. Panel (2) is further equipped with an intelligent PID (Proportional Integral Derivative) temperature controller to regulate its surface temperature. The panel (2) endowed with a water contact angle in the range of 100° to 115° ensure the nominal chance of interfacial wicking between fabric and sweating plane. The sweating plane contains a sweating zone (3) in the upper-middle position, consisting of an adequate number of sweating outlets (4). The location of the sweating zone (3) replicates the highest intensity sweat zone at the upper back of a sweating human torso [46]. The crescent-like arrangement of eight sweating outlets is a 2D reflection of a 3D curvature profile between the two shoulders of the torso. On the rear, the sweating outlets (4) are connected to the sweating glands (5), made of flexible, narrow-diameter silicone tubes that travel through a peristaltic pump (6) (Model: BF100, Flow accuracy: <0.5%, Lead fluid, PRC) and are submerged into the sweating liquid inside the container (7). The liquid container (7) is also equipped with a PID temperature controller to regulate the temperature of sweating liquid corresponding to the human perspiration temperature. Temperature sensors (K-type thermocouples) (8) are used to monitor the real-time temperature of the specimen under testing. The data logger (9) retrieves the data from the temperature sensors as per set interval and transmit it to the computer-based software for further analysis.

Three clamps (10R, 10L and 10T) are equipped to hold the specimen in place on the sweating plane. The clamps (10R and 10L) comprise a pair of metal bars bolted together at the bottom. The inner bar of each clamp can be turned out and in to firmly hold the specimen in place. The clamp (10T) consisting of an angle bar is hinged at the top to hold the specimen upper end. Further, the clamps (10R and 10T) are static at their position. While the clamp (10L) can be displaced right and left by rotating a driving bolt (11). The displacement of the clamp (10L) can be used to apply a certain pre-tension on the specimen under testing. The pre-tension can help to remove any slackness and creases in the fabric besides obtaining a uniform contact with the sweating plane. A scale bar (12), graduated in millimetres, is affixed on the top right corner of the panel (1) to directly read the displacement of the clamp (10L). Panel (1) with all its components is positioned between two metal column bars (13R) and (13L), supported by two 180-degree steering brackets connected with (13R) and (13L). The steering brackets are graduated in degrees to directly read and adjust the slope of the sweating plane. The column bars (13R) and (13L), at their base, are secured to a metal base-plate (14) (typical dimension: 550 ×450 mm×3mm) supported by a robust metal frame underneath. A container (15) placed just beneath the bottom edge of the panel (2) is used for liquid dripping collection. The apparatus is further equipped with three weighing balances (16, 17, and 18) to measure the real-time mass change of liquid supply, dripping and evaporation, respectively. The weighing balances (16) and (17 (Capacity: 6000 g, accuracy: 0.1 g, model: BX6000, Shimadzu, Japan) carrying the containers (7) and (15), respectively, are placed on the base-plate. The whole setup is then loaded on the weighing balance (18, (Capacity: 32000 g, accuracy: 0.1 g, linearity ±0.2 g, model: BX32KH, Shimadzu, Japan). All the weighing balances and data loggers are connected to a computer (19) for real-time data acquisition into the respective software.

Figure 3.1b reveals an apparatus used to prepare, transfer, and mount the specimen on *NSS* for testing. Typically, mounting a specimen on the *NSS* simply by hand is challenging because the fabric intrinsic flexibility is deterrent to its balancing on the upright sweating plane. A person's two-handed operation seems insufficient to keep the specimen evenly flat under a uniform stretch while mounting on *NSS*. Therefore, a systemic approach is demonstrated using the apparatus shown in Figure 3.1b. A horizontal bottom PMMA board (20) (40x550.0 mm) with two rubber strips (21), a tope loading flexible poly-amide sheet (23) (400 x700 mm) having some rubber strips (25) attached on it and functioning as dead weights, make up the whole apparatus.

In the bottom illustration of Figure 3.1b, a sample fabric specimen (22) of standard size (typically 450x550 mm) is shown. The specimen (22) is laid flat, lengthwise, on the board (20). Sheet (23) is placed in the middle, right above specimen (22), so that a portion of the specimen, about 25mm in width, is left uncovered on the top, right and left sides. The paper tapes (24) are used to secure the sheet (23) to the specimen beneath. Sheet (23) is then ready to carry and transfer the specimen to the *NSS* for mounting.

The clamps (10R) and (10L) are spaced apart at a distance of about 400mm. Sheet (23) and specimen (22) together are put on the sweating plane between the bar clamps (10R) and (10L) (Figure 3.1a). The top end of the sheet (23) is aligned with the top end of the panel (2). The piece of fabric extending above the sheet (23) is gripped in the tope clamp 10T, and then paper tapes (24) are removed to detach the specimen from the sheet (23). Subsequently, bar clamps are open and closed to grip the specimen on its right and left sides. Once the specimen is secured in the clamps, sheet (23) is gently removed from the top. The left bar clamp 10L is then slightly displaced towards the right, applying a certain pre-tension to the specimen.

3.2.1 Measuring Principle

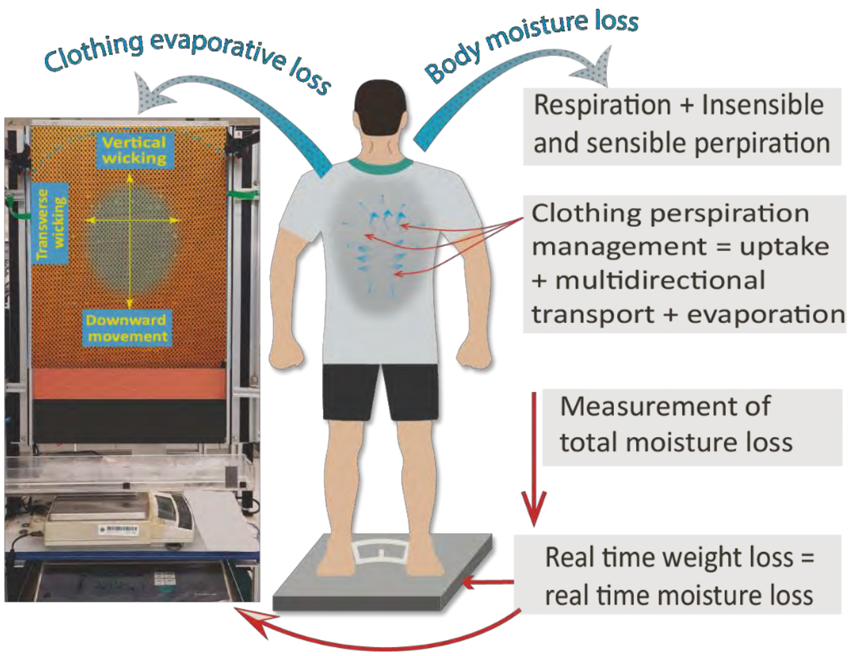

Figure 3.2. The measuring principle of NSS.

The instrument is designed to address the following fundamental questions about the liquid moisture management capabilities of fabrics, which have a direct impact on personal thermo-physiological comfort.

1. How quickly is sweat evaporated from the fabric? This is because evaporation is a decisive factor in the body heat dissipation and achieving personal thermal comfort.
2. How much sweat is accumulated in the fabric? This is because if more sweat is accumulated in the fabric, it may become heavier, sagging, sticky, sweaty, and uncomfortable.

3. How much liquid is dripped through the fabric? This is because if more liquid is drained through the fabric, it may dry faster.

NSS answers these questions simply by weighing separately the amount of liquid supplied, dripped, and evaporated through the fabric, using three weighing balances. The amount of liquid accumulated in the fabric is determined by subtracting the amount of liquid evaporated and dripped from the amount of liquid supplied as described by the following relation.

Liquid accumulation = liquid supplied – (liquid dripped + liquid evaporated)

The moisture evaporation rate, accumulation rate, and drying rate can all be calculated using the real-time curves of liquid evaporation and accumulation.

The NSS measurement principle is depicted in Figure 3.2. It employs the gravimetric principle, as do human trials, to measure body moisture loss through evaporation using a weighing balance. However, the main concern with human trials is that the evaporation may also take place directly from the skin (insensible sweating), and the role of fabrics in evaporating the liquid sweat cannot be evaluated independently [128]. The advantage of *NSS* is that it simulates only liquid sweating, which is supposed to accumulate and evaporate from the fabric surface so that the true contribution of fabric structure, composition and material properties to liquid accumulation, evaporation and transport can be evaluated autonomously.

3.3 Experimental section

3.3.1 Material

Eight kinds of commercial moisture management knitted fabrics (because of their greater demand in the leisure, activewear and sportswear industries)were tested. The fabrics varied in areal density, material, construction, and design, as indicated by their specifications, presented in Table 1. The fabrics were further tested for their absorbency and hydrophilicity using the drop absorbency test (AATCC79) and measuring the water contact angle, respectively. As shown in Table 1, unlike all pure polyester and polyester mix fabrics, the pure cotton fabric appeared to have some hydrophobic treatment (The details of hydrophobic treatment are unknown). It showed an average water contact angle of about 87°±0.82. However, it is important to note that the water drop could still penetrate the fabric over a period above 60 sec. In contrast, all other fabrics were found to be super-hydrophilic, showing quick wetting and wicking ability. Therefore, the measurement of true water contact angle was not applicable to them. All the fabrics were prewashed and dried according to ISO6330 standard test method [129]. The fabrics were then laser cut to size 450x550 mm, in an approximation to the size of a shirt panel. Essentially, the specimens were cut with long dimensions parallel to the wales, which correspond to the length of fabric in its roll and is often adapted in pattern layouts for fabric cutting during the process of garment making [130]

Table 3.1. Physical specifications and wetting parameters of fabrics

Code	Knit type	Fibre/Yarn specifications (denier)	Composition	Areal density (gm^{-2})	WPI / CPI	Thickness (mm)	Absorbency (sec)	WCA
K1	Pique-weft knit	253D	100% Cotton	244.97	27/51	0.66	60+	87±0.82
K2	Pique-weft knit	253D	65% PES/35% CO	225.41	28/50	0.62	<1	N.A.
K3	Bird eye-weft knit	75D/72F	45% PES/55%CM,	130.94	44/50	0.40	<1	N.A.
K4	Pique-weft knit	100D/96F	100% PES,	183.84	40/57	0.36	<1	N.A.
K5	Pique-weft knit	100D/96F	100% PES,	151.87	36/46	0.36	<1	N.A.
K6	Waffle-weft knit	50D/72F	100% PES,	96.13	57/52	0.20	<1	N.A.
K7	Small mesh-warp Knit	75D/72F	100% PES,	97.90	35/30	0.22	<1	N.A.
K8	Large mesh-warp knit	Un known	100% PES	140.6	22/21	0.32	1-3	N.A.

Note: - D: Denier, F: Number of filaments, PES: Polyester, CO: Cotton, CM: Coolmax®, WPI: Wales per inch, CPI: Courses per inch, WCA: Water contact angle

3.3.2 Experimental design

The fabrics were tested on *NSS* under controlled laboratory conditions with ambient temperature 20±0.5 °C, relative humidity 60±2.5%, and air velocity 0.1 to 0.3 m/s. To exclusively study the effect of fabric intrinsic contribution on dynamic liquid moisture management properties, the tests were performed at zero temperature gradient among the liquid supplied, sweating plane and the environment. The temperature of the sweating plane could only change because of evaporation from the fabric specimen. In addition, any change in the ambient temperature and relative humidity, which could affect the rate of evaporation, were tracked in real-time using a temperature and humidity recorder. Further, to simulate the active and resting periods during an exercise, each test consists of two phases: phase 1 (P1) consisted of one hour of sweating, and phase 2 (P2) consisted of one hour of drying.

To demonstrate and validate the accuracy, reproducibility, and potential of *NSS* in testing a wide variety of moisture management fabrics under various conditions, mimicking the real-life applications, we formulated the experimental plan consisting of three distinct sections as presented in Table 3.2.

Table 3.2. Design of experimental plan

Section 01	
Objective	To test and distinguish the dynamic liquid moisture management properties of a wide variety of fabrics in an accurate and reproducible manner.
Strategy	Eight different types of fabrics were tested on *NSS,* and the data were examined to see how the fabric overall specifications influenced its ability to perform dynamic liquid moisture management. The liquid was supplied to the fabric at a constant rate of 120 gh^{-1}, which may correspond to an extreme perspiration intensity at the upper back of the sweating human torso [31, 34, 46]. The orientation of the sweating plane was set vertically at an angle of 85° (manipulating the typical body posture during running [131]). Three specimens were examined for each fabric to confirm that the results were repeatable. The average results are discussed in section 3.4.
Section 2	
Objective	To validate the influence of adjustable sweat rate on dynamic liquid moisture management properties of the fabric.

Strategy	The slope of the sweating plane was set fixed at 85°, and the sweat rate was adjusted to 180, 120 and 60 gh^{-1} corresponding to an extremely high (1.5 $Lh^{-1}m^{-2}$), high (1.00 $Lh^{-1}m^{-2}$) and moderate (0.5 $Lh^{-1}m^{-2}$) sweating intensity at human upper back [31, 34, 46]. Three replicates of K3 fabric were tested at each sweat rate, and the average results are reported under section 3.5.
Section 3	
Objective	To validate the influence of slope of sweating plane on dynamic liquid moisture management properties of a fabric.
Strategy	The fabric dynamic liquid moisture management capabilities were tested at two different slopes of the sweating plane, viz. 85° and 65°, corresponding to a typically running and cycling body postures [132-134]. While the liquid supply rate was kept constant at 120 gh^{-1}. Three replicates were tested at each slope, and the results are described in section 3.6. Note: K3 fabric was chosen for experiments in sections 2 and 3 because of the Coolmax fiber's uniform wicking properties and, as a result, excellent reproducibility of results as found in section 1 and shown in Figure 3.11, K9.

3.3.3 Preparation of instrument and execution of test

Prior to testing, calibration of the feeding pump was carried out to ensure the desired perspiration rate of the sweating zone. The pump is equipped with an internal calibration function in which the volume of three consecutive dosages is measured against the set liquid volume and test flow rate. The values are then fed to the pump control panel, which compare and calculate the new values of motor revolutions to match the desired flow rate. The liquid (distilled water being used in current study) was filled in the supply container, and the pump was operated at priming mode to replace the air volume by moving liquid through sweating glands till the liquid emerges from the sweating outlets. The balances were also calibrated against the standard testing weight. The balance data were transmitted to the computer at every 5-second interval, in a comma-separated values (CSV) file format using the WinCT© communication program. After cleaning any liquid drops from the sweating plane, the specimen was placed over it under a precise extension of 10%. The data acquisition was put to start just ahead of loading the whole setup on the bottom weighing balance. Followed by a short interval of getting stability in the balance readings (about 10 min), the pump was turned ON to supply liquid to the fabric. By approaching the end of the set sweating duration, the feeding pump was set to automatically turn OFF. Similarly, the data acquisition from balances was set to auto-stop by completing the test period. The data collected were processed and analysed using Microsoft Excel (Microsoft Office 365) and Origin Lab (2021) software.

3.3.4 Definition, measurements, and calculations

Liquid accumulation

Gravimetric measurements were carried out on *NSS* employing a three-balance weighing system. The liquid supplied, dripped, and evaporated is measured individually by three weighing balances. From the relationship among the weight components of the liquid distribution, the amount of liquid accumulated in the fabric can be determined by Equation 3.1.

$$m_{accu} = m_{supp} - \left(m_{drip} + m_{evap}\right) \qquad (3.1)$$

Where, m_{accu} is liquid accumulated in the fabric, m_{drip} is liquid dripped down from the fabric, m_{evap} is liquid evaporated from the fabric.

The liquid accumulated in the fabric varies dynamically in both P1 and P2. In addition to fabric properties controlling the amount of liquid accumulated, the rate of liquid accumulation will be governed by the real-time rate of liquid supply, evaporation, and discharge.

Liquid evaporation

The mass of liquid evaporated is dynamically measured throughout the test. Hence for any interval of the test period, the average rate of evaporation in gh^{-1} can be found independently by Equation 3.2.

$$\text{Liquid evaporation rate } (gh^{-1}) = \frac{m_{evap}}{t_{evap}} \times 60 \qquad (3.2)$$

Where m_{evap} is the absolute mass of liquid evaporated and t_{evap} is the evaporation time.

Besides, the slope of the evaporation curve can be used to calculate the instantaneous rate of evaporation between any interval of time.

Liquid discharge

In the upright orientation of the sweating plane and fabric specimen placed over it, the liquid tends to flow downward through the fabric if the liquid supplied is sustained. A stage may arrive when the liquid accumulated at the bottom edge may start dripping. However, it should be noted that the onset of dripping is no indication of the maximum saturation capacity of the fabric. The liquid may tend to flow faster downward under the cooperative influence of capillary force and gravity as compared to its lateral and upward movement. The absolute amount of liquid discharge by dripping (m_{drip}) is dynamically measured throughout the test period. However, the dripping would stop after a while the liquid supply has been turned off. For the whole span of dripping the average discharge rate can be found by Equation 3.3.

$$\text{Liquid discharge rate (gh}^{-1}\text{)} = \frac{m_{drip\ P1+P2}}{t_{drip}} \times 60 \qquad (3.3)$$

Where $m_{drip\ P1+P2}$ is the absolute mass of liquid dripped during P1 andP2 and t_{drip} is the dripping time.

Intrinsic evaporation capacity (IEC)

The IEC is the percentage of the liquid evaporated during P1 to the dry mass of the fabric specimen as described in Equation 3.4.

$$\text{IEC} = \frac{m_{evap\ P1}}{m_{fabr}} \times 100 \qquad (3.4)$$

Where $m_{evap\ P1}$ is the mass of liquid evaporated during P1 and m_{fabr} is the initial dry mass of the fabric.

As the total surface area of all the fabric samples is constant, the term intrinsic evaporation capacity is proposed to readily differentiate among lighter and heavier fabric. Because, for sportswear and industrial workwear, lightweight evaporative cooling garments are always preferred to enhance comfort, performance, and productivity, especially in hot and humid environmental conditions.

***Intrinsic accumulation capacity** (IAC)*

IAC is the percentage of the maximum mass of liquid accumulated in the fabric during P1($m_{accu\ \ P1}$) to the initial dry mass of the fabric, as given in Equation 3.5.

$$\text{IAC} = \frac{m_{accu\ P1}}{m_{fabr}} \times 100 \qquad (3.5)$$

When selecting fabrics for evaporative cooling garments, lightweight fabrics with higher liquid accumulation potential could be preferable to attain comparable perspiration management to their heavier and thicker counterparts. Term, IAC is coined to easily distinguish the lightweight and highly absorbent fabrics in comparison.

Drying efficiency

The quick-drying ability of fabrics is highly preferred for enhanced thermo-physiological comfort, performance, and productivity. Consequently, drying efficiency (DE) is expressed as the percentage ratio of the liquid evaporated to the liquid retained in the fabric as described by Equation 3.6.

$$\mathrm{DE} = \frac{m_{evap\ P1+P2}}{(m_{supp\ P1} - m_{drip\ P1+\ P2})} \times 100 \qquad (3.6)$$

Where, $m_{evap\ P1+P2}$ is the total mass of liquid evaporate during P1 and P2,$m_{supp\ P1}$ is the mass of liquid supplied during P1 and $m_{drip\ P1+\ P2}$ is the total mass of liquid dripped during P1 and P2.

3.4 Results and discussion

Effect of fabric properties on liquid moisture management

This section discusses the liquid evaporation, accumulation, and discharge properties of eight fabrics given in Table 3.1. To further highlight the fabric appearance and surface structures, the microscopic images of fabric are shown in Figure 3.3. The one-way analysis of variance (ANOVA) test, at a confidence interval of 95%, was adopted to examine the significant differences in cumulative results of various fabrics.

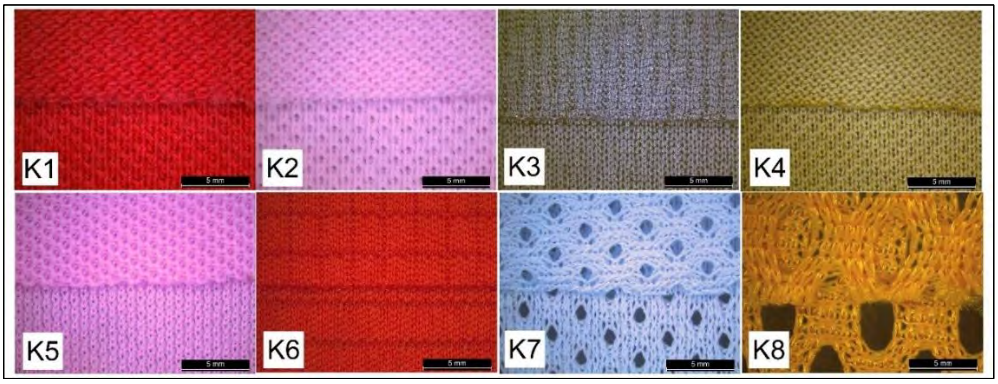

Figure 3.3. Surface structures of fabric.

3.4.1 Liquid evaporation

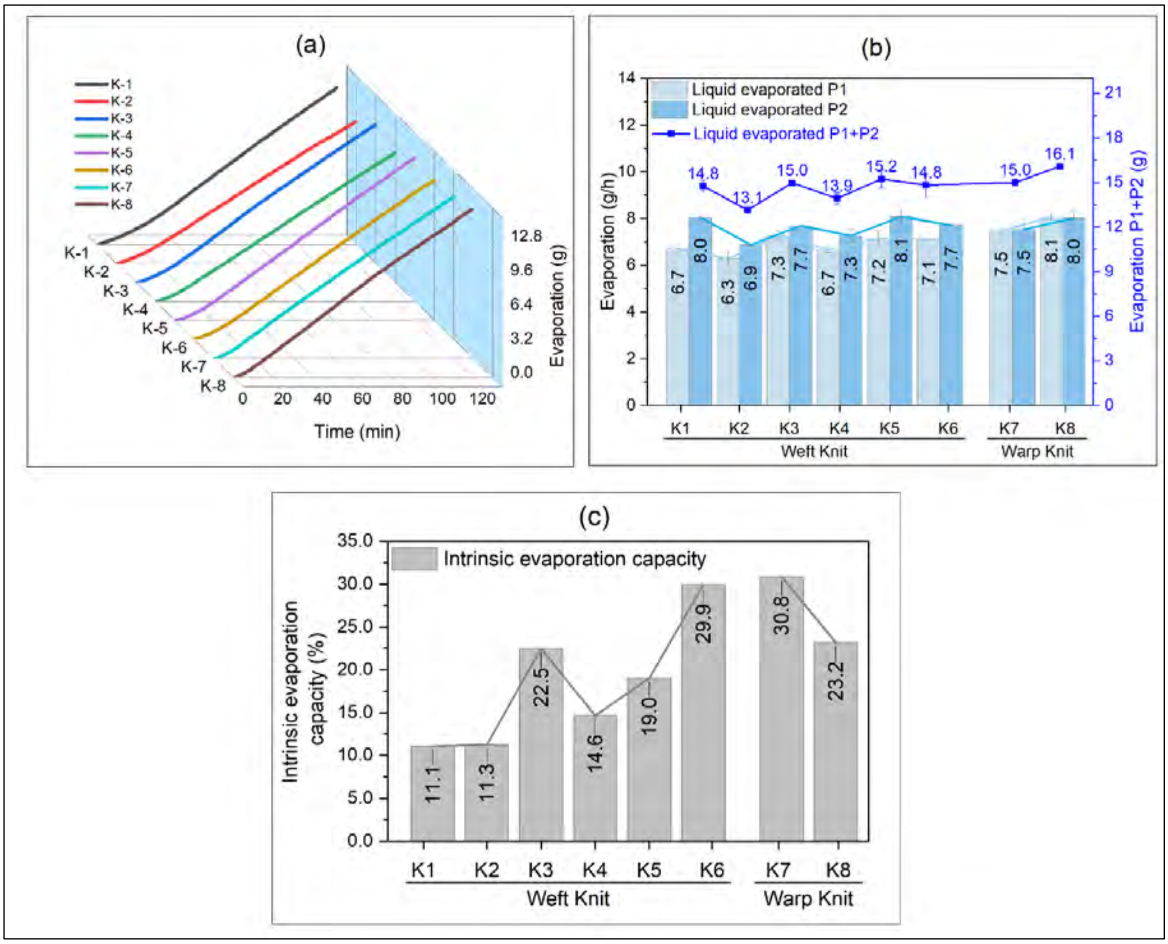

Figure 3.4. Liquid evaporation from fabric. (a): Real-time curves of mean evaporative mass loss over time. (b): The columns bars indicate the mean rate of evaporation during P1 and P2. The line plus symbol plot indicates the mean amount of cumulative liquid evaporated during P1 and P2. The error bars represent the standard deviations. (c) Intrinsic evaporation capacity of fabrics.

Figure 3.4 presets the liquid evaporation performance of fabrics. The real-time increase in evaporation over time is shown in Figure 3.4a. The slope of the evaporation curves can determine the evaporation rate for any given interval of time. The average evaporation rate during P1, P2 and their cumulative results are shown in Figure 3.4b. During P1, the K1 and K2 have shown a relatively lower evaporation rate of 6.7 and 6.3 gh^{-1}. This may be ascribed to the hydrophilic nature of cotton fibres present in these fabrics. The cotton fibres are cellulosic in nature, contain plenty of hydroxyl groups, which offer a strong affinity for water molecules. This may cause high liquid retention in cotton and, as a result, slow liquid transport and release. More importantly, evaporation can also be affected by the surface area of fabric covered by the liquid spreading through each interval of time during P1. A relatively low liquid spread rate in

K1 and K2 due to potential liquid absorption into cotton fibers is likely to reduce their evaporation performance. Because cotton is relatively hydrophobic in K1, a lower initial slope of its evaporation curves during P1 is possible due to the slow-spreading rate of liquid into K1 at this stage.

On the other hand, the K4, though it is pure polyester fabric, its evaporation rate of 6.7 gh^{-1} during P1 is also comparatively lower. The areal density of K4 is relatively higher among all other pure polyester fabrics, as shown in Table 3.1. Because of the dense and compact fabric structure, higher capillary pressure in the narrow capillaries may lead to increase flow resistance. Thus, the volume flow rate is expected to decrease with narrow capillaries, resulting in a lower spread area on the fabric surface. This may explain the relatively lower evaporation rate of K4 during P1. The K3, K5 and K7 have shown almost similar evaporation rates during P1. Although they all are composed of polyester fibre, they differ considerably in the areal density, fibre type, fibre fineness, construction, and gradients of surface roughness. The K3 fabric is a bird eye weft knit fabric composed of a mixture of conventional and profiled polyester fibres (Coolmax). While the K5 is the pique weft knit fabric made of conventional polyester fibres, and K6 is the waffle structure weft knit produced from micro denier polyester fibres. All three fabrics demonstrated quick wetting, wicking, and moisture transporting properties, thus resulting in a relatively higher rate of evaporation. However, the effect of fibre fineness and surface structure did not seem to affect considerably the rate of evaporation from these fabrics.

The warp knit mesh-type fabrics K7 and K8, in contrast, have shown a relatively higher tendency of liquid evaporation during P1. Both fabrics are made up of polyester fibres, with small to large mesh apertures in K7 and K8, respectively (as shown in Figure 3.3). Furthermore, the WCA of these fabrics is negligible, and the drop absorbency test results show their quick wetting and wicking ability, as shown in Table 3.1. It is important to note that the mesh-type construction, introducing plenty of see-through openings in fabric, when fixed on sweating plane, leaves a certain area uncovered that corresponds to the sizes of mesh openings. Additionally, the yarns running along the longitudinal direction of warp knit fabrics are aligned parallel to the gravitational liquid flow through the fabric; therefore, the resistance to liquid flow would be less than the weft knit fabrics.

Consequently, in association with yarn alignment and empty spaces, the liquid supplied in each interval of P1 could move along a larger distance conferring a broader wet area. In addition, the empty apertures of unrestricted airflow offer plenty of localised sites of vapour pressure gradients throughout the warp knit mesh fabric offering additional space for water molecules to release into air. In contrast, the vapour pressure gradient exists in one direction, normal to plane of fabrics, in the case continuous weft knit fabrics. Therefore, the coupling effect of localised vapour pressure gradient and a remarkably broader and faster spreading of liquid on warp knit mesh structure is assumed to promote the evaporation rate right from the early period of P1. As revealed in Figure 3.4 a, the evaporation curves of K7 and K8 are relatively steeper even in the first quarter of P1.

While comparing the rate of evaporation during P2 with that of P1, the K1 has outperformed all other samples. It is important to note that, by the end of P1, the surface area of the fabric covered by the spreading liquid is supposed to reach its maximum. Hence, in the case of K1, the existence of a hydrophobic finish could offer lower surface energy at the exterior of fibres allowing water molecules to escape into the air smoothly. This may explain the enhanced evaporation rate from the hydrophobically treated cotton during P2. Similarly, for remaining weft knit fabrics, the rate of evaporation during P2 is higher than that of P1, which may correspond to the liquid accumulation and maximum spread surface area of liquid in the fabric.

In the case of warp knit fabrics, however, the evaporation rate during P2 was the same as during P1 for K7, but it was somewhat lower for K8 when compared to P1. This could be attributed to the relatively lower amount of liquid accumulation in warp knit fabric (Figure 3.5) and substantially higher drying efficiency (Figure 3.8). Because of the increasing liquid content from top to bottom in the upright orientation of the fabric specimen under testing, the fabric may dry first at the top and then at the bottom. With the increasing drying time, the wet surface area may gradually reduce, lowering the evaporation rate during P2.

The cumulative evaporation for P1 and P2 is also indicated in Figure 3.4b to assess the overall performance of fabrics. The line and symbol plot shows that the hydrophobically treated cotton can provide better evaporation performance than the polyester-cotton blended hydrophilic fabric. Among pure polyester fabrics, the evaporation performance is similar except for K4. While comparing K5 with K4 (because both have the same yarn linear density and denier per filament), a relatively open pique knit structure in K5 can offer better evaporation performance, probably resulting from improved air permeability of the fabric.

Fabric evaporation performance is further assessed in relation to their dry mass, and the results are expressed in terms of intrinsic evaporation capacity, as shown in Figure 3.4c. The intrinsic evaporation capacity is to instantly highlight the fabrics which are lighter in weight and proficient in liquid evaporation. This could help to construct lightweight clothing for efficient sweat management in moderate to high-intensity physical exercises. The results revealed that the K3 and K6 among weft knit and K7 and K8 among warp knit fabrics could provide higher evaporation at a relatively lower fabric weight.

The one-way ANOVA results from Table 3.3 indicates that the fabric differs significantly in cumulative liquid evaporation ($p=0.00<0.05$). A post hoc Tucky test was conducted to identify these significant differences, and the pair-wise results of significance are presented in Table 3.4. The grey cells indicate the significantly differing pairs with a p-value < 0.05. In most cases, it is found that the total amount of liquid evaporated from K2 is significantly different, suggesting that the effect of the hydrophilic nature of cotton on evaporation is significant. In addition, the evaporation of K8-K4 pair is also significantly different ($p=0.001 <0.05$), indicating that the effect of mesh structure on evaporation could also be significant. While in all other pairs, with p-value >0.05, it may reflect that there is no significant effect of fabric areal density, thickness, and surface roughness gradient on the rate of liquid evaporation from fabric.

3.4.2 Liquid accumulation

The liquid accumulation properties of fabrics are illustrated in Figure 3.5. The real-time curves shown in Figure 3.5a, indicate the amount of liquid accumulated in the fabric over time. The phase-wise distribution of the liquid accumulated is presented in Figure 3.5b. The real-time curves show four consecutive stages of liquid accumulation around the whole test. During P1 (from 0-60 min), a linear curve indicates the steady rise of liquid accumulation in fabric, corresponding to the rate of liquid supplied and evaporated. With the onset of liquid dripping form fabric, except for K1 the slopes of the curves for all other fabrics, K2 to K6, tend to decrease quickly, indicating that the liquid accumulation is no more proportional to the rate of liquid supplied. However, a slight elevation of the curve by the end of P1, especially in the case of weft knit fabrics, indicates that accumulation still has been continued but a much slower rate. This is because the length of the specimen extending above the sweating zone allows the liquid accumulated to reach the extended vertical wicking height in the given test duration [6, 59, 135]. The length of the curve prior to bending indicates the period to start dripping, which is predominantly higher for K1 to K3 in the sequence; K1 > K2 > k3. The magnitude of line curvature at the commencement of dripping expresses the rate of change in liquid accumulation mutually decided by the rate of liquid supplied, evaporation and discharge. A large turn in the liquid accumulation curve of K1 amongst P1 suggests that the rate of liquid discharge has been increasing slowly. While in all other weft knit fabrics, the remarkably sharp turns of curves suggest a surge in the rate of liquid discharge causing the rate of liquid accumulation to decrease accordingly. At the end of P1, after the liquid supply has been stopped, a sharp ditch in curves indicates the residual liquid discharge, sustaining for a short interval of time during P2. Followed by the residual dripping, the consistent negative slope of the liquid accumulation curve reflects the drying of fabric at constant rate of evaporation. The considerably short time to start dripping is found in warp knit fabrics indicating a relatively lower liquid accumulation ability of such fabrics. A gentle transition in the rate of liquid accumulation at the onset of dripping in K7 and K8, indicates that the discharge rate at the start is not as fast as appeared in the weft knit fabric of same material.

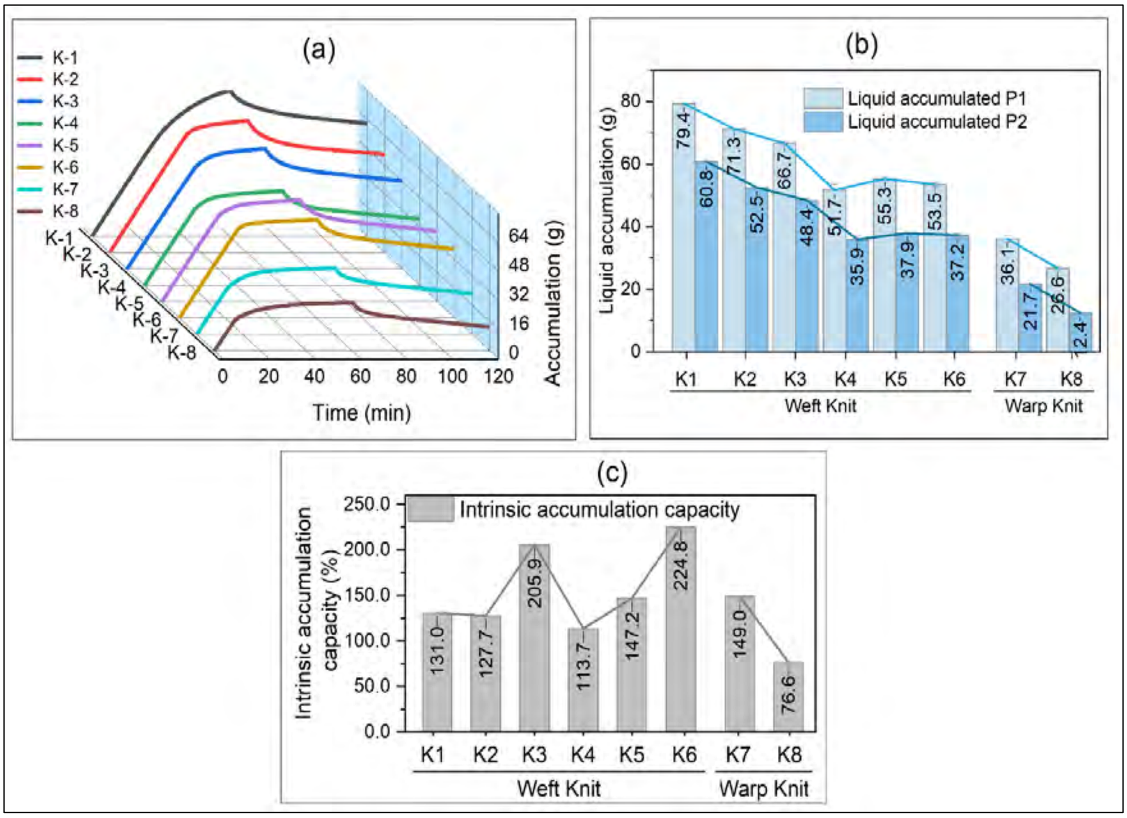

Figure 3.5. Liquid accumulation in fabrics. (a): Real-time curves of mean amount of liquid accumulated over time. (b): The columns bars indicate the mean amount of liquid accumulated during P1 and P2. The line plus symbol plot indicates the mean amount of cumulative liquid accumulated during P1 and P2. The error bars represent the standard deviations. (c): Intrinsic accumulation capacity of fabrics.

The comparative amount of liquid accumulated during P1 and P2 of fabrics is presented in Figure 3.5b. K1, being purely cellulosic in nature, shows the highest amount of liquid accumulation during P1. The second highest amount liquid accumulated in K2 can also be ascribed to the highly absorbent nature of constituent cotton fibres. The third highest liquid accumulation is found in K3. Even though K3 is entirely made of polyester fibers, the presence of profiled fibers may increase the fabric's specific surface area, resulting in greater liquid accumulation when compared to other polyester fabrics.[2, 3] Among other weft knit polyester fabrics, K4, K5 and K6 have shown similar amount of liquid accumulation despite widely varying in their areal density (K4=183.84 gm^{-2}, K5=151.87 gm^{-2}, K6=96.13 gm^{-2}). Since K4 and K5, both are made of same kind of yarn (100D/96F polyester), a relatively lower accumulation in K4 is expected due to its relatively compact structure induced by higher areal density. K6, on the other hand, is made up of micro denier polyester fibres (50D/72F), which also provide a higher specific surface area [136]. As a result, though the K6 has a lower areal density than K4 and K5, it accumulates a comparable amount of liquid. Overall, warp knit fabrics with a sequence of K7 > K8 show less liquid accumulation. The lowest accumulation in K8 may arise from its large size of mesh apertures (Figure 3.3) and apparently coarser yarn count (The yarn specifications are not kwon for K8 fabric). The amount of liquid accumulated by the end of P2 is also shown in Figure 3.5b, which is determined by the total amount of liquid discharged and evaporated by the end of P2.

IAC as described by Equation 3.5 is given in Figure 3.5c. K6 has the highest value of IAC followed by K3. Both K3 and K6 are made up of specialised fibres which tend to provide large surface area for higher liquid accumulation. Thus, the lightweight fabrics with superior IAC values can be easily identified and chosen to develop the lightweight but high-performance moisture management garments.

The one ANOVA findings (Table 3.3) show that the liquid accumulated P2 of various fabrics differs significantly ($p=0.000 < 0.05$). Table 3.4 shows that, except for K4 to K6, all other fabrics are significantly different in terms of liquid accumulation. The fact that $p > 0.05$ for K4 to K6 indicates that neither areal density nor the fabric thickness (Table 3.1) has a significant effect on liquid accumulation. Instead, it might be the nature of fibre constituents that decisively governs the amount liquid accumulation in fabrics.

Table 3.3. One-way ANOVA for cumulative liquid evaporation, discharge, and accumulation

Source	**DF**	**Adj. SS**	**Adj. MS**	**F-Value**	**P-Value**

Liquid evaporation P1+P2	7	16.099	2.2999	9.45	0.000
Liquid accumulation P2	7	5295.07	756.438	1109.14	0.000
Liquid discharge P1+P2	7	4968.01	709.715	1044.43	0.000

Table 3.4. Tukey simultaneous test for difference of means

Parameters	Liquid evaporation P1+P2	Liquid accumulated P2	Liquid discharge P1+P2
Difference of Levels	Adjusted P-Value	Adjusted P-Value	Adjusted P-Value
K2 - K1	0.018	0.000	0.000
K3 - K1	0.999	0.000	0.000
K4 - K1	0.470	0.000	0.000
K5 - K1	0.925	0.000	0.000
K6 - K1	1.000	0.000	0.000
K7 - K1	0.998	0.000	0.000
K8 - K1	0.070	0.000	0.000
K3 - K2	0.006	0.000	0.055
K4 - K2	0.557	0.000	0.000
K5 - K2	0.002	0.000	0.000
K6 - K2	0.013	0.000	0.000
K7 - K2	0.006	0.000	0.000
K8 - K2	0.000	0.000	0.000
K4 - K3	0.220	0.000	0.000
K5 - K3	0.997	0.000	0.000
K6 - K3	1.000	0.000	0.000
K7 - K3	1.000	0.000	0.000
K8 - K3	0.182	0.000	0.000
K5 - K4	0.073	0.109	0.003
K6 - K4	0.377	0.527	0.065
K7 - K4	0.200	0.000	0.000
K8 - K4	0.001	0.000	0.000
K6 - K5	0.966	0.956	0.705
K7 - K5	0.999	0.000	0.000
K8 - K5	0.459	0.000	0.000
K7 - K6	1.000	0.000	0.000
K8 - K6	0.097	0.000	0.000
K8 - K7	0.200	0.000	0.000

3.4.3 Liquid discharge

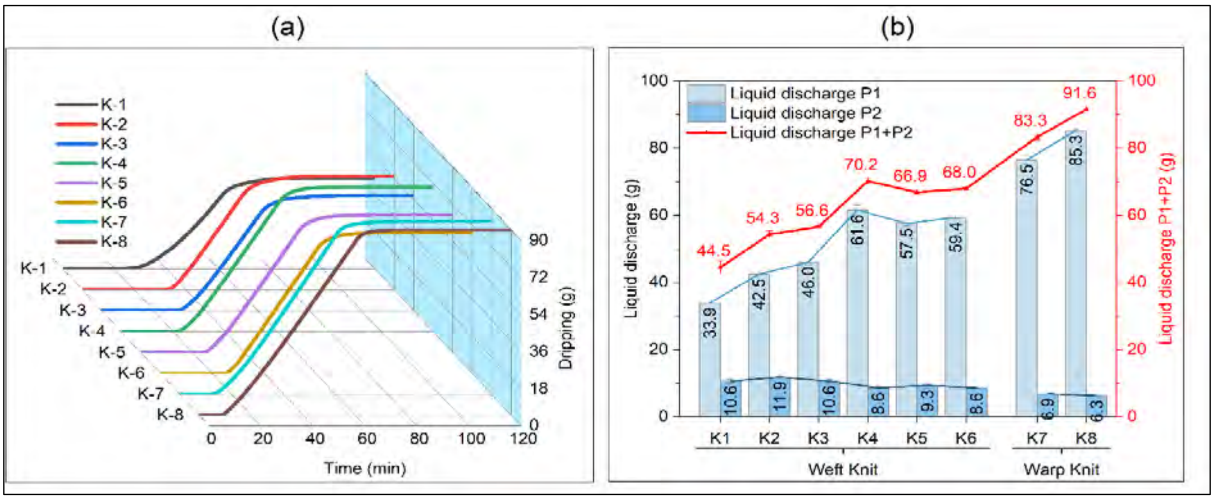

Figure 3.6. Liquid discharge from fabric. (a): Real-time curves of mean liquid discharged over time. (b): The columns bars indicate the average amount of liquid discharge during P1 and P2. The line plus symbol plot indicates the mean amount of cumulative liquid discharged during P1 and P2. The error bars represent the standard deviations.

Because of continuous sweating during P1, the area covered by liquid in fabric keeps on growing with time. The image of a fabric wet area shown in Figure 3.2, reveals that the growing amount of liquid may tends to flow faster in downward direction. As a result of the rate of liquid supplied, rate of evaporation, liquid permeability, and accumulation in fabric, a stage may occur during P1 when the liquid approaches the bottom edge. The upward and lateral capillary forces at the edge cause the incoming liquid to spread along and above the edge until the edge becomes supersaturated and liquid dripping begins.

The liquid discharge properties of the fabric are presented in Figure 3.6. The amount of liquid discharged over time is shown by the real-time curves in Figure 3.6 a. During P1, from 0 to 60 min, a segment of the flat curve indicates a period of no dripping. Afterwards, the almost steeper rise of curves represents a continuous liquid discharge by dripping. During P2, from 60 to 120min, the curves again tend to become flat, representing termination of liquid discharge followed by the end of liquid supply during P1. A sharp curve at the junction of P1 and P2 reflects the rapid fall in the dripping rate. During P1, among all other fabrics, except for K1, the linearity of curves indicates a constant rate of liquid discharge that may correspond to the constant rate of liquid supplied. However, in K1, the rate of liquid discharge is not as consistent as in other fabrics. This could be explained based on the higher rate of liquid absorption and a possibly lower rate of liquid transport through the pure cotton fabric. Cotton fibres are also prone to swelling due to liquid absorption, probably adding to the liquid flow resistance through the fabric. A progressively increasing area of saturation, on the other hand, could result in a gradually increasing liquid permeability through the fabric, as indicated by the increasing slope of the curve in the latter quarter of P1 [13]. However, after P1, the gentle shift in liquid discharge rate of cotton incorporated fabrics, K1 and K2, is illustrated by a somewhat large curvature of curves, suggesting a relatively slow and extended residual liquid dripping during P2. While the curves for all polyester-based weft knit fabrics, K3 to K6, show a reasonably significant decline in the rate of residual liquid discharge after P1. Similarly, the warp knit fabrics, K7 and K8, have demonstrated more quicker liquid discharge at the end of P1, as seen by the sharp turns of their curves at that time.

The relative distribution of liquid discharge during P1 and P2 and their cumulative liquid discharge are presented in Figure 3.6b. According to the results, the more liquid discharged during P1, the less during P2. When comparing phase-wise distributions, the liquid discharge of K1 to K3, compared to other fabrics is lower during P1. However, their residual discharge during P2 is greater. This could be due to the large amount of liquid accumulated in these fabrics, which was mostly achieved by cotton fibers in K1 and K2 and profiled polyester fibers in K3. On the other hand, with a small difference, a similar amount of liquid has been discharged from the other weft knit fabrics, K4 to K6, both during P1 and P2, which may correspond to their similar amount of liquid accumulation during P1, (Figure 3.5b). Similarly, the warp mesh knit fabrics, K7 and K8, have demonstrated the highest amount of liquid discharged due to their rapid liquid transport and low liquid accumulation potential. Overall, the liquid discharge through the fabric appears to be substantially impacted by the raw material, composition, and construction properties of the fabric.

Figure 3.7 depicts the mean discharge rate for the entire discharge duration, as well as the discharge span of various fabrics, to gain a clearer understanding of the liquid discharge characteristics of different fabrics. What stands out in Figure 3.7a is that the K4 and K8 fabrics have similar rates of liquid discharge, i.e., 76.3 gh^{-1} and 76.1 gh^{-1}, respectively. However, their discharge spans vary greatly. It is also worth noting that the commencement of the discharge span in mesh knits, K7 and K8, fabrics is approached earlier compared to other fabrics.

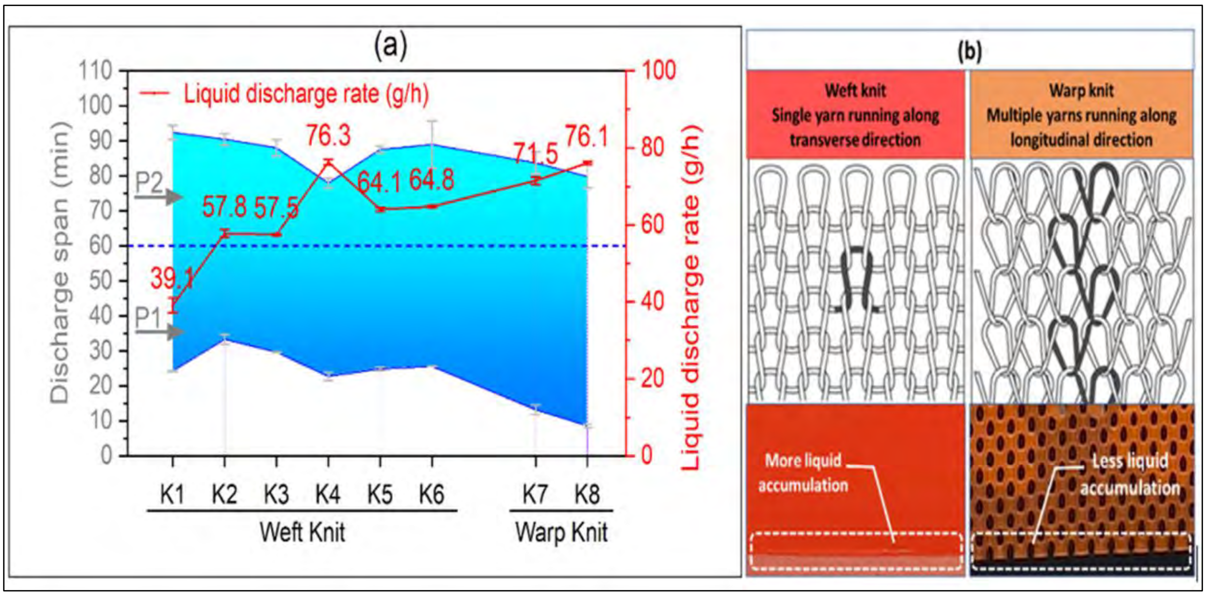

Figure 3.7. The discharge span of liquid and rate of discharge from different kinds of fabrics. (a) The shaded area represents the span of liquid discharge on the left y-axis. The lower and upper boundaries correspond to the time of dripping start and stops, respectively. While the reference line in the middle separates the P1 and P2. The line plus symbol plot correspond to the right y-axis and indicates the rate of discharge (gh^{-1}). The error bars represent the standard deviation. (b): The schematic of knit constructions and real images of warp and weft knit fabrics at their bottom edge.

To explain such difference in discharge onset, the fabric bottom edges of a warp knit (K8) and a typical weft knit fabrics are shown in Figure 3.7b. In the case of weft knit fabric, a dense layer of liquid accumulates at the fabric bottom edge before the dripping of liquid commences. The yarns that run down the fabric edge may formulate a network of inter-fibre and intra-yarn capillaries, allowing a large amount of liquid to be held. The smooth edge and perpendicular yarn arrangement to the direction of liquid flow through the fabric could result in dense pooling of liquid over the edge. As a result, as illustrated in Figure 3.7b, an image on the left, the liquid arriving at the edge of a weft knit fabric would spread and accumulates over it, forming a thickened layer. Because of the increased liquid collection along the edge, the surface tension of the liquid tends to rise. Consequently, the water molecules at the lowest bottom edge may be attracted by strong adhesive and cohesive forces until the weight of the accumulated liquid overcomes the surface tension and dripping occurs. Therefore, it is possible to realise a delayed onset of liquid dripping from weft knit fabrics.

In contrast, as illustrated in Figure 3.7b, a photograph on the right-hand side, the fabric bottom edge of warp knit fabric is not as smooth as in weft knit fabrics, due to the cut line passing through consecutive mesh openings. Furthermore, the yarns, which typically run along the length of warp knit fabric, are also trimmed at the edge. The irregular pattern and discontinuous yarn capillaries at the edge of warp knit fabric, prevent the large amount of liquid accumulation. Consequently, the warp knit fabrics caused an early onset of dripping during P1 and a rapid release of residual liquid dripping during P2.

Interestingly, a relatively low discharge rate and the longest discharge span of K1 fabric is probably due to the hydrophilic core and hydrophobic surface characteristics of cotton fibres in K1. As a result, the water above the surface can move quickly, whereas the water absorbed into cores would suffer a slow transport and release. Compared to K1, the higher discharge rate and shorter discharge span appears in K2, which means, the presence of polyester fibre along with hydrophilic cotton is found to enhance the water transport through polyester-cotton blended fabrics.

The remarkably different behaviour of K4 versus K5 fabric is probably due to its compact structure having an overall lower percentage of air voids than K5 (despite they share the same yarn specifications and resultant fabric thickness). Therefore, for a given rate of liquid supply, an early saturation may result in faster permeability of liquid in K4, so that an early dripping onset can occur [13]. Similarly, when the liquid supply to K4 is cut off, the higher permeability would also confer faster liquid draining. Besides, another possibility of enhanced liquid permeability in such surface-treated polyester fabrics may also lie in the poor stability of hydrophilic finishing against the applied sweating intensity. In this regard, a compact knit fabric like K4 might be more affected because, as anticipated by Laplace equation, higher capillary pursuer generated in narrow capillaries could force the liquid to move much faster [137].

The liquid surface tension and permeability could explain the onset and termination of liquid discharge from the fabric bottom edge. As the capillary pressure tends to reduce in the region of fabric saturation, the gravity-induced rise in liquid permeability could result in a growing amount of liquid at the bottom edge [13]. A stage arrives when the liquid gathered at the edge may attain a certain weight to overcome the liquid surface tension and falls apart [100]. The gradual loss of liquid accumulated at the bottom edge reduces the surface tension, allowing even smaller liquid drops to escape. However, as the saturation fades again during P2, the capillary forces reactivate, pulling the liquid back into the fabric and terminating the liquid discharge. The higher the amount of liquid accumulated during P1, the longer it may take to fade the saturation during P2, resulting in higher residual dripping during P2. Because warp knits accumulate less liquid than other fabrics during P1, their residual liquid discharge during P2 is also lower.

The one ANOVA results (Table 3.3) shows that the cumulative liquid discharge differs significantly among various fabrics (p=0.000<0.05). The pair-wise comparison in Table 3.4 shows that most fabrics have significantly different liquid discharge amounts, except for the following pairs: K2-K3 (p=0.05), K4-K6 (0.065) and K5-K6 (0.705). Since Coolmax fibres in K3 and micro denier polyester fibres in K6 causes more liquid to accumulate, despite significant differences in their structures, areal densities and thickness, their liquid discharge does not remain significantly different. In all other pairs, the P-value <0.05 suggests that the characteristic of fabric material, composition, and construction significantly affects the liquid transport and discharge.

3.4.4 Drying efficiency

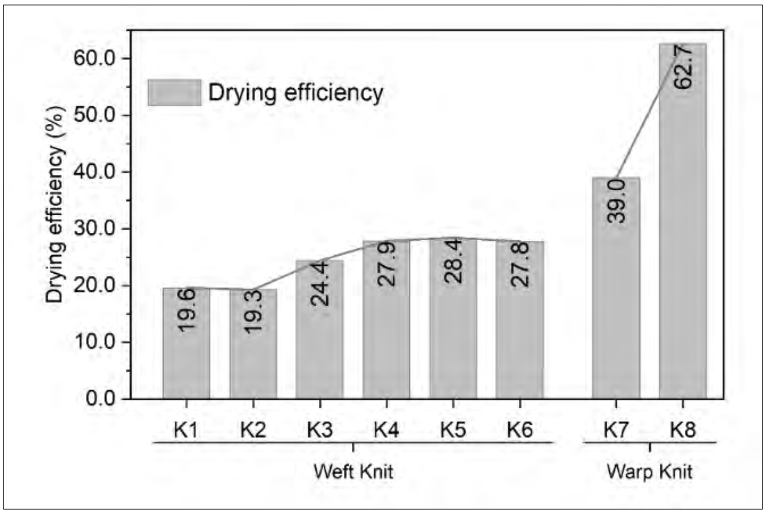

Figure 3.8. Drying efficiency of fabrics.

The drying efficiency of fabrics, as calculated by Equation 3.6, is given in Figure 3.8. It is evident that the highest drying efficiency, 62.7% and 39.0% of K8 and K7, respectively, corresponds to the warp knit polyester fabrics. Because warp knit fabrics have proved to show better overall evaporation performance and less liquid accumulation, the higher drying efficiency can be expected [138, 139]. Among weft knit fabrics, the drying efficiency of cotton-based fabrics, K1 and K2, is lower (K1=19.6%, K2=19.3%), suggesting that a large amount of liquid has been accumulated. Since the hydroxyl groups in cotton fibres tend to confine the water molecules, the slow liquid transport and release increase the drying time.

Among weft knit, the almost similar drying efficiency of K4 to K6correspond to their similar liquid accumulation and evaporation behaviour as revealed in Figure 3.5b and Figure 3.4b. On the other hand, a slightly lower drying efficiency of K3 could be attributed to the large amount of Coolmax fibers in its composition showing the higher liquid accumulation potential. Compared to K1 and K2, unlike cotton, there are no typical boding sites on conventional polyester fibres. As a result, any hydrophilic surface treatment applied to polyester fibres results in faster liquid transport and drainage. Consequently, polyester-based weft knit fabrics have a better drying efficiency than k1 and K2, implying that drying will be completed reasonably quickly. Until the fabrics differ greatly in liquid evaporation, the key to quick-drying is the reduced amount of liquid accumulation, which is also supported by the cotton Wicking Windows ™ and TransDRY® moisture management technologies [88].

3.5 Validation of liquid supplied rate on liquid distribution properties of fabrics

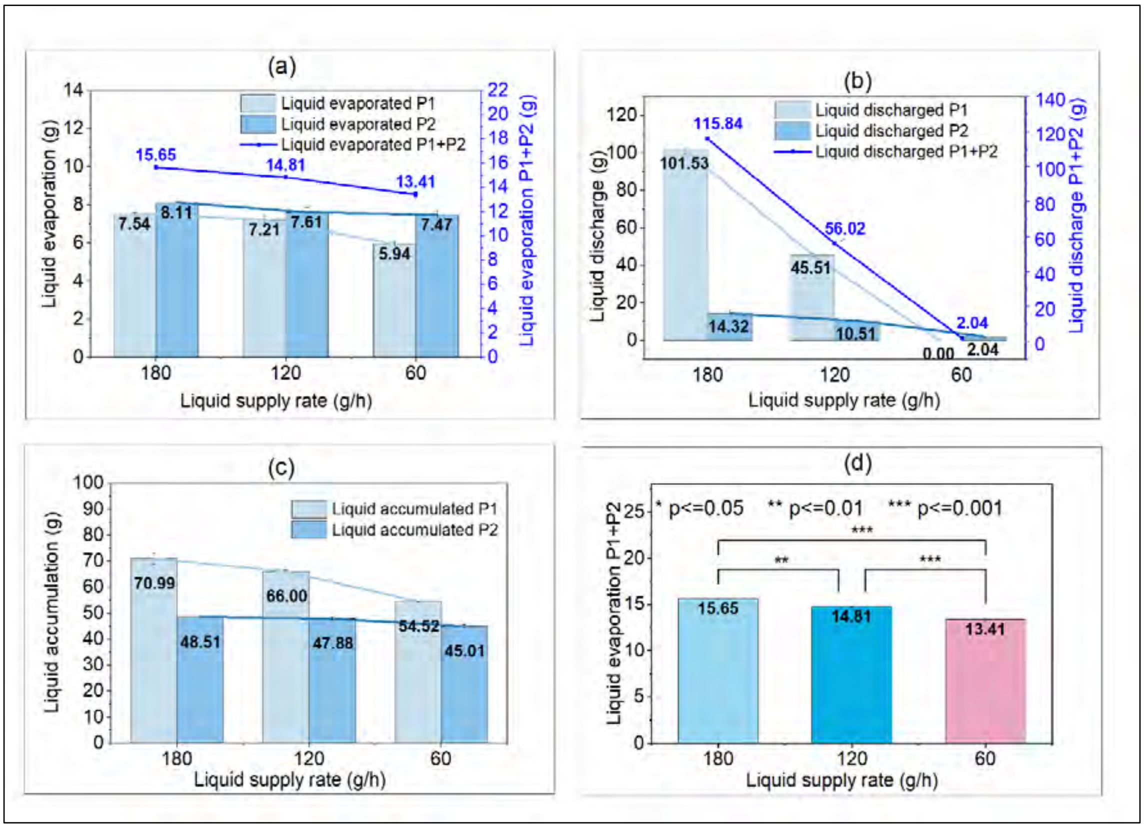

Figure 3.9. Validation of liquid supply rate on liquid evaporation, accumulation, and discharge from fabric. (a): Liquid accumulation versus liquid supply rate. (b): Liquid discharge versus liquid supply rate. (c): Liquid accumulation versus liquid supply rate. (d) Significance of difference in mean evaporation determined by one way ANOVA.

The adjustable liquid supplied rate of *NSS* was validated at three different supply rates of 180, 120 and 60 gh^{-1}, arbitrarily representing an extremely high, moderate, and lower sweating intensity. Three replicates of the same fabric were tested at each liquid supply rate, and the results are given in Figure 3.9. The comparison of mean evaporation during P1, P2 and cumulative of P1 and P2 from Figure 3.9a reveals that a higher supply rate tends to cause higher liquid evaporation (Liquid evaporation P1+P2: 15.65g @ 180 gh^{-1} > 14.81g @ 120 gh^{-1} > 13.41g @ 60 gh^{-1}). This is rather convincing as a relatively larger surface area of fabric is expected to be covered by faster liquid transport through the fabric at a higher rate of liquid supplied during P1. Similarly, by the end of P1, the maximum wetted area of fabric could also be higher. Consequently, higher liquid evaporation is expected at a higher liquid supply rate. As illustrated in Figure 3.9b, the comparative amount of liquid discharge during P1 confirms that the higher supply rate has caused a big volume flow rate through the fabric. At 60 gh^{-1}, the lowest liquid discharge of 2.04 g is observed only during P2. The amount of liquid discharge, on the other hand, has increased significantly from 56.02g to 115.84 g, equivalent to the supply rate of 120 gh^{-1} and 180 gh^{-1}, respectively. In the same way, from Figure 3.9c, the amount of liquid accumulated in the fabric is also observed to increase with the increase in liquid supply rate, indicating the resultant spread area would also be greater to enhance evaporation. In Figure 3.9d, the one-way ANOVA results, performed at 95% confidence intervals, suggest that the effect of liquid supply rate is significant on cumulative liquid evaporation from fabric.

3.6 Validation of inclination of sweating plane on liquid distribution properties of fabrics

The inclination of the sweating plane of *NSS* is validated at 85° and 65°, corresponding to an almost straight and lean body posture. Three replicates of the same fabric were tested on each slope at a constant liquid supply rate of 120 gh^{-1}, and the results are illustrated in Figure 3.10. It can be seen from Figure 3.10 a that phase-wise, as well as cumulative liquid evaporation, is relatively higher at a lean position of 65° slope. Additionally, liquid accumulation during P1 and P2, as shown in Figure 3.10b, is higher at 65°slope, so the liquid discharge is relatively lower (Figure 3.10c). While changing the slope from 85° to 65°, resultant increase in liquid accumulation and decrease in liquid discharge suggest that the liquid spreading in upward and lateral directions of fabric has been promoted. In addition, the relative influence of the gravitational component on the downflow of liquid would also be reduced at a lower inclination. As a result, progressively increasing wet area of the fabric is about to enhance evaporation. Moreover, at a 65° slope, the possibly enhanced exposure of fabric to air currents from the roof-mounted air-conditioners and intensity of the roof lights could have an added effect on increasing evaporation. In Figure 3.10d, the independent t-test results are plotted, showing that the effect of the slope on the cumulative amount of liquid evaporated is highly significant.

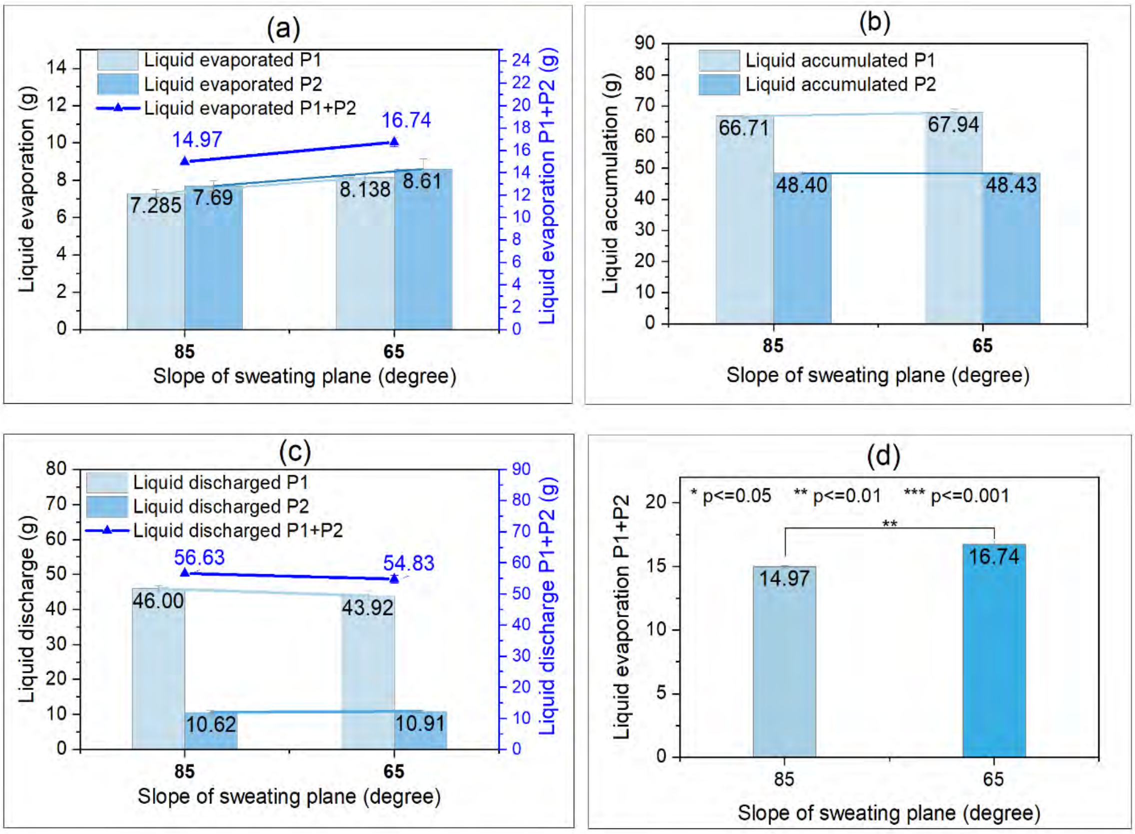

Figure 3.10. Validation of sweating plane inclination on liquid evaporation, accumulation, and discharge from fabric

3.7 Reproducibility, uncertainty, and accuracy of measurements

The most sensitive measurement by NSS is the mass of liquid evaporated, measured throughout the test by the bottom scale. In addition, the rate of liquid evaporation is also very sensitive to changes in temperature and humidity of the testing room atmosphere. Therefore, the reproducibility of the results was verified by testing three specimens for each fabric and comparing the total mass of liquid evaporated in each test. For each fabric, K1 to K8, the real-time evaporation curve for each test of three repeats is shown in Figure 3.11. The coefficient of variation (CV) and uncertainty also known as standard error (SE) (as measured by; $SE = S.D/\sqrt{N}$, where S.D is the standard deviation, and N is the number of test repeats) are provided in Figure 3.11 (K9) for the mean mass of liquid evaporated. The identical trends of evaporation curves in K1 to K8, the values of SE < 0.50g, and CV <6.0%, as shown in K9, validate the good reproducibility of the results. In the case of the highest value of CV (5.6%) and SE (0.48g) observed in K6, the curves of two tests, K6-1and K6-3, were highly reproducible while K6-2 lagged in evaporation. When the root cause was investigated, it was discovered to be a relative rise in ambient relative humidity from 66.5 % to 69.6 % during this test.

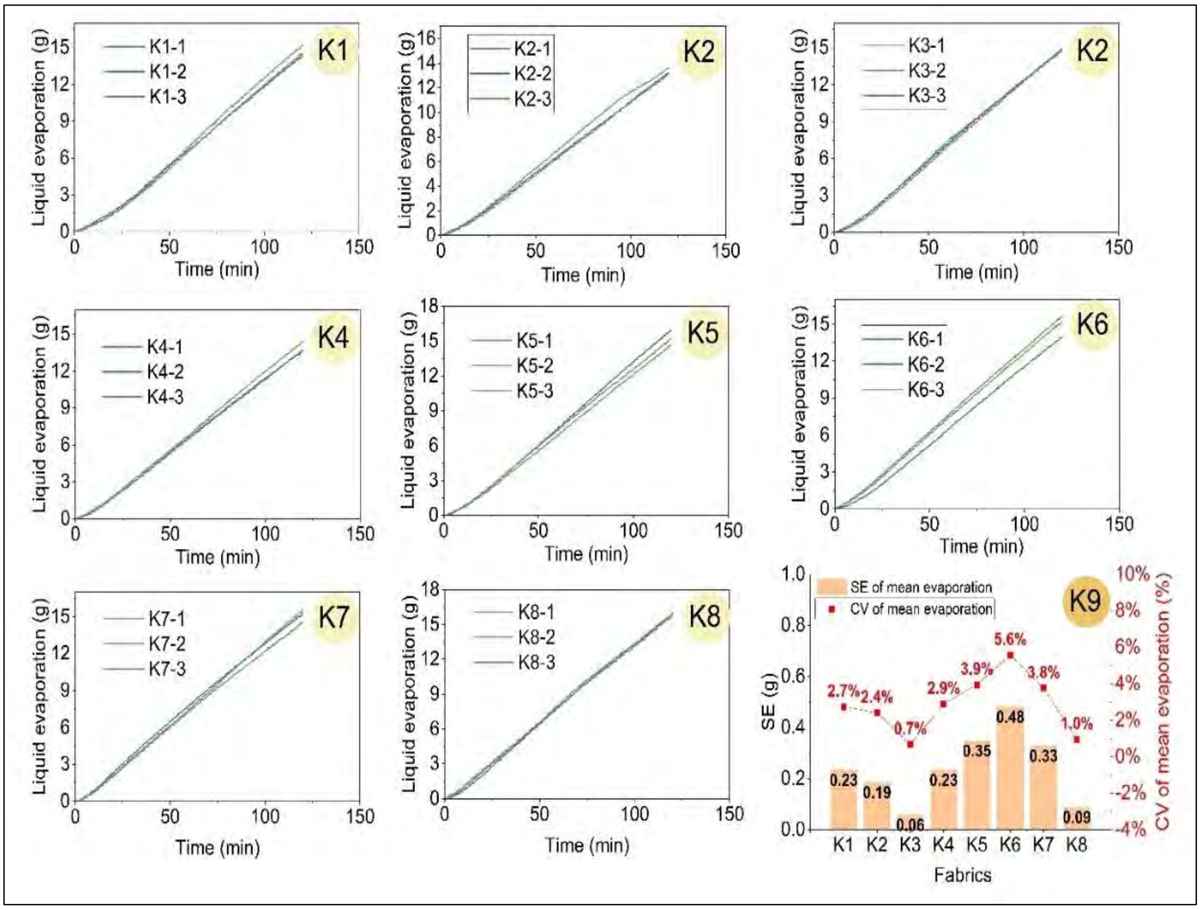

Figure 3.11. Reproducibility of results for the mean mass of liquid evaporation, K1-K8. CV and SE of mean evaporation, K9.

As the evaporation is immediately affected by the change in ambient conditions, the liquid dripped and accumulated may also vary accordingly. Besides, variations in results may also occur due to inconsistencies in sample size, fabric composition, and structural properties, fabric moisture management treatments, manual handling operations, amount of liquid supplied, as well as drift and linearity errors of weighing system. Therefore, to confirm the accurate working of the weighing system comprising of three balances, the sum of the liquid evaporated, dripped, and accumulated is verified against the known value of liquid supplied (Equation 3.7).

$$m_{acuu} + m_{drip} + m_{evap} = m_{supp} \quad (3.7)$$

Where, m_{supp}, m_{drip} and m_{evap} are measured directly by three weighing balances, while the m_{acuu} is determined from the difference between the initial dry mass and the wet mass of the fabric at the end of the test. The discrepancy in the total mass of liquid accumulated, dripped, and evaporated to the mass of liquid supplied is described in terms of "Error percentage" as shown in Equation 3.8.

$$Error\ \% = \frac{m_{supp} - (m_{acuu} + m_{drip} + m_{evap})}{m_{supp}} * 100 \qquad (3.8)$$

Thus, the "accuracy percentage" can be found by Equation 3.9.

$$Accuracy\ \% = 100 - Error\ \% \qquad (3.9)$$

The measurement accuracy of twelve different tests was randomly verified as described above, and the histogram of accuracy is shown in Figure 3.12. In 75% of tests, the accuracy percentage is higher than 99%, and for the remaining 25% of tests, the score is above 98%, which is also acceptable.

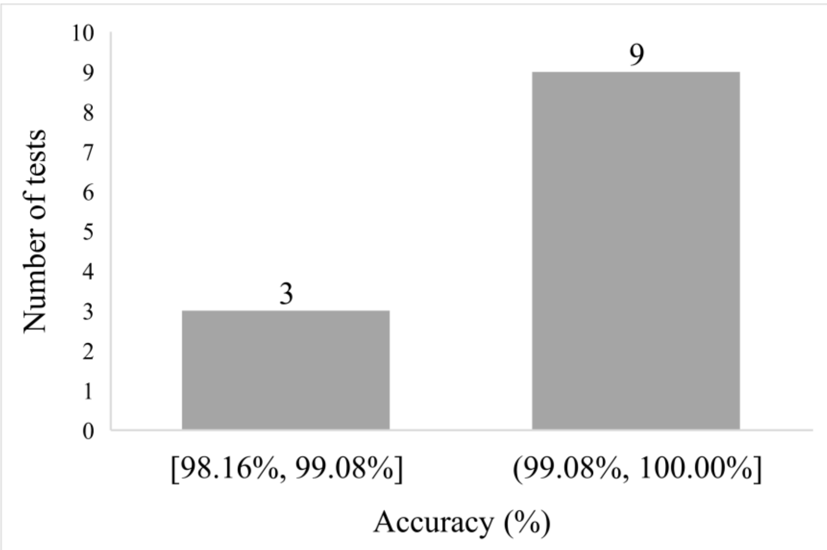

Figure 3.12. Measurement accuracy of the instrument.

3.8 Conclusions

The purpose of this article was to present a new instrument for evaluating the fabric dynamic liquid moisture management properties by simulating a fabric-sweating skin interaction and adjustable body posture. Based on the gravimetric measurement principle of *NSS*, subjected to a specific sweating intensity, the fabric dynamic liquid accumulation, evaporation, discharge, and drying properties can be measured simultaneously in one test. Furthermore, liquid wetting, wicking, spreading, and transporting through fabric can all be observed at the same time. Moreover, fabric intrinsic accumulation capacity and intrinsic evaporation capacity can also be investigated, which are essential to the development of lightweight and high-performance moisture management apparel. Eight different types of moisture management fabrics were tested on NSS, and the results were quite useful in differentiating the fabric unique specifications. Some cotton-based fabrics showed higher liquid accumulation, lower liquid discharge and evaporation performance. Nonetheless, in a pure cotton fabric with a relatively hydrophobic surface, the evaporation rate was low at first but increased gradually afterward. The evaporation performance of polyester-based weft knit fabrics with different knit designs was found to be comparable. However, their ability to store and discharge liquid was discovered to be affected significantly by constituent fibre specifications and fabric density. The warp knit mesh type fabrics excelled all other fabrics in terms of evaporation and quick-drying ability. The sweating intensity and slope of the sweating plane were found to have significant effects on fabric liquid moisture distribution properties. The measurement system accuracy was investigated in terms of the agreement between the cumulative mass of liquid evaporated, dripped, and accumulated and the known mass of liquid supplied. The measurement accuracy ranged from 98 to 100 percent, with the majority of tests exceeding 99 percent. Measuring the mass of liquid evaporated was reasonably reproducible, with a maximum coefficient of variation being less than 6%.

Chapter 4

Further instrumentation and evaluation of fabric liquid and moisture management performance at simulated skin and sweat temperatures

4.1 Introduction

For functional apparel, especially sportswear and activewear, the liquid and moisture management properties of the fabrics, namely their ability in sweat absorption, distribution, evaporation, draining and drying, are critical to wear comfort and performance. Such properties should be measured for quality evaluation and product development.

Despite a great deal of research developed on measuring the fabric liquid transport properties, some critical aspect of fabric liquid and moisture management remains unexplored to what extent, with increasing liquid content in the fabric, the strength of capillary forces changes affecting the downflow rate of liquid. Similarly, the fabric's post-sweating drying properties are critical to wet-thermal comfort as well as controlling the post-exercise chilling effect and should be measured during a drying phase immediately following the sweating phase.

Existing instruments or measurement techniques, however, are unable to simulate the profuse sweating and drying phases consecutively in order to measure the concurrent and real-time liquid moisture management and drying abilities of fabrics in a more practical scenario. In most existing bench scale instruments, the continuous sweating process, the varying sweating rate, the temperature of skin and sweat, and the orientation of the fabric on the body cannot be fully simulated and the measurements of sweat accumulation, spreading, evaporation, dripping and drying, cannot be obtained simultaneously.

Though the non-temperature control version of NSS reported in Chapter 3 can measure the fabric liquid and moisture management properties, including evaporation, draining and drying, concurrently and in real-time, the measurements were not taken under the simulated skin and sweat temperatures. In addition, the system could not characterize the fabric in-plane multidirectional flow of liquid under the simulated sweating condition. It was envisioned that a new version of NSS offering simulated skin and sweat temperature control along with potential of measuring multidirectional flow rates can reveal more insights.

4.2 Design, construction, and operation of NSS

The NSS was designed and developed to measure the fabric rates of liquid accumulation, evaporation, dripping and drying simultaneously in addition to examining the transport rate of liquid through the fabric in upward, lateral, and downward directions at the given rate of sweating. The schematic diagram of the instrument is shown in Figure 4.1.

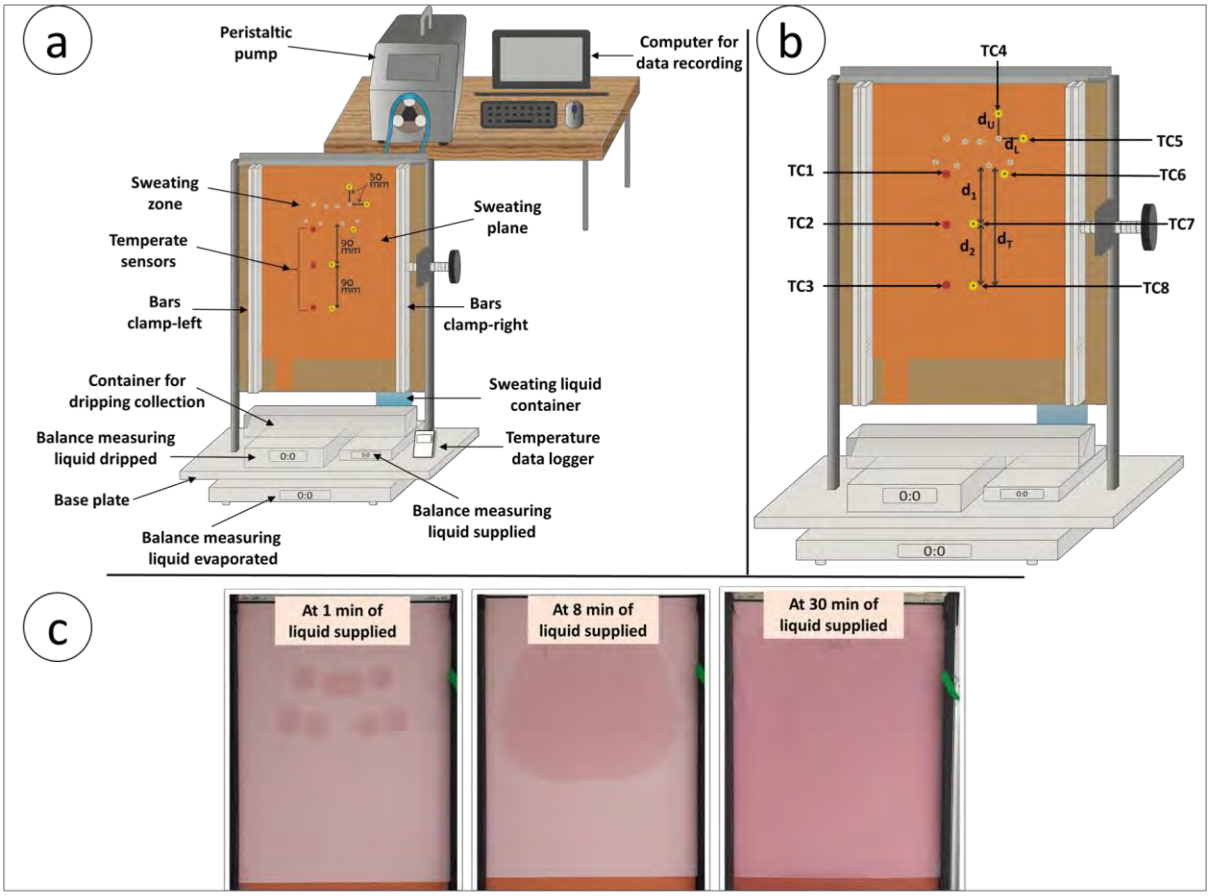

Figure 4.1. (a) Schematic diagram of NSS; (b) Temperature sensors arrangement for temperature monitoring and regulation; (c) Typical spreading pattern of liquid on the fabric under testing.

NSS employed three calibrated electronic measuring balances to accurately measure the amount of liquid supplied, dripped, and evaporated over time. The fabrics' dynamic rates of liquid accumulation, evaporation, dripping and drying can be determined from the data retrieved by three balances. The detailed description of the NSS construction, methodology, operations, and weight measuring principle has been explained in Chapter 3. Herein, the strategy used to regulate sweat and sweating plane temperature, as well as measure the multidimensional liquid flow rate and changing rate of liquid downflow with increasing liquid content, will be discussed in detail. The sweating plane of NSS was further equipped with temperature sensors (k-type thermocouples, ETA, TT-K-30, 260 degrees, wire diameter: 0.25mm) to monitor and regulate the surface temperature of the sweating plane at the average sweating skin temperature. Fig. 1b summarized the arrangement of temperature sensors for the sweating plane temperature regulation and monitoring. The typical spreading style of liquid into a moisture management fabric as observed on NSS is shown in Fig. 1c, which reflects that the wetting area expands over time eventually wetting the entire sample. The liquid evaporation from fabric tends to decrease the temperature of the sweating plane under the wet area of the fabric by a magnitude defined by the temperature difference between the sweating plane and the testing room environment. In order to study the fabric liquid evaporation and drying properties at a simulated sweating skin temperature, the temperature of the sweating plane was regulated by a Proportional-Integral-Derivative (PID) temperature controller. It should be noted that the heating panel that controls the temperature of the sweating plane was made up of a single heating element. Therefore, upon activation of temperature regulation, the temperature of the whole sweating panel changes equally. Consequently, the temperature under the dry and wet area of the fabric, as indicated in Fig. 1c at 8 min of liquid supplied, cannot be regulated independently.

In order to control the temperature of the wet area of the sweating plane, which should closely simulate the sweating skin temperature, instead of using single-point temperature control, the temperatures at three critical locations are monitored using three temperature sensors and their average is fed into PID to regulate the sweating plane temperature. The temperature of the sweating plane becomes uniform once all three points are covered by the expanding wet area of the fabric. From Fig. 1b, the average response of three temperature sensors TC1-TC3 was used by the PID temperature controller to regulate the sweating plane temperature at 36±1.5 °C. As sweating begins, the spreading liquid into the fabric triggers a temperature drop by evaporation first at TC1. The decrease in average temperature, in turn, activates the PID to regulate the average temperature of the sweating plane accordingly, as a result, TC2 and TC3 will undergo a rise in temperature. It was found that the temperature rises under the dry area of fabric was momentary and dropped immediately as approached by the growing wet area of liquid in the fabric. Once all three temperature sensors TC1-TC3 are covered under the wet area, as indicated in Fig. 1c on the extreme right position, the temperature of the sweating plane under the whole wet area becomes identical. Another set of three temperature sensors TC6-TC8 was used to cross-check and record the average temperature of the sweating plane throughout the test using a temperature recorder (Anbai, AT4208)

To simulate the sweat conditions, a thermostatic water bath equipped with a PID temperature controller was used to regulate the temperature of the sweating liquid at 35±1 °C. In addition, to prevent the sudden drop of liquid temperature while passing through the pump head, the whole path of liquid movement, from the thermostatic water bath to the sweating outlets, was additionally insulated and heated by integrating a flexible heating element running along the pump tubing. To achieve the desired sweat temperature, the temperature of the thermostatic water bath and that of heating element in the path of the liquid transport are adjusted appropriately through preliminary trials. A temperature sensor was fixed in one of the sweating outlets to constantly monitor and record the temperature of the sweating liquid in sweating intervals.

4.2.1 Measurement of liquid accumulation, dripping and drying by the gravimetric measuring principle:

The mass related parameters of liquid and moisture management like liquid evaporation, liquid accumulation, liquid dripped, IEC, IAC were measured according to the relations explained earlier in Chapter 3. Herein, the DE has been redefined by Equation 4.1.

$$\text{DE} = \frac{m_{evap\ P2}}{m_{reta}} \times 100 \qquad (4.1)$$

Where, $m_{evap\ P2}$ is the mass of liquid evaporated during P2 and m_{reta} is the mass of liquid retained in the fabric described by the mass of liquid accumulated in the fabric by the end of P1 minus the mass of liquid dripped during P2 as given by Equation 4.2.

$$m_{reta} = (m_{accu\ P1} - m_{drip\ P2}) \qquad (4.2)$$

It is possible that some liquid dripping may occur during P2 after the liquid supply is turned off at the end of P1. Since any amount of liquid dripped from the fabric does not contribute to evaporation, the DE is determined by the percentage of the liquid evaporated during P2 from the liquid retained in the fabric. It is worth noting that while the DE for some fabrics during P2 may reach 100%, the drying rates and drying times of such fabrics cannot be distinguished by DE. Therefore, the drying rates and calculated drying times of fabrics were additionally measured.

The drying rate (g/min) of fabric was determined from the slope of the liquid accumulation curve during P2 according to Equation 4.3.

$$\text{Drying rate} = (-1) \times (\text{Slope of the linear region of liquid accumulation curve during P2}) \quad (4.3)$$

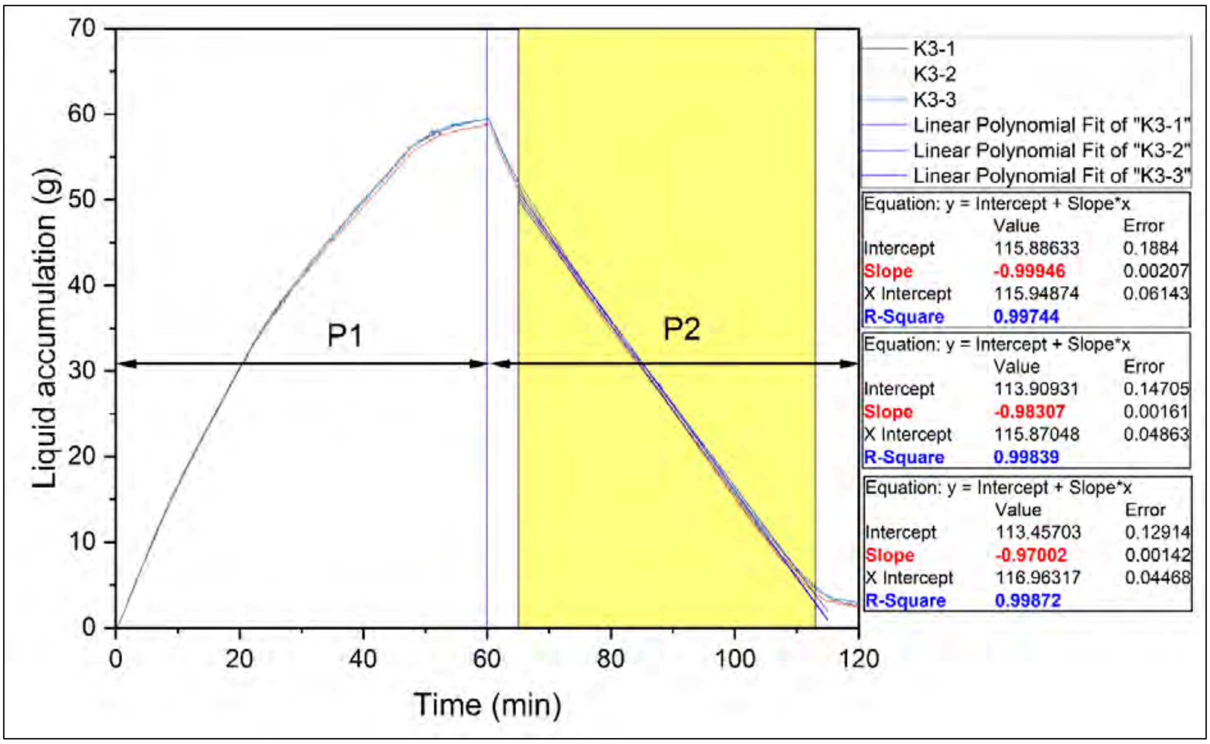

Figure 4.2. Calculation of drying rate from liquid accumulation curve during P2. The selected area under the yellow box is used to calculate the slope of the curve. The data in the right-side boxes show the slope and coefficient of determination for each curve.

Figure 4.2 represents three real-time liquid accumulation curves produced by three repeated tests of a fabric K-3 on NSS (K-3 just taken as an example). The slopes of the curves during P1 represent the weight gain by the liquid accumulation in fabric versus time, while the slopes of the curves during P2 represent the weight loss by liquid dripping and evaporation from fabric versus time. The weight loss may be accelerated at the start of P2 by trailing dripping of liquid from the fabric, but after that, it solely depends on the rate of liquid evaporation. It is evident from Figure 4.2, that after about 10 minutes of liquid dripping during P2, the curves become almost linear indicating the constant rate of drying. Therefore, to prevent the effect of liquid dripping on the calculation of the drying rates, linear regression was applied in the selected linear regions as highlighted by the yellow box. The results of linear fitting for three tests are shown in the side boxes, where the "slopes" representing the drying rates (g/min) are marked red and the coefficient of determination R^2 are marked blue. In each test, the value of R^2 >0.99 implies that the fabric dried at a constant rate of drying in the selected region. It must be noted that the drying on NSS is taking place at the simulated skin temperature in an upright position. A significant amount of excess liquid may accumulate at the fabric's bottom edge, causing the drying rate to decrease significantly while the edge is drying. The phenomenon is visible in Figure 4.2 at the later stage of P2, where the accumulation curves appear to flatten over time. The average drying rates and calculated drying times of fabric are further discussed in section 4.3 under "Drying rates and calculated drying times of fabrics."

The calculated drying time (min) of the test fabric was measured according to Equation 4.4.

$$\text{Drying time} = \frac{m_{reta}}{Drying\ rate} \qquad (4.4)$$

4.2.2 Measurement of upward, lateral, and downward liquid flow rates.

The fabric in-plane directional liquid flow rates are measured by detecting temperature variations at the moving liquid front through the fabric. Once the liquid supply is activated, the liquid spreads into the fabric around each sweating outlet. The temperature of fabric tends to drop because of liquid evaporation under wet state. The temperature change at the liquid front flowing into the fabric is recorded by temperature sensors placed at fixed distances around the sweating outlets. After sweating begins, the temperature change at the certain temperature sensor such as TC4, TC5, TC7 and TC8 indicate the time required by the liquid front to travel the distance between the sweating outlets and the temperature sensor. Because the liquid has the potential to spread into the fabric in all directions around the sweating zone, the flow rates of liquid into the fabric at the given rate of sweating (liquid supplied) were measured in terms of upward flow rate (UFR), lateral flow rate (LFR), and downward flow rates (DFRs) for ease of understanding and analysis. For estimation of vertical and lateral flow rates, TC4 and TC5 were fixed respectively, at a distance of 50mm apart around a common sweating opening as shown in Figure 4.1b. The relative difference in upward and lateral flow rates measured concurrently was found to be useful in determining the natural wicking tendency of liquid along a specific direction of the fabric. The UFR and LFR can be calculated according to Equations 4.5 and 4.6.

$$UFR = {d_U}/{t_4} \qquad (4.5)$$

$$LFR = {d_L}/{t_5} \qquad (4.6)$$

Where d_U is the vertical distance of 50mm and t_4 is the time taken by liquid to reach the TC4. Similarly, d_L is 50mm lateral distance and t_5 is the time taken by liquid to reach TC5.

Since the fabric sample is tested in an upright direction on NSS, the increasing liquid content in the fabric would tend to flow downward over time. Therefore, it is crucial to evaluate the fabric moisture management ability i.e., stability of capillary forces and wicking consistency against the increasing sweat load in the downward direction. Because, in case of poor wicking ability, the fabric may get saturated quickly beneath the sweating zone, and a swift increase in liquid permeability through fabric may occur. Keeping in view, the DFRs were measured over two consecutive distances below the sweating zone viz, d_1=90mm and d_2=90mm as shown in Figure 4.1b. TC7 monitors the time interval t_7 for liquid flow over d_1 while TC8 examines the time interval t_8 for liquid flow over d_1+d_2= d_t=180mm. The downward flow rates over d_1 and d_2 can be calculated by Equations 4.7 and 4.8.

$$DFR_{d1} = {d_1}/{t_7} \tag{4.7}$$

$$DFR_{d2} = {d_2}/{t_8 - t_7} \tag{4.8}$$

The relative difference of DFR_{d1} and DFR_{d2} helps in determining whether the fabric capillary pressure is high enough to sustain the downward capillary flow rate of liquid with increasing liquid content, or if the liquid permeability, the flow rate of liquid through the fabric, would tend to increase over time. A positive value of relative percentage difference between DFR_{d1} and DFR_{d2} indicates the increase in liquid permeability, and the magnitude of the value indicates the extent of the increase. Conversely, the zero or negative value of relative percentage difference would imply the presence of strong capillary forces and robust wicking potential of the fabric against increasing liquid content. The presence of stable and higher capillary pressure in the fabric would cause more liquid to accumulate in the whole fabric, making it suitable for long lasting evaporative cooling effects.

4.3 Experimental section

Eight commercial moisture management fabrics reported in Chapter 3 were utilized again. Hereby, Table 4.1 recall the fabric physical characteristics to facilitate the result and discussion of measurements made at new version of NSS. Tests were conducted under controlled environmental conditions of 20±1 °C temperature, 66±2.5% relative humidity (RH) and an air velocity of 0.1 to 0.3 m/s. The sweating plane inclination was adjusted vertically at 85°. The distilled water was to simulate the sweating liquid and sweating rate was set at 120±1 gh^{-1}. The average temperature of sweating plane and sweating liquid was controlled at 36±1.5 °C and 35±1 °C respectively. The temperatures of the sweating plane and sweating liquid were continuously recorded at a sampling rate of $1s^{-1}$.

The tested specimen was fixed on the sweating plane delicately with the specimen carrying template. A constant extension of 5mm was applied to each specimen. Immediately after the test specimen was fixed, the instrument load measuring system was set into operation. The data from each balance were collected and recorded for every 5-second interval. In each test, a 30-minute loading period was provided before sweating to stabilise balance readings and temperature of sweating plane and specimen. Each test consisted of two phases with one hour of continuous sweating in phase 1 (P1) and one hour of continuous drying in phase 2 (P2). Three specimens of each fabric were tested, and the data were analysed for the average and standard deviations to check that the reproducible of results. The data collected were processed and analysed using Microsoft Excel (Microsoft Office 365) and Origin Lab (2021) software.

Table 4.1. Physical specifications and wetting parameters of fabrics

Code	Knit type	Fibre/Yarn specifications (denier)	Composition	Areal density (gm^{-2})	WPI/ CPI	Thickness (mm)	Absorbency (sec)	WCA
K1	Pique-weft knit	253D	100% Cotton	244.97	27/51	0.66	60+	87±0.82
K2	Pique-weft knit	253D	65% PES/35% CO	225.41	28/50	0.62	<1	N.A.
K3	Bird eye-weft knit	75D/72F	45% PES/55% CM,	130.94	44/50	0.40	<1	N.A.
K4	Pique-weft knit	100D/96F	100% PES,	183.84	40/57	0.36	<1	N.A.
K5	Pique-weft knit	100D/96F	100% PES,	151.87	36/46	0.36	<1	N.A.
K6	Waffle-weft knit	50D/72F	100% PES,	96.13	57/52	0.20	<1	N.A.
K7	Small mesh-warp	75D/72F	100% PES,	97.90	35/30	0.22	<1	N.A.

	Knit								
K8	Large mesh-warp knit	Un known	100% PES	140.6	22/21	0.32	1-3	N.A.	
Note: - D: Denier, F: Number of filaments, PES: Polyester, CO: Cotton, CM: Coolmax®, WPI: Wales per inch, CPI: Courses per inch, WCA: Water contact angle									

4.4 Reproducibility and accuracy of measurement

4.4.1 Reproducibility of weight measurements

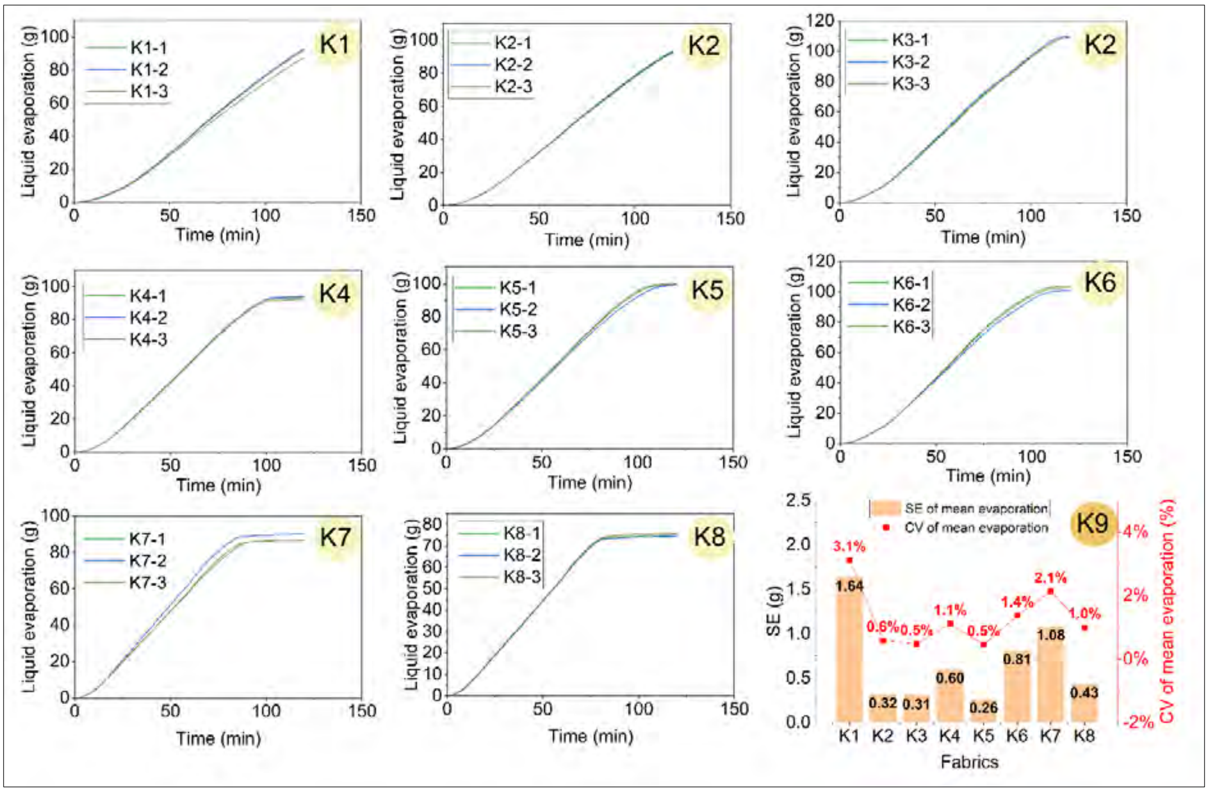

Figure 4.3. Reproducibility of liquid evaporation over time

The reproducible and accurate measurement of liquid evaporation from fabrics at the simulated sweat and sweating skin temperature is the key measurement of NSS. This is because the evaporation of the liquid is measured throughout the whole test and is more sensitive to variations in set temperatures, ambient conditions, sampling variations and irregularities in the instrument's operations. Therefore, three replicates of each fabric were tested, and the reproducibility of results was investigated in terms of replicability of real-time evaporation curves, coefficient of variation and standard error (uncertainty) of mean values. The real-time evaporation curves for three repeats of each fabric, K1 to K8, are presented in Figure 4.3. The identical shapes and replicating curves of three tests in each fabric confirm the high reproducibility of dynamic liquid evaporation measurements by NSS. Similarly, the highest observed value of CV=3.1% and SE=1.64 validate that the average measurements of liquid evaporation from repeated tests are highly reproducible.

The weight measuring system of NSS is comprised of three balances which produce measurements for the amount of liquid supplied, dripped, and evaporated independently. Because all liquid supplied into the fabric is distributed in the form of liquid evaporation, accumulation, and/or dripping from the fabric, the sum of the liquid evaporated, accumulated, and dripped was verified against the known mass of liquid supplied as described by Equation 4.9 to check the accuracy of system measurements.

$$m_{acuu} + m_{drip} + m_{evap} = m_{supp} \tag{4.9}$$

Where, m_{supp}, m_{drip} and m_{evap} are measured directly by three weighing balances, while the m_{acuu} is determined from the weight difference between dry and wet fabric at the end test. Any relative difference between the mass of liquid supplied and distributed would yield an error. The error percentage ($Error$ %) was determined by Equation 4.10.

$$Error\ \% = \frac{m_{supp} - (m_{acuu} + m_{drip} + m_{evap})}{m_{supp}} * 100 \tag{4.10}$$

While the “accuracy percentage” ($Accuracy$ %) was measured according to Equation 4.11.

$$Accuracy\ \% = 100 - Error\ \% \tag{4.11}$$

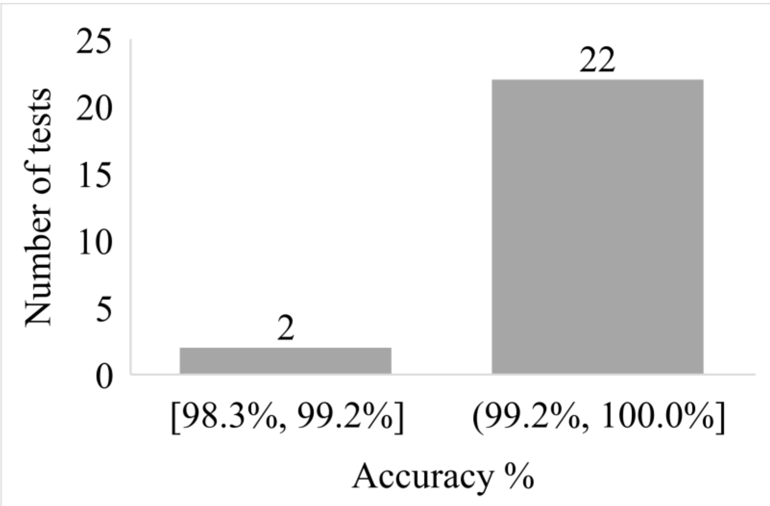

Figure 4.4. Measurement accuracy percentage of the instrument.

The $Accuracy$ % of all 24 tests (8 fabrics x 3 repeats of each fabric) was investigated and presented in Figure 4.4. In 22 tests out of 24, the $Accuracy$ % was observed above 99%. While in the remaining 2 tests, the $Accuracy$ % was even higher than 98%, which was also good enough.

4.4.2 Reproducibility of NSS sweating plane and sweat temperatures

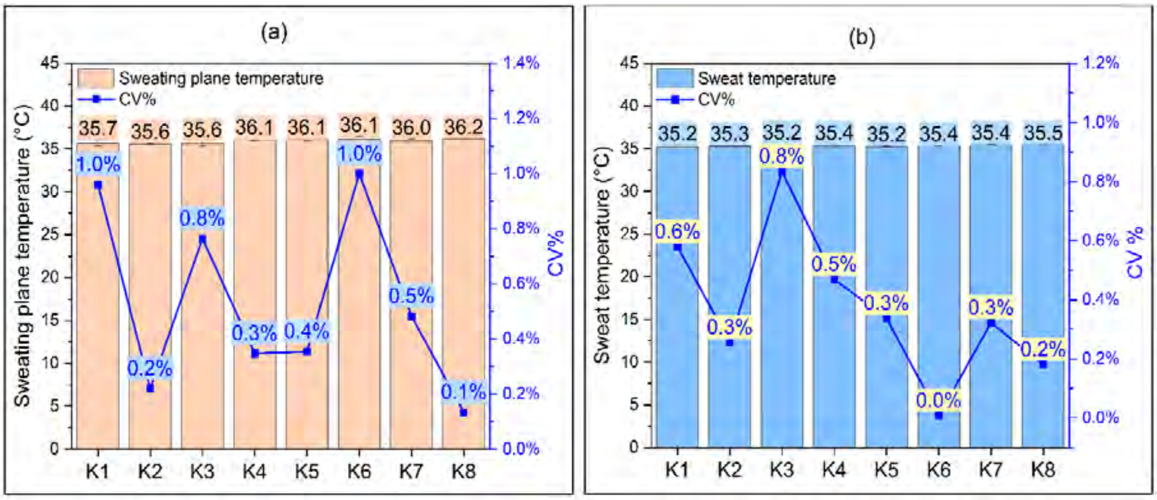

Figure 4.5. Reproducibility of sweating plane and sweat temperature

The average sweating plane temperature during P1 and P2 and the average sweat temperature during P1 are presented in Figures 4.5a and 4.5b respectively. Temperatures were recorded throughout the test, and the average of three repeats is plotted in column bars, with error bars indicating the standard deviation. A line-symbol plot is also used to show the temperature coefficient of variation (CV) for three repeats of each test. The average sweating plane temperature (simulated skin temperature) varies slightly from fabric to fabric with a maximum temperature CV of 1%. Similarly, for three repeats of each fabric, the average sweat temperature was found to be very consistent, ranging between 35.2°C and 35.5°C, with a CV of less than 1%. The reproducibility of simulated skin and sweat temperatures on NSS is confirmed by these identical results from the PID temperature control functions of NSS. As a result, the NSS measurements of liquid evaporation, as shown in Figure 4.3, are also found to be very consistent and reproducible in each fabric.

4.5 Results and discussion

This section discusses the fabric liquid evaporation, accumulation, dripping and drying properties of eight diverse kinds of fabrics as presented in Table 4.1 The absolute average values and their standard deviations were measured and reported for each phase of the test.

4.5.1 Liquid evaporation

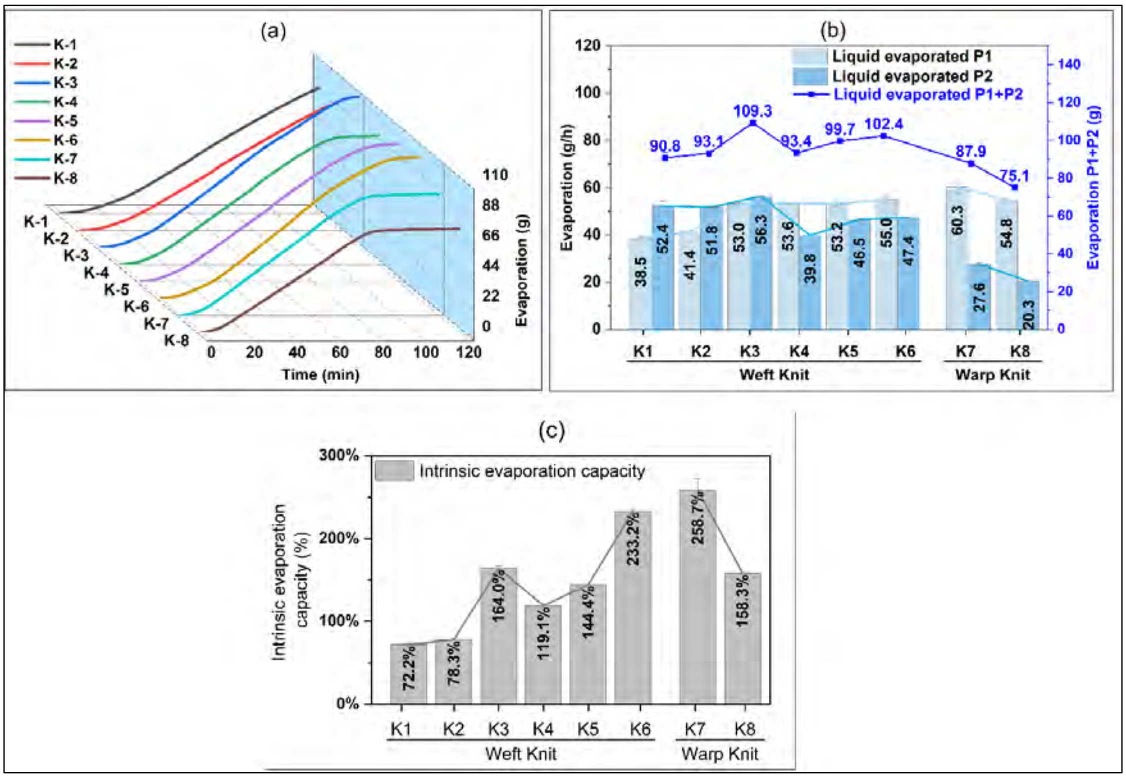

Figure 4.6. Liquid evaporation from fabric. (a): Real-time evaporation curves. (b): Average mass of liquid evaporated during P1 and P2 is indicated by column bars. The cumulative mass of liquid evaporated during P1+P2 is indicated by a line plot. The error bars represent the standard deviations.

The liquid evaporation results are summarized in Figure 4.6. The real-time evaporation curves in Figure 4.6a indicate the mass of liquid evaporated versus time. The slopes of curves at any given interval of time determine the rate of evaporation. The careful examination of real-time curves reveals that the rate of liquid evaporation is slow at the start of P1, gradually increases over P1, and finally tends to fall during P2. The rate of increase in evaporation is relatively much slower in K1 and K2 and much faster in K7 and K8. From K3 to K6 the rise in the rate of evaporation during P1 appears to be identical. The differences in liquid evaporation rates during P1 can be attributed primarily to the composition and construction of knit fabrics. K1 is made up of pure cotton while K2 comprised 35% of cotton and 65% of polyester fibres. Cotton fibre is inherently hydrophilic and tends to absorb and retain a large amount of water in it. The water molecules being polar are bounded at the polar sites (OH^{-1}) in the cellulose of cotton fibre. Moreover, cotton fibre has a hollow lumen structure in its core, which promotes liquid absorption and slows liquid spread through the fabric. Consequently, the wet area relatively grows slowly in pure cotton or cotton mix fabrics because of which the rate of evaporation is observed to increase slowly in K1 and K2.

On the other hand, K3 to K8 are all composed of pure polyester fibres. The standard moisture regain of polyester fibre is 0.4% and it does not tend to absorb liquid into the cores of the fibres. Generally, polyester fabrics are made moisture management by their hydrophilic surface treatment which promotes the liquid wetting and spreading at the surface of fibres. As a result, in polyester fabrics, the relatively increasing rate of evaporation at an early stage during P1 may result from their faster spreading rate of liquid. The comparatively much faster increase in evaporation rate was observed in K7 and K8, which may be due to their warp knit mesh construction. The yarn running parallel along the length of the warp knit fabric, combined with the see-through mesh opening, might speed up the rate of liquid transport through the fabric. The wider the size and greater the number of mesh openings, the smaller the area of the fabric traversed by the liquid. As a result, the liquid spreads much faster on warp knit mesh fabrics, and K7 and K8 exhibit higher evaporation at the start of P1.

The evaporation tendency is seen to decrease in comparison to P1 during P2, terminating more quickly in K7 and K8, somewhat later in K4, K5 and K6, much later in K3, and remaining almost constant in K1 and K2. This is because the presence of water in the fabric is necessary for evaporation to continue. To maintain evaporation, the K1 and K2 may absorb and contain water for a longer period. The K3 fabric is primarily composed of Coolmax® fibre, which increases liquid accumulation due to its multichannel surface and large specific area. Among K4 to K6, the yarn count and areal density of fabric K4 are relatively higher (Table 4.1) which may result in greater packing density resulting in a relative decrease in the liquid accumulation during P1 and liquid evaporation during P2. In K5 and K6 the decrease in the rate of evaporation appears later than in K4 and starts decreasing at an identical time which may indicate the similar amount of liquid accumulated in them. Despite the remarkable lower areal density and thickness of K6 compared to K5, the higher specific area induced by micro denier polyester fibres in K6 may cause comparable liquid accumulation in K6. The sharply decreasing rate of evaporation in K7 and K8 is attributed to their remarkably lower liquid accumulation capacity (Figures 4.7b and 4.7c).

The average rate of liquid evaporation in each phase is presented in Figure 4.6b. Comparing the amount of liquid evaporated during P1 vs P2, it can be evaluated that all pure polyester fabrics, K3 to K8, have demonstrated a relatively higher amount of liquid evaporated during P1 ranging between 53 to 60.3 gh^{-1}. K8 outperformed the others, achieving 60.3 gh^{-1}, followed by K6 (55.0 gh^{-1}), K8 (54.8 gh^{-1}), K4 (53.6 gh^{-1}), K5 (53.2 gh^{-1}), and K3 (53.0 gh^{-1}). In comparison, pure cotton and cotton mixed fabrics, K1 and K2, demonstrated a limited potential for liquid evaporation during P1 with 38.5 gh^{-1} and 41.8 gh^{-1}, respectively. However, when compared to P1, there was a significant increase in the amount of liquid evaporated during P2 for K1 and K2. Similarly, K3 also exhibited a slight increase of liquid evaporated during P2. Nonetheless, among all remaining fabrics, K4 to K8, the liquid evaporated during P2 was significantly reduced when compared to P1, with the difference being especially pronounced in K7 and K8. The increase or decrease in liquid evaporated during P2 among the various fabrics studied can be explained conclusively by the following rule: "the more liquid accumulated in a fabric during P1, the longer it will continue liquid evaporation during P2." Therefore, the liquid evaporated during P2 was observed higher among K1 to K3, with K3 outperforming at 56.3 gh^{-1} followed by K1 at 52.4 gh^{-1} and K2 at 51.8 gh^{-1}. The total amount of liquid evaporated during P1+P2 may indicate the overall performance of the fabrics' liquid evaporation, and the test fabrics may be ranked in the following order; K6 > K5 > K4 > K2 > K1 > K7 > K8.

Figure 4.6c shows the IEC values of fabrics, which distinguish the lightweight fabrics with the highest potential for liquid evaporation during P1 in the following order: K7>K6>K3>K8 >K5>K4 >K2>K1. The fabrics K1, K2, and K4 fabrics are comparatively thicker and heavier, whereas K6 and K8 are thinner and lighter (Table 4.1).

4.5.2 Liquid accumulation

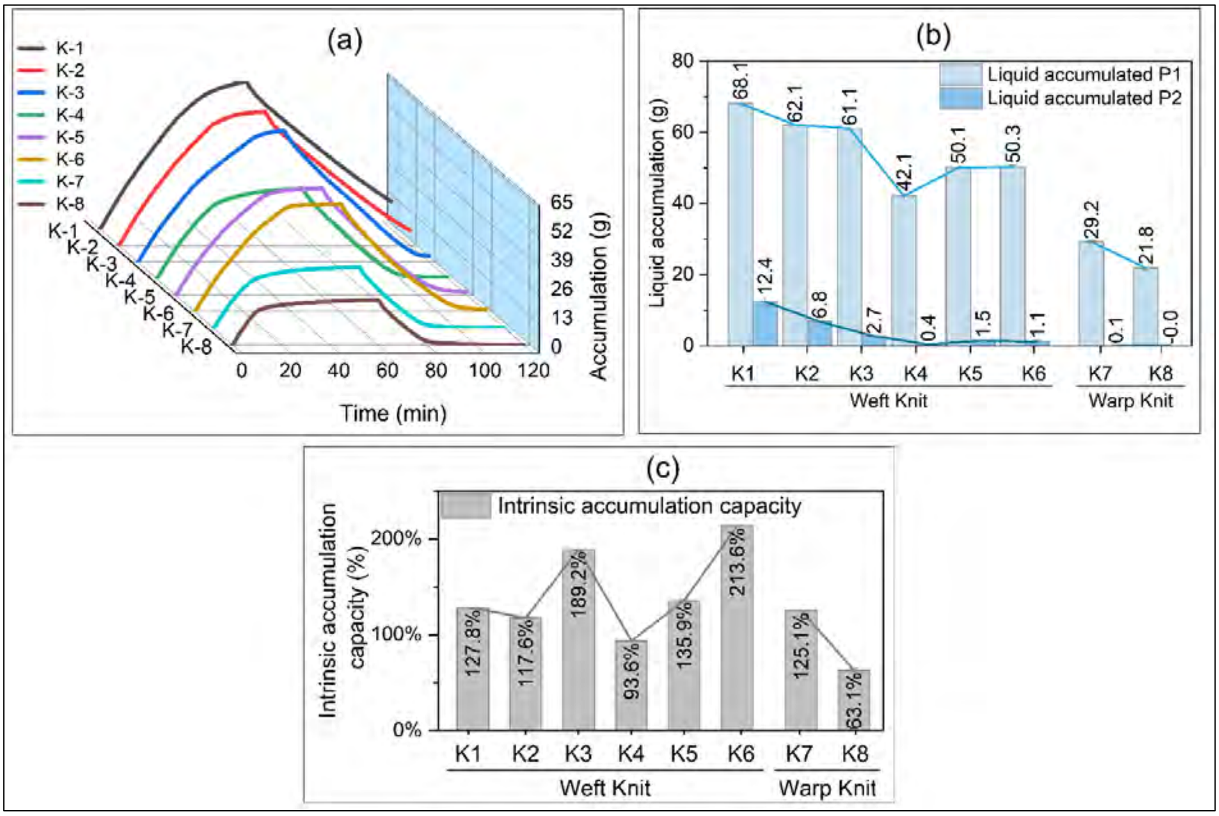

Figure 4.7. Liquid accumulation in fabrics. (a): Real-time liquid accumulation curves (b): Liquid accumulated during P1 and P2 is represented by column bars with error bars indicating standard deviations. (c): Intrinsic accumulation capacity of fabrics. The error bars represent the standard deviations.

The liquid accumulation properties of fabrics are summarized in Figure 4.7. Figure 4.7a shows the relationship between the weight of liquid accumulated in fabrics versus time consecutively both during P1 and P2. The rise of curves in P1 indicates the weight gain of liquid accumulated in the fabric while the fall of curves during P2 represents the weight loss in liquid accumulated by dripping and evaporation. The rate of weight gain is mutually decided by the rate of liquid supplied, evaporated, and dripped through the fabric during P1. The initial linear portions of curves correspond to the prior dripping period and primarily depend on rates of liquid supplied and evaporation from fabric. The bending of curves during P1 indicates the start of dripping, which reduces the rate of liquid accumulation in fabrics. The flattening of curves at the start of dripping in K7 and K8 indicates that dripping significantly reduced the rate of liquid accumulation. In contrast, because dripping appears to be delayed in these fabrics, the effect of dripping on the rate of liquid accumulation is less pronounced in K1 to K3. In general, the liquid accumulation curves of all fabrics during P1 exhibit three deflections: a steeper portion at the start, a gentle downward deflection in the middle, and bending and straightening of curves at the end. A gentle deflection in the middle section, where the rate of liquid accumulation slightly decreases, indicates the period when, even though dripping has not yet begun, the rate of evaporation may reach its maximum due to the spreading area of liquid in fabric. The magnitude of decrease in the rate of liquid accumulation, as shown by the flatness of curves during P1, is mutually determined by the rate of liquid dripping, evaporation and spreading into the fabrics. If the liquid wicking and spreading continued until the end of P1, the rate of liquid accumulation did not drop sharply after dripping started, as shown by K1 to K3.

Because the liquid supplied is terminated at the end of P1, the liquid accumulated during P2 will decrease over time, indicating the post-sweating drying behaviour of fabric at simulated skin temperature and upright body orientation. Except at the beginning of P2, where some liquid dripping may continue for some time, the rate of weight loss in the remaining period of P2 is primarily governed by the rate of liquid evaporation. P2 curves can also be divided into three sections for ease of analysis. A short non-linear and a steeper portion at the beginning (caused by dripping), a significant linear portion in the middle (showing drying at the constant rate of evaporation), and a rapidly decreasing slope towards the end (the drying rate is slowed down to the end). Figure 4.7a shows that, except for K1 and K2, all other fabrics dry largely or completely during P2. Because the fabrics are held nearly vertically on NSS, the portion above the edge may dry faster than the bottom. As a result, the rate of weight loss by evaporation appears to slow down at the end.

The average amount of liquid accumulated in both P1 and P2 is shown in Figure 4.7b where the maximum liquid accumulated in the fabric at the given rate of liquid supplied can be evaluated during P1. The variation in liquid accumulation can be explained based on fabric material, composition, density, knit structure and knit type. The K1, being pure cotton fibre indicated the highest liquid accumulation (68.1g), followed by K2 (62.1g) and K3 (61.1g). The K2 with 35% of cotton fibres in addition to 65% polyester is the second highest in liquid accumulation. The cotton fibres are hydrophilic and showed a strong affinity for water molecules owing to the polar nature of their cellulosic molecules. Moreover, a hollow lumen is present in the cotton fibres where more liquid can be absorbed into the core of fibres imparting higher liquid accumulation ability to pure cotton and cotton mix fabrics. Additionally, the liquid may also accumulate among the inter-yarn and intra-yarn interstices in the fabric. It should be noted that K3 is pure polyester, yet its liquid accumulation is comparable to that of

K2. In addition to 45% of traditional polyester, the presence of 55% Coolmax® fibre fibres in K3 imparts higher specific area and capillary pressure resulting in its higher wicking ability and liquid accumulation. The K4 and K5 are both pure polyester fabrics and composed of the same yarn count (100D/96F), however, the liquid accumulation in K4 (42.1g) is less than that of K5 (50.1). The thickness of both fabrics is the same (o.36mm), but the areal density of K4 (183.84 gm-2) is greater than that of K5 (151.87 gm-2) indicating that yarns in K4 are more closely packed and liquid accumulation may decrease in the relatively dense structure. K5's structure, on the other hand, is relatively loose, allowing more liquid to accumulate within larger pores. It should be noted that the liquid accumulation in K6 (50.3g) is also identical to that of K5 (50.1g) though the yarn count (50D/72F), areal density (96.13 gm^{-2}) and thickness (0.20mm) of K6 differ significantly from that of K5. Despite its lower areal density and thickness, K6 may achieve higher liquid accumulation due to fine micro denier polyester fibres. Because increasing the fineness of the fibres increases the specific surface area (total surface area per unit mass) of the fabric, which results in greater liquid accumulation in K6. K7 and K8 warp knit fabrics have shown overall lower liquid accumulation, which may be attributed to their open mesh construction, and yarn alignment parallels the direction of liquid flow through the fabric, promoting more liquid dripping and less liquid accumulation.

By the end of drying phase P2, it is found that comparatively more moisture is contained in cotton-based fabrics K1 and K2, while all polyester-based fabrics K3 to K8 are about to dry. The drying properties of fabrics during P2 are further explained in terms of drying efficiency, drying rate, and drying time in the next section.

According to the IAC of the fabrics shown in Figure 4.7c, K6 (213.6%) and K3 (189.2%) fabrics can achieve the highest liquid accumulation per unit mass of the fabric, which can be attributed to the higher specific surface area produced by micro denier polyester and Coolmax® polyester fibres in K6 and K3, respectively. Higher IAC values imply that excessive management can be performed by even lightweight fabrics.

4.5.3 Evaluation of drying efficiency, drying rate, and drying time

Drying efficiency of fabrics

Fabric drying efficiencies are measured during P2 using Equation 4.1. The DE values of the fabrics shown in Figure 4.8 display that the fabrics with DE% >95%, K4, K7, and K8, followed by K6, K5 and K3 are almost dry. In contrast, the relatively lower DE% of cotton-based fabrics, i.e., K1 (87.9%) and K2 (93.2%), implies that the more cotton fibres in a fabric, the longer it may take to dry completely. Because drying phase P2 lasts for 60 minutes, a 100% DE value during P2 does not distinguish between fabrics that have dried earlier.

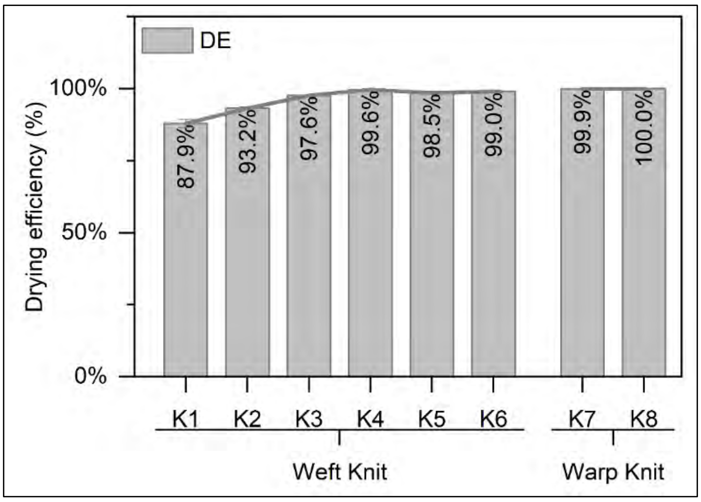

Figure 4.8. Drying efficiency of fabrics.

Drying rates and drying times of fabrics

To further distinguish the fabric drying performance the drying rates and calculated drying times of fabrics as determined by Equations 4.3 and 4.4 respectively, are presented in Figure 4.9.

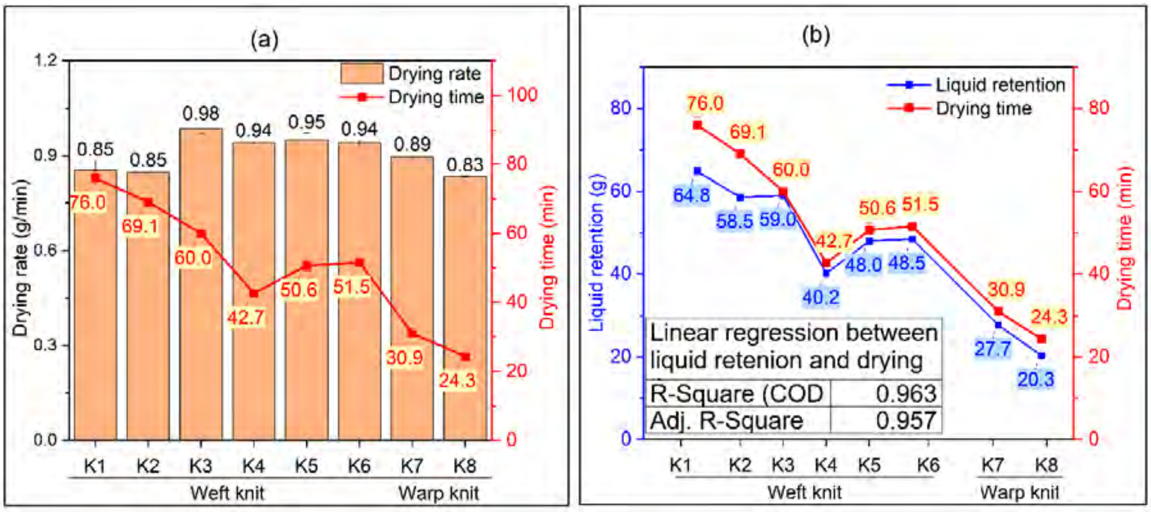

Figure 4.9. Drying properties of fabrics; (a) relationship between drying rate and drying time of fabrics. (b) Relationship between liquid retention and drying time of fabrics. The error bars represent the standard deviations.

Figure 4.9 shows that pure polyester weft knit fabrics, K3 to K6, have higher drying rates, with K3 having the highest drying rate of 0.98 g/min. The drying rate of K4 to K6 is also higher, ranging from 0.94 to 0.95 g/min. However, the drying rates of K1 and K2 in weft knit fabrics are similar (0.85 g/min) but lower when compared to pure polyester weft knit fabrics. Similarly, polyester warp knit fabrics also dry at relatively slower rates, with K7 (0.89 g/min) drying noticeably faster than K8 (0.83 g/min).

The drying dynamics of fabrics can be explained based on the types of liquid accumulated contained in fabrics. Today it is known that fabrics may contain up to five different types of moisture: 1) primary moisture: in the case of cotton and other natural fibres, it is the moisture that is inside the cells of the fibre. This moisture is only removed with a lot of heating. If it is eliminated, the material dries out with the consequent change in the mechanical properties of the fibre. 2) secondary moisture (swelling water): applies to natural fibres. It is the water that is absorbed by the fibre and that produces its swelling. 3) tertiary water, which exists as multilayers on the surface of fibres, located in the external pores of the fibres (Capillary water of the intra-yarn spaces, between fibres). It occurs in all synthetic fibres and also in natural ones, due to the micro and nanopores on their surface. It is what gives the sensation of a "slightly damp" fabric. 4) quaternary or bulk water: it is the one that is located between the threads or fibres (Capillary water of the inter-yarn spaces, between yarns). It is what gives the look and feel of "wet fabric" and can be partially removed by squeezing. 5) excess moisture (overloaded water): it is the one that is deposited above and below the surface of the fabric [139]. If the fabric is hung vertically, the liquid moisture in excess may run along the surface of a fabric, rather than inner capillary flow [55]. It is normally the moisture that drips off.

All of the fabrics from K3 to K8 are made of hydrophobic polyester fibres. As a result, the majority of the water retained in these fabrics could be tertiary and quaternary. Because fabrics are tested in a nearly vertical orientation on NSS, any excess water accumulated in such fabrics will quickly drip off. As a result, the evaporation of capillary water present in the inter-yarn and intra-yarn spaces would determine the drying rates of these fabrics. Moreover, due to the higher wicking ability of polyester fabrics, the water spreads faster and wider over the larger surface area which gives rise to a higher rate of evaporation and thus drying. In contrast, the primary and secondary water of cotton fibres in K1 and K2 dries slowly resulting in substantially lower drying rates. The lower drying rate observed in warp knit fabric K7 and K8 is possible due to their lower liquid accumulation. In addition, the most of surface free water will gather at the edge of the fabric in a hanging orientation, and the nominal capillary water present in the upper portion of the fabric would dry quickly, leaving the fabric wet area smaller and smaller towards the bottom. With rapidly decreasing wet are of fabric the rate of surface evaporation would also decrease yielding an average lower drying rate in warp knit fabrics. In addition to drying rates, the calculated drying times of fabrics are also plotted in Figure 4.9a. The drying times (minutes) are not found to correlate with the drying rates of fabrics. Instead, they appear to correlate strongly (value of adjusted R^2 >0.95) with the amount of liquid retained in the fabric as presented in Figure 4.9b. Therefore, it's important to note that the drying rate alone cannot determine a fabric's ability to dry quickly until the amount of liquid retained in the fabric is considered.

4.5.4 Liquid discharge

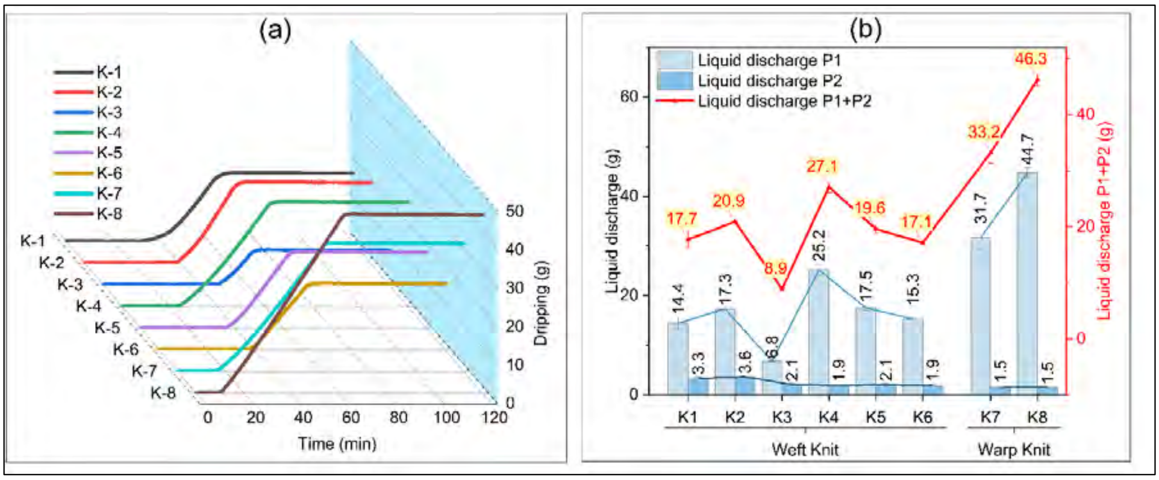

Figure 4.10. Liquid discharge from fabric. (a): Real-time liquid discharge curves. (b): The average liquid discharge during P1 and P2 is indicated by column bars. The cumulative liquid discharged during P1 and P2 is indicated by a line plus symbol plot. The error bars represent the standard deviations.

The liquid dripping behaviour of fabrics is shown in Figure 4.10. Figure 4.10a represents the real-time amount of liquid collected as dripping over time in both P1 and P2. While the average amount of liquid dripped during P1 and P2 separately as well as cumulatively (P1+P2) are summarised in Figure 4.10b. Because of the continuous liquid supplied during P1, the liquid continues to spread in hydrophilic fabrics over time. Figure 4.1c depicts a typical liquid spreading pattern in the fabric, indicating that liquid can spread in all directions around the sweating zone. A push-pull effect caused by continuous liquid feeding and capillary pressure in the fabric causes the liquid to spread throughout the fabric. Because of the vertical inclination of the NSS fabric, the increasing liquid content in the fabric would tend to spread down under the combined influence of capillary pressure and gravitation force. When the liquid reaches the fabric's edge, it tends to accumulate and spread along the edge until its weight overcomes the cohesive and adhesive forces and drips off. The dripping is caused by excess water accumulating at the fabric's edge. Figure 4.10a shows that liquid dripping begins more quickly in warp knit fabrics with K8 followed by K7, whereas in weft knit fabrics (K1 to K6), dripping begins faster in K4 and fairly late in K3. While K1-K2 and K5-K6 appear to be similar in terms of time to start dripping. The steeper and more linear portions of the curves indicate a constant rate of dripping, which may correspond to a constant rate of liquid supplied. Nonetheless, the rate of dripping in K1 is observed to gradually increase, which could be attributed to the higher flow resistance provided by the highly absorbent and swelling nature of its cotton fibres. Since K2 also contains some cotton fibres, a similar but less pronounced effect can also be seen.

Figure 4.10b illustrates an identical trend of the cumulative (P 1+P2) and average amount of liquid dripped during P1 (b). The highest amount of liquid dripping is observed in K7 and K8 among warp knits and in K4 among weft knits. The open mesh construction and parallel orientation yarns along the direction of liquid flow in K7 and K8 may accelerate the liquid drainage through fabrics. However, in K4 the higher liquid drainage may arise from its higher packing density, poor stability and wicking performance of moisture-wicking treatments resulting in higher liquid permeability with increasing liquid saturation in fabric. In contrast, the superior moisture-wicking and liquid-containment properties of Coolmax® fibres in K3 were responsible for the lowest liquid discharge. The liquid that dripped in K1, K2, K5, and K6 is comparable, on the other hand. It is noteworthy that the liquid drained during P2 is much smaller compared to that during P1 because a significant portion of liquid supplied during P1 at an elevated temperature (35C) is evaporated from fabric at the simulated skin temperature (36C). The other major portion of liquid supplied is either accumulated or dripped from the fabric during P1. Consequently, by the end of P1, the liquid accumulated at the edge will reduce greatly to drip during P2.

4.6 Measurement of fabric in-plane directional flow rates of liquid at NSS

The liquid supplied from each sweating outlet in the sweating zone of NSS comes in direct contact with the fabric replicating a real-time fabric-sweating-skin interaction. In the case of hydrophilic fabrics with quick wetting and wicking properties, the sweating droplets are absorbed quickly into the fabric. The continuous liquid supply on NSS in conjunction with the capillary flow of liquid in the fabric creates a push-pull mechanism that causes the liquid to spread all around the fabric. However, the natural tendency of liquid flow may vary along its length and width direction due to the unique construction, composition, and finishing treatment of the fabrics. Similarly, in the case fabric increasing liquid accumulation under prolonged sweating, the flow rate of liquid through the fabric in a downward direction may accelerate induced by gravity and must be evaluated against increasing sweating rate to examine the wicking-durability of fabrics for appropriate applications. For instance, some ordinary moisture management fabrics may spread a small amount of liquid faster to dry quickly. However, upon continuous sweating or supplying a large amount of liquid under certain conditions, liquid sweat may drain from such fabrics very quickly because they cannot accumulate large amount of liquid for a prolonged evaporative cooling effect. Therefore, while testing fabrics on NSS, the in-plane directional flow rates of liquid through fabrics were also investigated at continuous sweating, by detecting temperature variations at the liquid front. The UFR, LFR, DFR_{d1} and DFR_{d2} as explained in section (4.2.2) are presented in Figure 4.11. All the fabric specimens employed in this work are knit fabrics, which consist of courses and wales of yarn running along the length and width of fabrics, respectively. The length of the test samples was kept along the wales direction. The UFR and LFR may correspond to the liquid flow rate along the wales (length) and course (width) of the fabric, respectively.

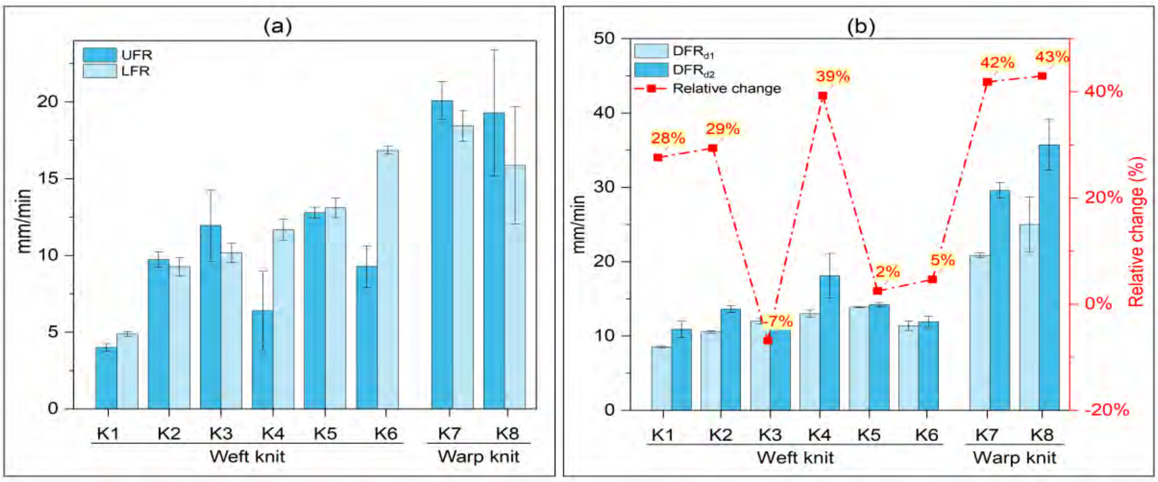

Figure 4.11. Flow rates of liquid through fabrics as measured at continuous and constant rates of liquid supplied on NSS. (a) The upward and lateral flow rate through the fabric is measured around a common sweating outlet. (b). Downward flow rates of liquid produced from all sweating outlets of NSS

Regarding UFR and LFR as shown in Figure 4.11a, it was found the warp knit fabrics, K7 and K8, with mesh-type construction have exhibited comparatively higher flow rates, where UFR is slightly greater than LFR. This greater propensity for liquid movement in an upward direction can be attributed to the potential vertical alignment of yarns in warp knit fabrics.

Furthermore, the liquid moved only along the yarns surrounding mesh openings, whereby the existence of numerous mesh openings reduced the overall covered area available for liquid transport. Consequently, the flow distance per unit of time appears to be greater in the warp knit fabrics. Among weft knit fabrics (viz. K1 to K6), K1 had the lowest flow rates of UFR and LFR, which is possibly caused by the slightly hydrophobic surface characteristics of K1 as revealed by the WCA of 87 and drop absorbency time of 60+ sec given in Table 4.1. In fabrics K2, K3 and K5, the spreading rate of liquid along the course and wales direction were almost identical. Against the hygroscopic cotton fabrics (viz. K1 and K2), pure polyester fabrics indicated a higher wicking potential as evidenced by their higher flow rates of UFR and LFR. While in K2, the mixture of polyester and cotton fibres also demonstrated relatively fast and uniform liquid flow rates along the courses and wales of the fabric. As indicated by LFR > UFR in K5 and K6, the liquid spread faster along the course direction in these two fabrics.

To observe the fabric in-plane directional liquid behaviours, Figure 4.12a illustrates the typical spreading patterns of liquid into fabrics recorded after 8 minutes of continuous sweating. The interval of 8 min was selected to compare the spread areas for the same amount of liquid supplied prior to the dripping of liquid, which was about to start in K8, beyond this period. The liquid spreading areas were determined by image analysis using Adobe Photoshop CC 2019.

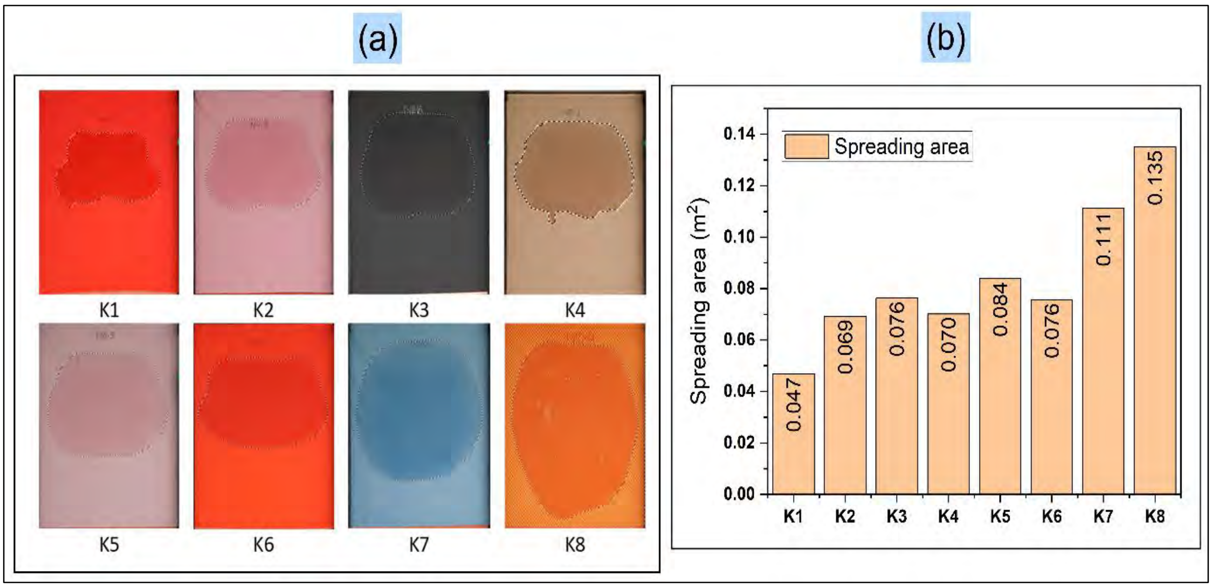

Figure 4.12. Validation of down flow rate by spreading the area of the liquid. (a) Typical spreading pattern liquid on fabric's surface (b) Spreading area of liquid at 8min of liquid supply.

The remarkably higher values of LFR vs UFR in K4 and K6 from Figure 4.11a can be verified by their apparent elliptical spreading pattern of liquid in Figure 4.12a. Wherein, the predominant flow of liquid along course direction may correspond to the specific orientation of yarn loops in the unique pique and waffle knit construction of K4 and K6, respectively, which may work together in tuning the directional flow of liquid.

The characteristics of the bulk flow of liquid through the fabric in a downward direction are summarised in Figure 4.11b. The column bars show the DFR_{d1} and DFR_{d2}, while the line plot indicates their relative percentage difference. The value of DFR_{d2} being measured near the bottom edge determines the ultimate downward flow rate of liquid through the fabric. Overall, DFR_{d2} values were higher than DFR_{d1}, which may be explained by the increasing downward liquid flow rate in the fabric after liquid accumulation [13]. Among the tested fabrics, warp knit fabrics (K7 and K8) had much greater values of DFR_{d2} than DFR_{d1}, which also resulted in larger spread area, as shown in Figures 4.12a and 4.12b. The relatively higher value DFR_{d2} of K4 among the weft knit fabrics may be caused by its relatively high capillary force resulting from its relatively high areal density among the polyester weft knit fabrics.

In addition to the value of DFR_{d2}, the relative difference between DFR_{d1} and DFR_{d2} is important to evaluate the change in liquid permeability with increasing liquid content in the fabric. A remarkably higher DFR_{d2} over DFR_{d1} by 42% and 43% is observed in warp knit fabrics, K7 and K8, respectively. The K1, K2 and K4 have also shown a noticeable rise in liquid permeability of 28%, 29% and 39% respectively. The rise in liquid permeability is generally explained on basis of liquid saturation in fabric. It is found that the liquid permeability varies directly with the increase in saturation while the capillary pressure varies inversely [13]. At a saturation below 100%, the capillary pressure will hold the liquid within the capillaries of the fabric. Therefore, the fabrics showing a remarkable rise in liquid permeability may get saturated faster, and the bulk of liquid may start flowing along the surface of the fabric rather than the inner capillary flow [55]. In contrast, the fabrics K5 and K6, where a small positive difference is observed between DFR_{d1} and DFR_{d2}, have shown relatively stable capillary flow in the downward direction at the increasing liquid content in the fabric over time. Interestingly, in the case of fabric K3 consisting of polyester-Coolmax® fibres, the negative value of relative difference implies the superior wicking potential of fabric causing the growing amount of liquid in fabrics to spread wider in all directions. Consequently, the saturation is delayed, and higher capillary pressure prevents the permeability of the liquid to rise over time. That is why the K3 fabric has shown higher liquid accumulation, evaporation, and lower liquid discharge as measured by NSS.

The different spreading patterns seem to correlate well with the varying directional flow rates of liquid in fabrics as revealed by NSS. The fitted linear regression analysis was used to test if the NSS flow rates explained the area covered by liquid during 8 minutes of sweating, and the results are shown in Figure 4.13. The regression was significant at $P<0.01$ for UFR, with $R^2=0.75$, $P<0.05$ for LFR with $R^2=0.58$, $P<0.001$ for DFR_{d2} with $R^2=0.88$ and $P<0.0001$ for DFR_{d1} with $R^2=0.96$. The spread area was positively related to all rates of directional flow; however, it was found to change almost linearly with the downward flow rate DFR_{d1} with the highest value of $R^2=0.96$. Indeed, the spread area was also in a strong relationship with DFR_{d2} and UFR, yet due to their apparently higher association with warp knit fabrics, they might overestimate the spread area for weft knit fabrics. Since flow rates were measured with a continuous liquid supply, they are more realistic for simulating fabric liquid sweat dispersion along different directions in contact with a body high-intensity sweating zone.

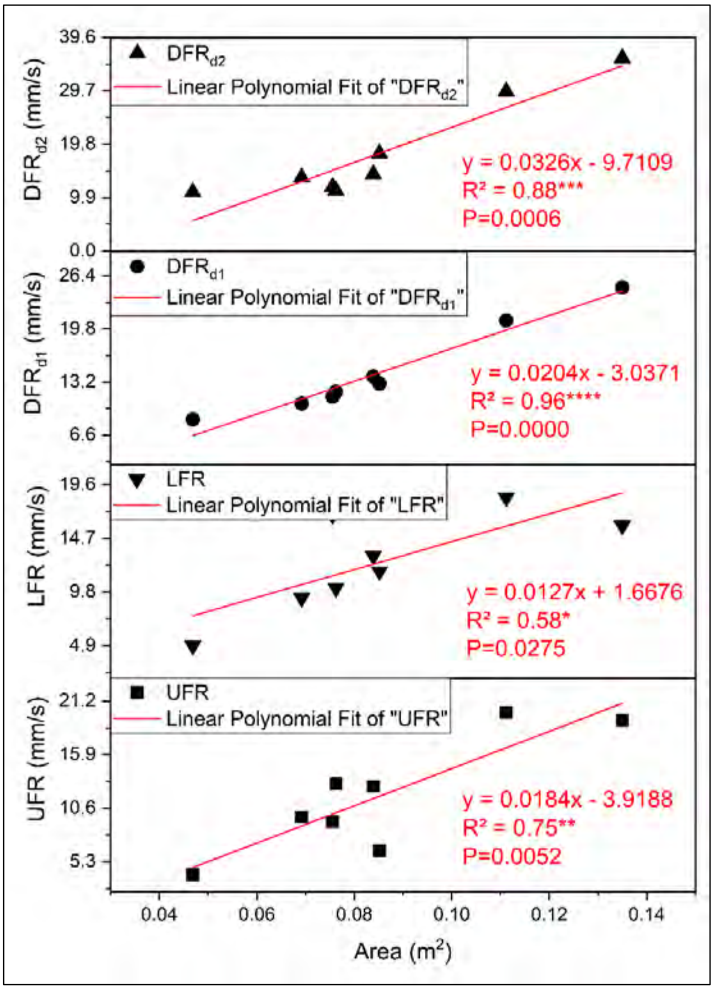

*Figure 4.13. Linear regression relation between 8min spread area and NSS directional flow rates of liquid. The results are significant at * P≤0.05, **P≤0.01, ***P≤0.001, ****P≤0.0001*

4.6.1 Correlation between NSS flow rates and liquid mass distribution

Pearson correlation coefficients between the NSS flow rates and liquid mass distribution i.e., accumulation, evaporation, and discharge, are presented in Table 4.2.

Table 4.2. Pearson correlation coefficient between NSS flow rates and liquid mass distribution for 8 fabrics

NSS Flow rates →	**UFR**		**LFR**		**DFR_{d1}**		**DFR_{d2}**	
NSS liquid distribution↓	***r***	**P**	***r***	**P**	***r***	**P**	***r***	**P**
Liquid accumulation during P1	-0.76	0.03	-0.81	0.02	-0.94	0.00	-0.93	0.00
Liquid evaporation during P1	0.69	0.06	0.89	0.00	0.65	0.08	0.54	0.17
Liquid discharge during P1	0.62	0.10	0.56	0.15	0.90	0.00	0.96	0.00
r: Pearson correlation coefficient, P-Value: < 0.05 indicates the correlation is significant								

Liquid accumulation during P1 is found to be in a significant negative correlation with all parameters of NSS flow rates. In particular, it is highly negatively correlated with the downward flow rates; DFR_{d1} (*r* =-0.94, P <0.01) and DFR_{d2} (*r* =-0.93 P<0.01) suggesting that higher the rate of liquid flow through the fabric, lower the liquid accumulation. Alternatively, the liquid discharged from fabric also is likely to increase with increasing liquid flow rates, especially in the downward direction. Consequently, a significant and strong positive correlation between liquid discharge during P1 and DFR_{d1} (*r* =0.90, P<0.01) and DFR_{d2} (*r* =0.96, P<0.01) is obtained. In addition, the liquid evaporation during P1 was also found to be positively correlated with the flow rates in different directions. However, the correlation is higher and more significant with LFR (*r*=0.89, P<0.01) compared to UFR (*r*=0.69, P>0.05) and downward flow rates (*r*=0.65 and 0.54, P>0.05), which may be due to the fact that the LRF is not influenced by gravity and solely depends on the fabric material, structure and wettability in addition to the applied rate of sweating. In contrast, liquid flow in a downward direction can accelerate due to gravity with increasing liquid accumulation in fabrics as observed in K1, K2, K4, K7 and K8 (Figure 4.11b). If a higher DFRs or UFR is accompanied with a higher LFR, the liquid can spread more in surrounding areas and evaporate faster. Thus, the liquid evaporation during P1 is found to be in a significant and strong positive correlation with the LFR.

Besides, Figure 4.14 shows the correlation between liquid evaporation during P1, and the wet area of fabric measured at the 8th min of sweating. The value R^2=0.52 shows a moderate positive correlation between the two parameters, which implies that liquid evaporator P1 will increase with the wet area yet cannot be completely explained by the area of spreading. Because the increase in spreading area can contribute to evaporation mainly before dripping. After that, the rate of spreading will slow down and liquid evaporation during P1 will mainly depend on the specific material, composition, structure, and wettability of fabrics. Therefore, a single factor, such as spreading area cannot fully explain the mass of liquid evaporated under continuous and prolonged sweating. Instead, numerous factors may interact with each other, hence an instrument like NSS would be beneficial to realistically investigate the fabric liquid and moisture management performance.

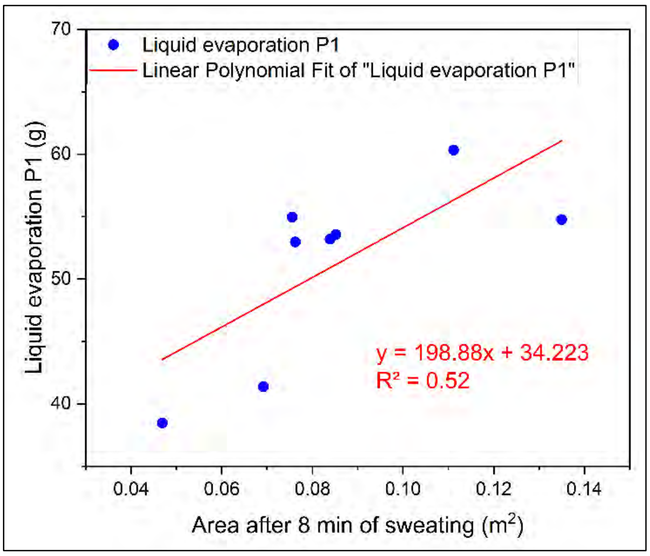

Figure 4.14. Relationship between liquid evaporation during P1 and area of liquid spreading after 8 min of sweating

4.7 Correlation between NSS and MMT results

To compare the NSS results with that of the moisture management tester, MMT, fabrics were tested on MMT according to the standard test method of AATCC 195, and results are summarised in Table 4.3. Among all weft knit fabrics, K1, pure cotton, has the highest values of OMMC (0.99) and OWTC (649.9), indicating the highest potential for overall moisture management and one-way liquid transport. However, the fabric has relatively higher wetting times at the top (8.7s) and exceptionally high wetting times at the bottom (25.4s), indicating that liquid cannot quickly transfer from the top to the bottom.

Table 4.3. Moisture management properties of fabrics by MMT

Fabrics		Wetting Time Top(sec)	Wetting Time Bottom(sec)	Top Absorption Rate(%/sec)	Bottom Absorption Rate(%/sec)	Top Max Wetted Radius (mm)	Bottom Max Wetted Radius (mm)	Top Spreading Speed (mm/sec)	Bottom Spreadin g Speed (mm/sec)	Accumulative one-way transport index(%)	OMMC
		WT_t	**WT_b**	**MAR_t**	**MAR_b**	**MWR_t**	**MWR_b**	**SS_t**	**SS_b**	**OWTC**	**OMMC**
K1	Mean	8.73	25.37	92.92	267.89	11.00	28.00	0.83	5.55	649.88	0.99
	S.D	4.00	8.58	20.67	102.65	2.24	4.47	0.26	2.06	142.77	0.03
K2	Mean	3.06	3.27	33.93	24.15	22.00	20.00	4.34	4.05	-60.82	0.29
	S.D	0.28	0.28	1.63	3.28	2.74	0.00	0.25	0.08	24.93	0.02
K3	Mean	2.90	2.72	33.80	33.22	25.00	23.00	5.29	5.38	38.69	0.41
	S.D	1.14	1.14	2.11	1.91	3.54	2.74	0.92	1.13	32.68	0.04
K4	Mean	4.06	4.17	52.63	40.58	20.00	20.00	3.79	3.79	-122.03	0.31
	S.D	0.58	0.57	4.60	4.26	0.00	0.00	0.33	0.26	13.05	0.01
K5	Mean	1.91	1.91	41.93	34.49	25.00	25.00	10.79	10.74	-68.05	0.32
	S.D	1.00	1.01	6.88	4.05	0.00	0.00	10.01	9.98	13.87	0.01
K6	Mean	3.02	3.00	56.30	51.01	23.00	24.00	5.44	5.48	-127.35	0.36
	S.D	1.05	1.02	2.12	6.90	2.74	2.24	0.69	0.75	29.48	0.02
K7	Mean	2.60	2.50	59.26	49.93	30.00	30.00	7.71	7.64	-75.42	0.36
	S.D	0.61	0.56	4.50	9.39	0.00	0.00	0.30	0.29	24.86	0.03
K8	Mean	2.64	2.46	48.10	49.12	30.00	30.00	9.33	9.39	84.25	0.51
	S.D	0.29	0.47	9.32	14.93	0.00	0.00	1.55	1.13	83.07	0.13

Table 4.4. Pearson correlation between NSS and MMT results

NSS Results →		**UFR**	**LFR**	**DFR_{d1}**	**DFR_{d2}**	**Liquid accumulation during P1**	**Liquid evaporation during P1**	**Liquid discharge during P1**
MMT Result ↓								
Wetting Time Top(sec)	***r***	-0.68	-0.73	-0.49	-0.34	0.50	-0.71	-0.25
	P	0.06	0.04	0.22	0.41	0.20	0.05	0.55
Wetting Time Bottom(sec)	***r***	-0.60	-0.71	-0.45	-0.33	0.51	-0.71	-0.25
	P	0.12	0.05	0.26	0.43	0.20	0.05	0.55
Top Absorption Rate	***r***	-0.39	-0.28	-0.17	-0.05	0.13	-0.33	0.03
	P	0.34	0.50	0.68	0.91	0.76	0.42	0.94
Bottom Absorption Rate	***r***	-0.51	-0.61	-0.36	-0.25	0.42	-0.62	-0.18
	P	0.20	0.11	0.39	0.56	0.31	0.10	0.67
Top Max Wetted Radius	***r***	0.93	0.83	0.80	0.68	-0.75	0.80	0.54
	P	0.00	0.01	0.02	0.06	0.03	0.02	0.17
Bottom Max Wetted Radius	***r***	0.58	0.35	0.64	0.63	-0.51	0.27	0.55
	P	0.14	0.40	0.09	0.10	0.20	0.53	0.16
Top Spreading Speed	***r***	0.78	0.69	0.69	0.53	-0.64	0.67	0.47
	P	0.02	0.06	0.06	0.17	0.09	0.07	0.25
Bottom Spreading Speed	***r***	0.63	0.44	0.61	0.48	-0.50	0.41	0.44
	P	0.09	0.28	0.11	0.23	0.21	0.32	0.28
Accumulative one-way transport	***r***	-0.39	-0.68	-0.26	-0.18	0.42	-0.67	-0.15
	P	0.34	0.06	0.53	0.67	0.31	0.07	0.73
OMMC	***r***	-0.37	-0.58	-0.21	-0.12	0.33	-0.58	-0.08
	P	0.37	0.13	0.62	0.77	0.43	0.13	0.85

r: Pearson correlation coefficient, P-Value: < 0.05 indicates the correlation is significant

Besides, the bottom maximum wetted radius (28 mm) appeared more than twice the top maximum wetted radius (11mm). Similarly, the bottom absorption rate (267.9 %/s) and bottom spreading speed (5.6 mm/s) were exceptionally higher compared to top (92.9 %/s) and (o.8 mm/s), respectively. As Table 4.1 shows a higher WCA of 87±0.82 for K1, there is the possibility that liquid penetrates the fabric gradually but could not spread fast into the fabric. As a result, under the influence of its contact pressure and gravity, it may diffuse gradually to the bottom and result in exceptionally high OMMC and OWTC. In such conditions, it is not sure how realistically the value of OMMC and OWTC will correlate with the real-time fabric liquid moisture management performance and need to be investigated by some suitable method.

Considering other weft knit fabrics, K2 (Polyester-cotton blend, 225.41GSM) and K5 (Polyester 100%, 151.87 GSM) have shown similar properties with a lower overall moisture management capacity (OMMC=0.3 and 0.3 respectively) accompanied with a poor one-way transport ability (OWTC=-60.8 and -68.1), respectively, suggesting the liquid may not easily diffuse form skin side to the outer surface of the fabric. However, they showed a very fast wetting time of 2s to 3s, and medium absorption rates on top and bottom (MAR_t= 33.9 %/s and 41.9 %/s at the top, MAR_b=24.2 %/s and 34.5 %/s at the bottom, respectively), large maximum wetted radius (MWR_t=22.0mm and 25.0 mm at the top, MWR_b= 20.0mm and 25.0mm at the bottom, respectively) and very fast spreading speeds (SSt=4.3 mm/s and 10.8mm/s at the top, SSb=4.0mm/s and 10.7 mm/s at the bottom, respectively), indicating that the liquid can spread easily on both sides of each fabric, whereas K5 would spread even more faster and wider than K2 [140].

K3 fabric, composed of pure polyester and Coolmax®, on the other hand, has shown a fair positive once-way transport capacity with a value, of OWTC=38.7, along with medium absorption rates (MAR_t= 33.80 %/s at the top, MAR_b=33.22 %/s at the bottom) very fast wetting times (WT_t=2.9s and WT_b=2.7s) and spreading speeds (SSt=5.3 mm/s, SSb=5.4mm/s), as well very large spreading radii (MWR_t=25.0mm and MWR_b=23.0mm), indicating that liquid while spreading into fabric, can easily diffuse from skin side to the outer surface of the fabric, where it can evaporate to the environment.

K4 and K6, on the other hand, have demonstrated quick wetting with relatively slow absorption rates (MAR_t= 24.2 %/s and 34.5 %/s at the top, MAR_b=22.0 %/s and 25.0 %/s at the bottom, respectively), large wetted radii (MWR_t=20.0mm and 23.0 mm at the top, MWR_b= 20.0mm and 24.0mm at the bottom, respectively) and high spreading speeds (SSt=3.8 mm/s and 5.4mm/s at the top, SSb=3.8mm/s and 5.5 mm/s at the bottom, respectively) but have shown increasingly poor and negative one-way transport capacities (OWTC= -122.0 and -127.4, respectively), indicating that the liquid cannot diffuse effortlessly from inner to the outer surface of a fabric, instead, may tend to accumulate on the side of the fabric, adjacent to the skin. In addition, the OMMC of K4 and K6 were found to be just fair, at 0.3 and 0.4, respectively.

Among warp knit fabrics, the OWTC of K7 is negative at -75.4 but that of K8 is positive at +84.3, yet both have demonstrated very fast wetting (WT_t=2.6s and 2.6s, WT_b=2.5s and 2.5s, respectively), remarkably higher absorption rates (MAR_t= 59.26 %/s and 48.10 %/s at the top, MAR_b=49.93 %/s and 49.12 %/s at the bottom, respectively), extremely fast spreading speeds (SSt=7.7mm/s and 9.3mm/s, respectively, SSb=7.6mm/s and 9.4 mm/s respectively) and exceptionally large wetted radii on both sides (MWR_t=30.0mm, and 30.0 mm, MWR_b= 30.0mm and 30.0mm, respectively), indicating that they can absorb quickly and spread very swiftly and widely, on each side of the fabric. Particularly, K8 spreads more quickly than K7, which may be explained by its noticeably bigger size of mesh openings. As a result, a lower liquid accumulation and higher liquid evaporation can be expected from such fabrics.

Table 4.4 shows the Pearson correlation coefficients between the MMT and NSS results for 8 fabrics. This reveals that the NSS rates of liquid flow i.e., UFR, LFR, DFR_{d1}, and DFR_{d2} are negatively correlated with the MMT parameter of wetting times, absorption rates, one-way transport, and overall moisture management capacity. However, the correlation is significant only between LFR and wetting times on the top and the bottom ($r= -0.73$, $P<0.05$ and $r= -0.71$, $P<0.05$, respectively), suggesting that the lateral flow rate of liquid on NSS will increase on fabrics having shorter wetting times. This is understandable because quick wetting can help the liquid spread faster, as evidenced by the top spreading speed of all polyester-based fabric compared to K1 in Table 4.3. In contrast, NSS flow rates are positively correlated with MMT parameters of spreading speeds and maximum wetted radii. Particularly, there is a significant and very high correlation of UFR with maximum wetted radius at the top ($r=0.93$, $P<0.05$) followed by a strong correlation with spread speed at the top ($r=0.78$, $P<0.05$). This implies that similar characteristics measured on the same side of the fabrics are found to be correlated, which may be explained by the fact that the same surface of the fabric is presented to the sensors for SS_t and MWR_t on MMT and UFR on NSS. Similarly, the maximum wetted radius at the top is also strongly and significantly correlated with LFR ($r=0.83$, $P<0.05$) and DFR_{d1} ($r=0.80$, $P<0.05$). However, unlike NSS, MMT's maximum wetted radius does not indicate the dominant direction of liquid flow along a specific direction of the fabric, such as course or wales in knit fabrics. Nevertheless, on NSS, the relative difference between UFR and LFR can differentiate the flow rate of liquid along the specific course or wales directions, as illustrated in Figures 4.11a and 4.12a in case of fabric, K4, and K6.

In addition to NSS liquid flow rates, the Pearson correlation coefficients established between NSS liquid mass distribution i.e., accumulation, evaporation, and discharge during P1 and MMT parameters are also summarised in Table 4.4. The liquid accumulation during P1 is found to be positively correlated with the MMT parameter of wetting time, absorption rates, OMMC, and one-way transport capacity, and negatively correlated with spreading speeds and maximum wetted radii. Nonetheless, the correlation was significant only between maximum wetted radius top and liquid accumulation during P1 ($r=-0.75$, $P<0.5$) indicating that a fabric capable of spreading liquid widely can better prevent the localized accumulation of liquid in fabric. As a result, it can evaporate fast and drip more when subjected to the rate of continuous sweating on NSS.

While no significant correlation is found between the amount of liquid discharge during P1 and the parameters of MMT. However, a moderate positive correlation is observed between liquid discharge during P1 and maximum wetted radii on top and bottom ($r=0.54$ and 0.55 respectively), indicating that there is a 55% chance of an increase in liquid discharge during P1 on temperature-controlled NSS for the respective increase in wetted radii on MMT.

On the other hand, liquid evaporation during P1 was also found to be in a significantly positive correlation with maximum wetted radius at the top ($r=0.80$, $P<0.05$) while significantly negatively correlated with wetting times at the top and bottom ($r=-0.71$, $P<0.5$). This implies that the quick wetting and large wetted area as indicated by short wetting time and large maximum wetted radius at the top on MMT can better explain the fabrics liquid evaporation P1 on NSS. Besides, the liquid evaporation P1 was discovered to be moderately negatively correlated with the MMT indices of moisture management properties, viz. OWTC at $r=-0.67$ and OMMC at $r=-0.58$, however, the correlations were not statistically significant.

According to the results of MMT, K1 with values of OMMC=0.99 and OWTC=649.88 should have the highest moisture management performance, however, its liquid evaporation P1 was lowest among all fabrics. Similarly, K4 and K6 with negative values of OWTC=-122.03 and -127.35 respectively, and low values of OMMC=0.31 and 0.36 respectively, should demonstrate poor moisture management properties, yet their liquid evaporation P1 is found maximum among other weft knit fabrics. Likewise, the absorption rate of K4, K6, K7 and K8 are almost identical, but they vary greatly in their liquid accumulation during P1. As well, the top spreading speed in K5 (10.79 m/s) is slightly higher than in K8 (9.33 m/s), yet the liquid discharge P1 in K8 is 27.2g higher than in K5. Therefore, in summary, it implies that the liquid evaporation, as well as accumulation and discharge from fabric, can be affected by a variety of factors such as fabric materials, construction, wettability, sweating rates, temperature gradients, environmental conditions, natural and forced convection, thus cannot be explained reliably by the parameters of MMT, particularly when based on a small set of data from a diverse range of fabrics as employed in the current study. Hence, should be measured practically and precisely on an instrument like NSS with controllable sweat and skin temperatures.

Furthermore, when comparing NSS to other instruments, the basic differences in measuring principles and capability must be considered. MMT, for example, measures directional liquid transport using an electrical principle, whereas the NSS uses a gravimetric principle to measure the evaporation rate, moisture accumulation rate, and drying rate, as well detection of temperature variations at the liquid front to measure the fabric in-plane directional flow rates of liquid. In further contrast, the flow rates on NSS are measured at the simulated skin temperature under continuous sweating, whereas the effect of temperature and evaporation are neglected on MMT.

4.8 Comparison of measurements at temperature-controlled and non-temperature-controlled versions of NSS

The NSS parameters of liquid evaporation, accumulation, and discharge during P1, measured at temperature-controlled NSS (Chapter 04) and non-temperature-controlled NSS (Chapter 03), are compared in Figure 4.15 in terms of magnitude and interaction. Corresponding to the original response of fabrics to continuous sweating, the values measured during P1 have been selected for comparison. While, the drying efficiencies of fabrics, corresponding to P2 are compared in Figure 4.16.

Figure 4.15a. reveals that against the non-temperature-controlled NSS at 20.0 °C, the fabrics' liquid evaporation during P1 has substantially increased when measured on temperature-controlled NSS at about 36.0°C and 35.3°C simulated skin and sweat temperatures, respectively. Among weft knits, the evaporation increased 5.5 and 6.6 times in K1 and K2 fabrics, respectively. The presence of non-hygroscopic polyester fibres with hygroscopic cotton fibres in K2 has shown an additional rise of 1.1 times in liquid evaporation during Phase one (viz. P1).

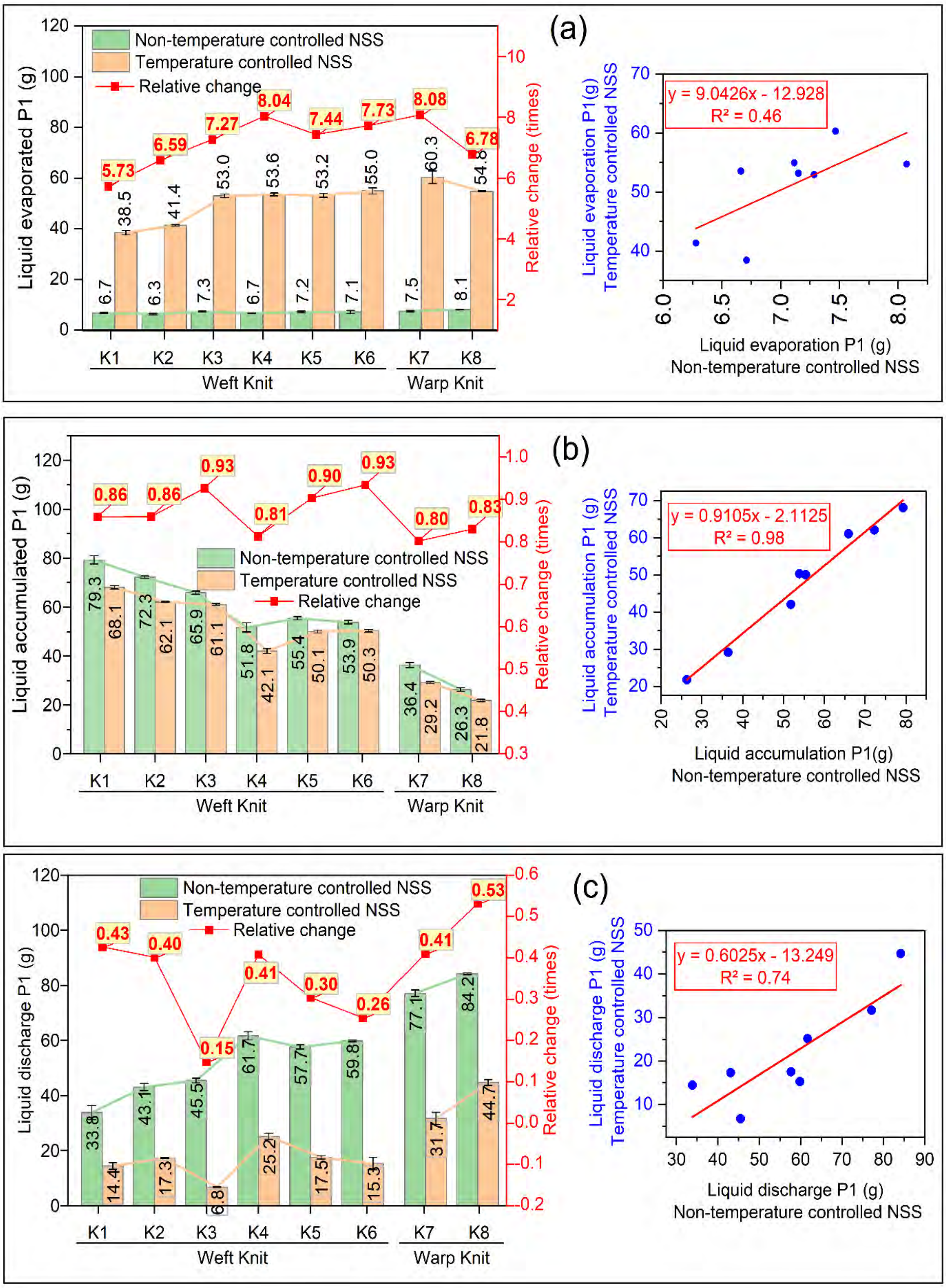

Figure 4.15. Comparison of measurements by the non-temperature control and temperature-controlled version of NSS. (a) Comparison of liquid evaporation. (b) Comparison of liquid accumulation. (c) Comparison of liquid discharge.

Among pure polyester weft knits (K3, K4, K5 and K6), the evaporation has increased by more than 7 times showing an obvious advantage of pure polyester fabrics over cotton and cotton-mix fabrics in evaporating the liquid. In the case of hygroscopic cotton fibres, the liquid is absorbed and trapped inside the fibres' cores by potential hydrophilic sites, while it spreads at the surface of hydrophilic polyester fibres where it can easily diffuse into the environment.

In the case of warp knits polyester fabrics (viz. K7 and K8), against their behaviour at non-temperature-controlled NSS, the liquid evaporated at temperature-controlled NSS is found higher in K7 with a total rise of 8.08 times as compared to the 6.78 times in K8. It should be noted that under the impact of temperature, where the magnitude of liquid evaporation increases the range of liquid evaporation also increases and a difference between the highest and lowest values reaches up to 21.8g on temperature-controlled NSS as opposed to 1.8g of non-temperature-controlled NSS. In addition, the sequence in which different fabrics evaporate the mass of liquids during P1, also changed and a moderate positive correlation was noticed between the liquid evaporation during P1 at non-temperature and temperature-controlled NSS with a value of R^2=0.46.

Figure 4.15b. compares the fabric liquid accumulation, at non-temperature and temperature-controlled NSS. The results show that at elevated temperatures, liquid accumulation is slightly reduced but the order of fabric in liquid accumulation remains almost the same as indicated by a very strong positive correlation of R^2=0.98. Among all specimens, K1 to K8, the liquid accumulation at temperature-controlled NSS is found to vary between 0.80 to 0.93 times its values at non-temperature-controlled NSS. Specifically, K3 and K6 have shown the lowest reduction in liquid accumulation at elevated temperatures which can be ascribed to their large capillary pressure and volume-specific area arising from the profiled fibres viz. Coolmax® in K3 and micro denier polyester in K6 [141, 142]. Since the amount of liquid accumulation at temperature-controlled NSS doesn't seem to be affected largely by increasing evaporation, therefore will be chiefly governed by the amount of liquid supplied in addition to the fabric's intrinsic fibres composition, type and fabric structure.

The amount of liquid discharge is compared in Figure 4.15c. Since, at the elevated temperature, for the given amount of liquid supplied during P1, the amount of liquid accumulation is found to vary slightly but liquid evaporation has increased significantly, the liquid discharge is reduced accordingly. It is reduced by close to half in K8 and more than half in K1 to K7 when compared to non-temperature-controlled NSS measurements. The highest decrease in liquid discharge is observed in K3 and K6, which may be a sign of reduced rate of saturation and thus the speed of liquid flow through the fabric induced by remarkably higher rate of evaporation at the simulated skin and sweat temperatures. Nonetheless, the value of R^2=0.74 indicates a strong positive correlation between the amount of liquid discharged during P1 at both the non-temperature and temperature-controlled NSS.

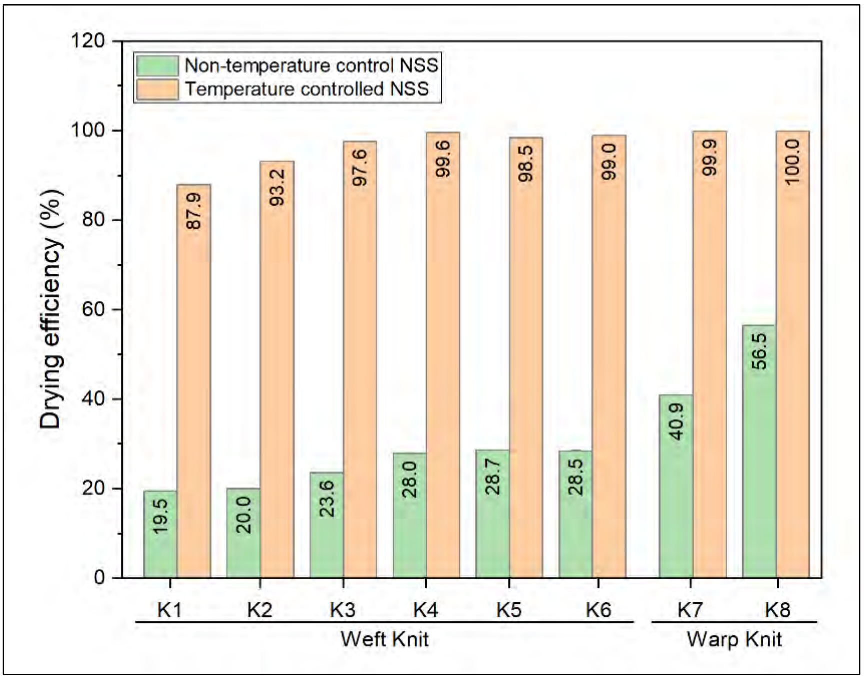

Figure 4.16. Comparison of drying efficiency measured on non-temperature controlled and temperature controlled NSS

Figure 4.16 compares the drying efficiency of fabrics, measured at temperature-controlled and non-temperature-controlled NSS. It is found that at elevated temperatures of temperature-controlled NSS, the drying efficiency of all fabrics has improved to a large extent. In fabrics, K1 and K2, it reached 87.9% and 93.2% starting from 19.5% and 20.0% of non-temperature controlled NSS, respectively. The competitively higher drying efficiency of K2 implies that instead of pure cotton the blend of polyester and cotton can improve the drying properties [143]. While, among all pure polyester fabrics, the drying efficiency is found to reach 97.6% in K3, 98.5% in K5 and above 99% in the remaining ones.

In summary, the comparative evaluation indicates that the simulated skin temperature of NSS can better simulate the end-use conditions and offers realistic measurements of fabric liquid moisture management and drying properties. The increase in evaporation and drying efficiency is due to the increased natural convection induced by the large temperature difference between the NSS and ambient conditions. The effect was more pronounced in pure polyester fabrics when compared to the fabrics containing hygroscopic cotton fibres.

4.9 Relationship between NSS parameters of liquid mass distribution and rates of wicking by standard wicking tests

In this section, investigations are made to find any possible correlation between the standard wicking tests and NSS measurements of liquid mass distribution. The fabrics tested on NSS were further tested for vertical and horizontal wicking properties and fitted linear regression analysis was performed to identify the possible relationships.

4.9.1 Vertical wicking rates of fabrics

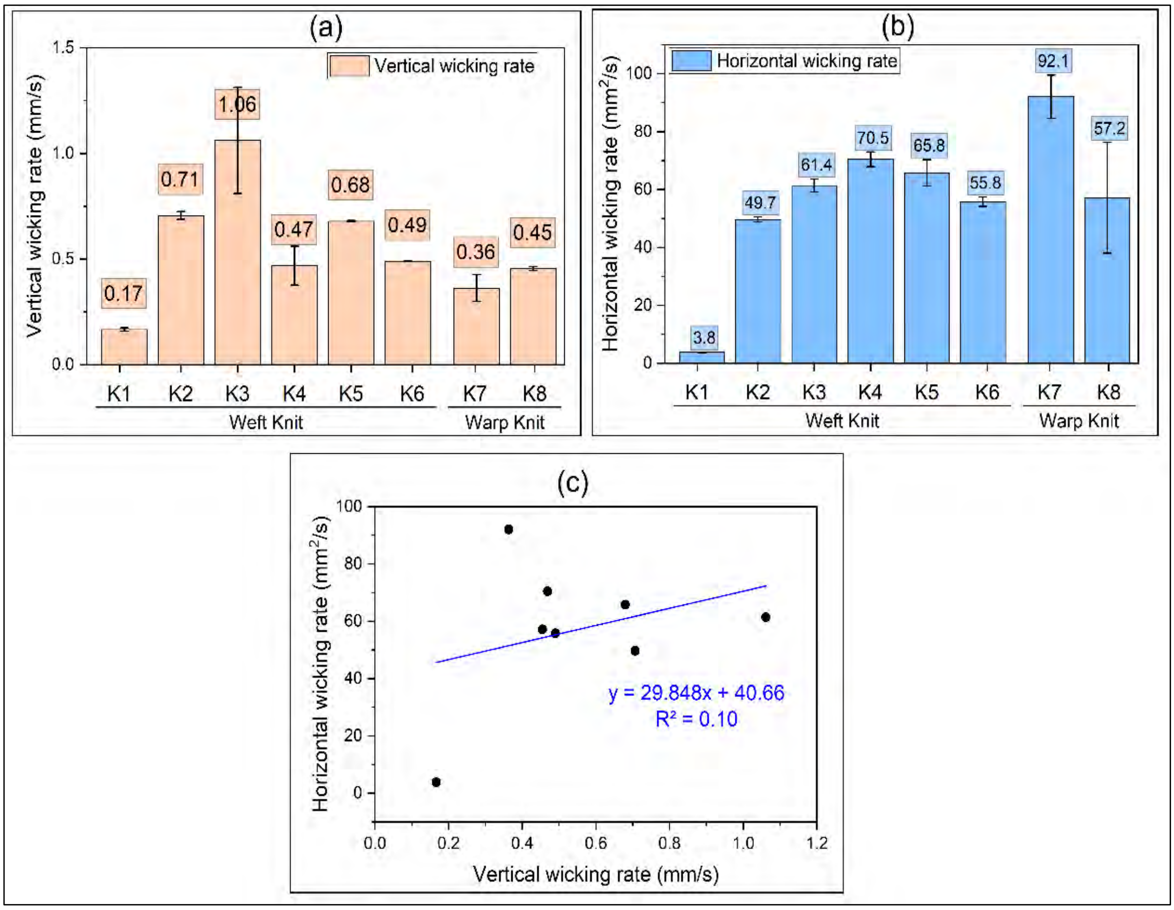

Figure 4.17. Wicking test results (a) Vertical rate of wicking (b) Horizontal rate of wicking

The vertical wicking was measured according to AATCC 197 [144]. Three fabric strips with dimensions 2.5cm x 35cm, were cut from each fabric. The strips were hung vertically over a horizontal bar and the bottom edges were immersed about 5mm into an indefinite reservoir of distilled water. The wicking height of water in each strip was recorded in the unit of mm for the first 2.0 ±0.1 min and the rate of vertical wicking was determined by the ratio of wicking distance to the wicking time. After three strips of each fabric were tested, the average rate of vertical wicking was examined in the units, mm/s, and results are shown in Figure 4.17a. Among weft knit fabric the fabric K3 has the highest vertical wicking rate of 1.06 mm/s possibly owing to the superior wicking action of Coolmax® fibres constituting about 45% of its composition with 55% of conventional polyester fibres.

The second highest rate of vertical wicking is 0.71 mm/s in K2, a blend of 65% polyester and 35% cotton fibres. Among other weft knit polyester fabrics, K5 is rising high at 0.68mm/s followed by K6 and K4 at 0.49 mm/s and 0.47 respectively. The lowest vertical wicking rate is found in K1, a pure cotton fabric, which is expected because of its higher absorbency time of 60+s and WCA of about 87°. While in the case of warp knit fabrics, K8 has a higher vertical wicking rate (0.45 mm/s) compared to K7 (0.36 mm/s). As a result, the fabrics can be arranged in the following descending order based on their vertical wicking rate.: K3>K2>K5>K6>K4>K8>K7>K1.

4.9.2 Horizontal wicking rates of fabrics

The horizontal wicking rates were determined according to the standard test method; Horizontal wicking of textiles AATCC198 [118] with a little modification. About 1 ml of distilled water was supplied at the centre of each fabric for 1 min using a peristaltic pump. A video of liquid transport in fabric was recorded by a mobile phone camera (Samsung A50) capturing the real-time area of water spreading in the fabric. The areas covered in 2.0 ±0.1 min was calculated by image analysis technique using a computer-based software; Adobe Photoshop CC 2019. Three specimens were tested for each fabric and the average rate of horizontal wicking was measured in the units, mm^2/s, by dividing the area covered by 120 sec.

Figure 4.17b presents the horizontal wicking rates of fabrics, where the lowest spreading rate of 3.8 mm^2/s is found in fabric K1 because of its hydrophobic characteristics. Among other weft knit fabrics, K4 spreads at 70.5 mm^2/s followed by K5, K3, K6 and K2 at 65.8 mm^2/s, 61.4 mm^2/s, 55.8 mm^2/s and 49.7 mm^2/s respectively. In the case of warp knit fabrics, the K7 spreads at 92.1 mm^2/s showing the highest overall rate of spreading among all fabrics under investigation. While K8 has a comparatively lower spreading rate of 57.2 mm^2/s, falling in the range of weft knit fabrics. It is interesting to note the vertical wicking rate of K7 was much lower among all fabrics except K1, yet it outperformed all others in horizontal wicking rate. Similarly, the vertical wicking rate of K3 was higher than that of K4 and K5, yet its horizontal wicking rate was lower than that of those. Figure 4.17c indicates almost no correlation with the value of R^2=0.10 for linear regression between the vertical and horizontal wicking rates of given fabrics. This implies that in a diverse set of fabrics the rate of liquid spreading cannot be determined reliably by the respective vertical wicking rates of fabrics.

4.9.3 NSS parameters of liquid mass distribution versus the rate of vertical wicking

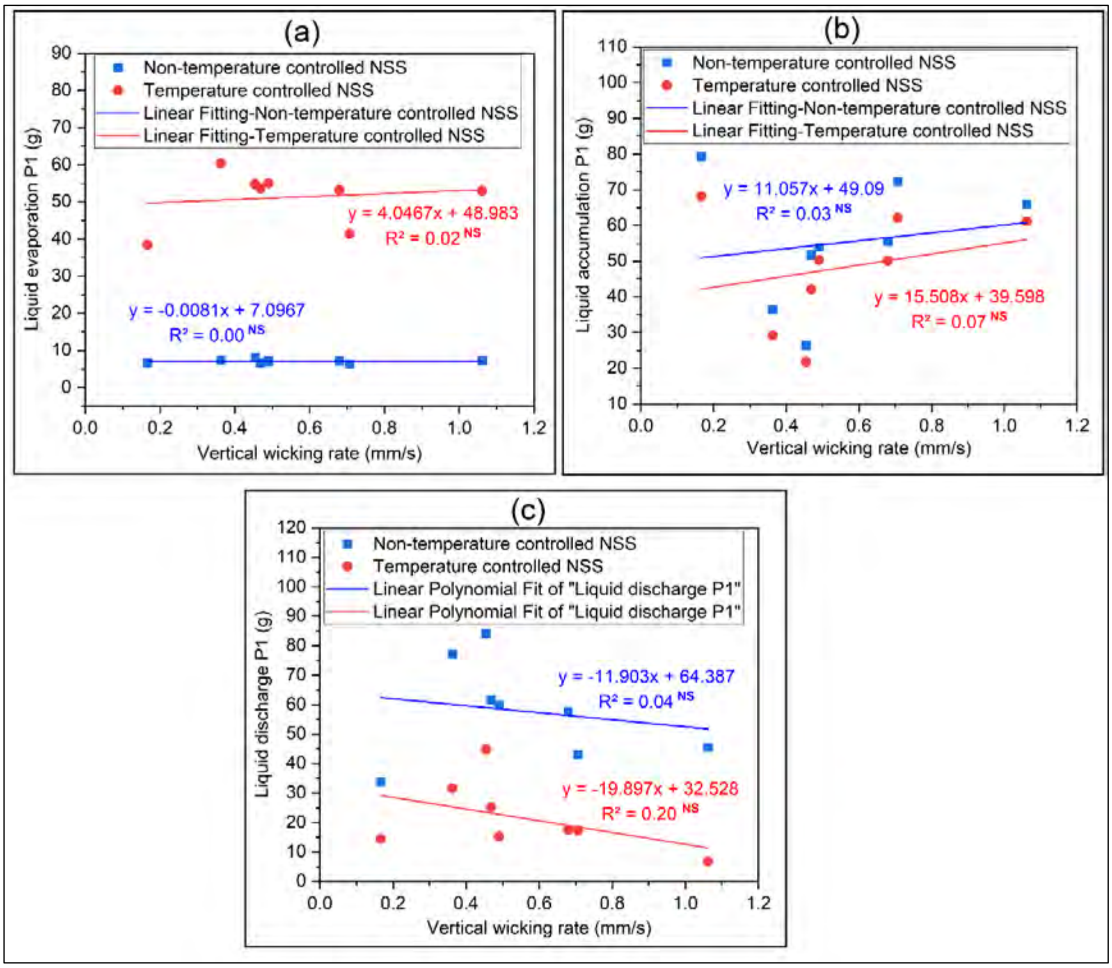

Figure 4.18. Relationship between rate of vertical wicking and (a) amount of liquid evaporation, (b) amount of liquid accumulation and (c) amount of liquid discharged

The relationship between the amount of liquid evaporation, accumulation, and discharge, determined during P1 on both non-temperature and temperature-controlled NSS, and the rate of vertical wicking are presented in Figures 4.18 a, b, and c respectively. The R^2 value of_0.21 and lower reflects a negligible correlation in all cases. This might be possible because of the entirely different working principle of NSS and the standard vertical wicking test. As, the water is supplied from an indefinite reservoir to the bottom edge of the fabric strip in a vertical wicking test, where it is wicked upward against the direction of gravity. In contrast, on NSS the liquid is supplied to the upper middle area of the fabric at a rate much lower than that from an indefinite reservoir. Moreover, the liquid supplied in the fabric can spread in all directions and the impact of gravity-induced flow in a downward direction cannot be neglected any longer under continuous sweating. These differences may justify the insignificant and negligible correlation between the rate of vertical wicking and NSS measurements of liquid mass distribution.

4.9.4 NSS parameters of liquid mass distribution versus the rate of horizontal wicking

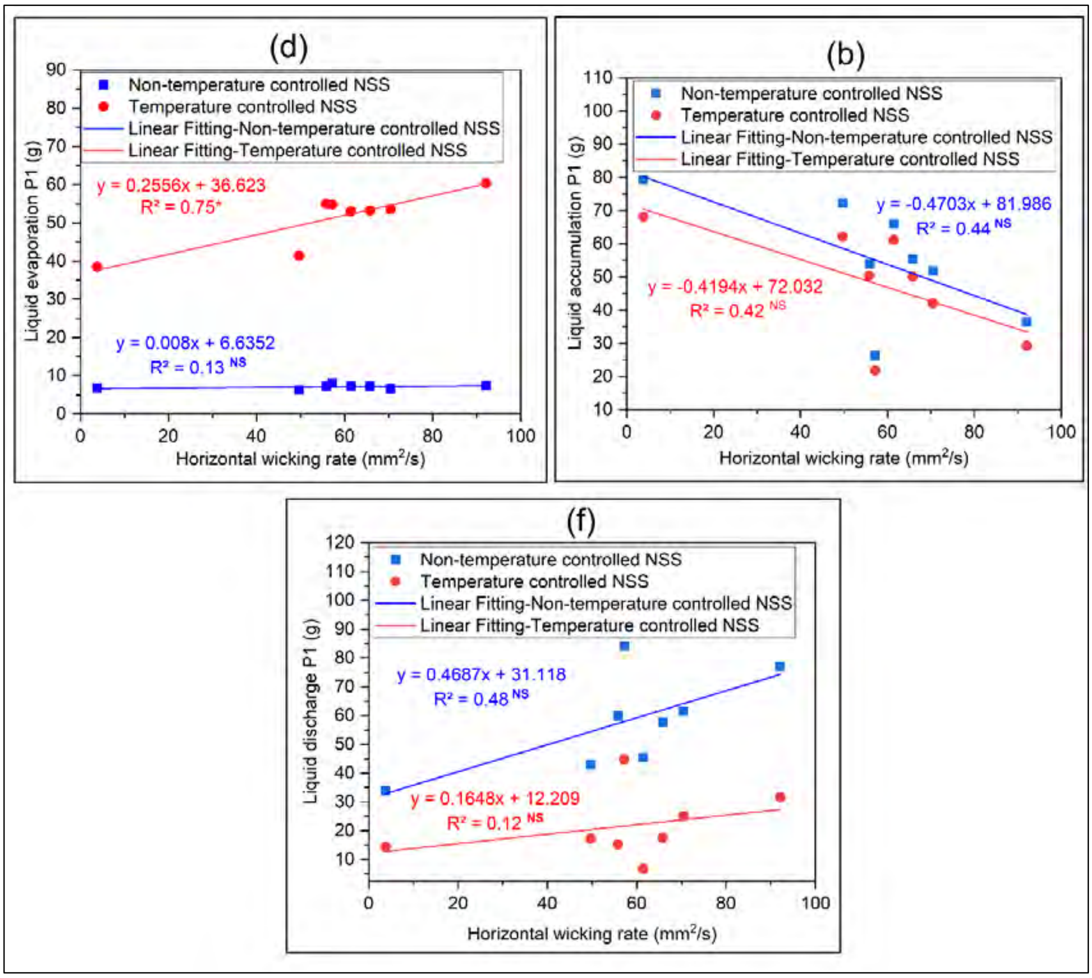

Figure 4.19. Relationship between rate of horizontal wicking and (a) amount of liquid evaporation, (b) amount of liquid accumulation and (c) amount of liquid discharged

Figure 4.19 presents the correlation between the NSS parameters of liquid mass distribution and fabrics rates of horizontal wicking tests using linear regression analysis. Figures 4.19 a, b, and c, show the relationship between the rate of horizontal wicking and the mass of liquid evaporation, accumulation, and discharge respectively, as recorded during P1 for both non-temperature and temperature-controlled NSS.

From Figure 4.19a, the correlation between liquid evaporation and rate of horizontal wicking is not significant at non-temperature-controlled NSS (R^2=0.13^{NS}) and becomes significant and highly positive when measured at the temperature-controlled NSS (R^2=0.75*). Since, at non-temperature-controlled NSS, the values of liquid evaporation during P1 in fabrics vary within a narrow range of 1.8g, therefore is less predictable by the corresponding spreading rate of liquid in the horizontal wicking test. However, at the simulated skin and sweat temperatures of NSS, where the mass of liquid evaporation increases substantially, the range of evaporation become also broader at 21.8g. Perhaps because of this increase in variations, the rate of horizontal wicking is found to be significantly correlated with the rate of liquid evaporation at high temperatures.

Figure 4.19b, on the other hand, shows a moderate negative but not-significant correlation between the rate of horizontal wicking and liquid accumulation during P1 at both, non-temperature (R^2=0.44) and temperature-controlled NSS (R^2=0.42). A possible explanation for this equal strength of the association is the almost uniform behaviour of fabrics liquid accumulation during P1 at both normal and elevated temperatures of NSS.

Figure 4.19c shows a moderate positive but not significant correlation (R^2=0.48^{NS}) between the liquid discharge during P1 and horizontal wicking rate for non-temperature-controlled NSS, and negligible correlation ((R^2=0.12^{NS}) for temperature-controlled NSS. Since, at elevated temperatures, the mass of liquid discharge during P1 is reduced substantially because of a substantial increase in liquid evaporation during P1 but small decrease in liquid accumulation during P1the range of variation in liquid discharge narrows down to 30.3g from 50.3g at no-temperature control NSS. Possibly, this narrowing of range and changing sequence of fabrics in the mass of liquid discharge during P1 at temperature-controlled NSS is likely to make it less predictable by the corresponding change in horizontal wicking rate.

4.10 Conclusions

This chapter introduced the NSS as a cutting-edge instrument for the quantitative evaluation of fabric dynamic liquid moisture management properties at adjustable sweating rates, simulated skin and sweat temperatures and vertical orientation of a body posture. NSS measured the fabric rates of liquid accumulation, evaporation, dripping and drying simultaneously by simply weighing dynamically the amount of liquid supplied, evaporated, and dripped through fabrics. In addition, NSS also measured the rates of liquid flow through the fabric along upward, lateral, and downward directions concurrently by detecting the waterfront through temperature measurement. The eight kinds of unique moisture management knit fabrics were tested and results revealed that the measurements from NSS were highly reproducible and accurate. Higher liquid accumulation was observed among pure cotton (K1), polyester-cotton mix (K2), polyester-Coolmax® (K3) and polyester micro denier fabrics (K6). Lower liquid accumulation and higher liquid dripping were observed in mesh fabrics (K7 and K8). The higher evaporation was found in pure polyester fabrics with good wicking properties (K3 to K8).

Overall, higher drying rates were observed in pure polyester weft knit fabrics (K3 to K6) that accumulated enough liquid for prolonged evaporation. The drying times of fabrics were found to correlate strongly with the amount of liquid retained in the fabrics. Despite having a smaller covered area by open mesh warp knit fabrics (K7 and K8), they demonstrated greater potential for liquid evaporation during the sweating phase and quick-drying ability (low drying time) during the drying phase. The liquid accumulation and evaporation abilities of fabrics were discovered to be greatly influenced by the knit types, nature of raw material, fibres and their composition rather than the areal density and thickness of fabrics under observation. Fabric intrinsic accumulation capacity and intrinsic evaporation capacity were additionally investigated, which readily differentiated the lightweight fabric with a higher potential for liquid accumulation and evaporation as desired for lightweight and high-performance moisture management apparel. The measurement accuracy as investigated by the total amount of liquid accumulated, evaporated, and dripped against the known mass of liquid supplied, was found to range from 98% to 100% with most tests exceeding 99%.

The rates of liquid flow through fabrics, determined by NSS itself, were found to be primarily determined by the knit type, knit design, and the inherent wicking potential of the fabrics' fibres. Against the bulk flow of liquid produced by continuous sweating, the fabrics containing polyester-Coolmax® (K3), polyester micro denier (K6) and polyester with durable moisture management finish (K5) exhibited consistent downward flow rates of liquid, showing great potential for excessive sweat management. Liquid accumulation P1 was discovered to be significantly negatively correlated with UFR, LFR, and DFRs, whereas liquid evaporation was found to be significantly positively correlated with LFR only. The liquid discharge during P1 was in significant positive correlation with the DFRs.

While correlating the results of NSS and those of MMT, the correlation was found significant and higher between the flow rates of NSS and “Top Maximum Wetted Radius” as well “Top Spreading Speeds” on MMT. Likewise, the liquid evaporation was also in strong association with “Top Maximum Wetted Radius” as well “Top Spreading Speeds” on MMT, instead of “Bottom Maximum Wetted Radius” and “Bottom Spreading Speeds” as one could expect intuitively. Similarly, in contrast to expectations, the liquid evaporation during P1 was discovered to be strongly negatively associated with "Accumulative one-way transport" and moderately negatively correlated with "OMMC." The liquid accumulation during P1, however, was fairly positively related with “Bottom absorption rate” and substantially negatively associated with “Maximum wetted radii” and “Spreading speeds” on each side of fabric. Nonetheless, the liquid discharge during P1 was only moderately positively related to the “Maximum wetted radii”.

When compared to the non-temperature-controlled NSS, at temperature-controlled NSS, the amount of liquid accumulation rose about 5.7 to 8.1 times and spanned over a larger range while fluctuating the position of fabrics in the relative degree of evaporation. The liquid accumulation was decreased only by a small amount whilst almost maintaining the fabric sequence of relative liquid accumulation. The liquid discharged was also reduced accordingly.

While comparing NSS results with standard vertical and horizontal wicking tests, the linear regression revealed that the amount of liquid evaporation, accumulation, and discharged, measured at both, temperature controlled, and non-temperature controlled NSS was in a very weak relationship with the vertical wicking rate of fabric. While the horizontal wicking rate was found in strong significant relation with the amount of liquid evaporation only at temperature-controlled NSS with the value of R^2=0.75*. On the other hand, a moderate correlation was identified between the amount of liquid accumulation and horizontal wicking rate with R^2 equals 0.44 and 0.42 for non-temperature controlled and temperature controlled NSS, respectively. Moreover, in the case of liquid discharge, the horizontal wicking rate was in moderate relation for non-temperature controlled NSS with R^2=0.48, and in very weak correlation for temperature controlled NSS with R^2=0.12.

Chapter 5

Study of nature-inspired fibrovascular capillary bed patterns for efficient profuse sweat management

5.1 Introduction

Efficient thermal-moisture management for comfort and functional performance is key to activewear. Clothing designed for personal moisture management should regulate both sensible and insensible perspiration from the body to minimise the wet-thermal discomfort while sweating [145-148]. Sweat evaporation is a key medium of body cooling by heat dissipation especially in hot weather when ambient temperature becomes equal or rises above the skin temperature. Whereas clothing worn next to sweating skin may act as a barrier for heat dissipation, vapour transmission, and liquid evaporation between the body microclimate and the environment. Therefore, it is necessary to develop clothing with properties like quick sweat absorption, fast-spreading and evaporation across the sweating regions so the wearer can feel cool and dry [149-151].

Many advancements in the development of moisture management fabrics have been reported in recent years, enhancing the fabric's absorption, wicking, evaporation, and quick-drying properties [152-154]. A wide range of fibres including, synthetic, natural, regenerated, and advanced functional fibres such as profiled fibres, multilobe fibre cross-sections, micro-denier fibres, bi-component fibres, cool touch, hydrophobic synthetic fibres endowed with hydrophilic functions have been introduced to construct moisture management fabrics [136, 155-157]. Similarly, with advances in yarn manufacturing techniques, the use of various novel blends and a variety of yarns such as Trans dry®, hollow yarn, soft twisted, plied yarns, soft-core spun yarn, and elastic yarns have been reported in the construction of activewear moisture management fabrics [42, 149, 158-163]. Likewise, it is found that fabric structures and finishing patterns can also significantly govern moisture management properties. Double-layer knit fabrics have a wettability gradient with a partial hydrophobic layer on the inner side and a super hydrophilic layer on the outer side is found of great potential to minimise the wet sensation, and stickiness and improve the one-way liquid transport for faster evaporation [28, 43, 44, 164-166]. In addition, the fabric structures with mesh openings are found favourable for high air-permeability, good heat and moisture vapour transmission especially desired for garments of tropical environments [150, 160, 167-169]. On the other hand, biomimicry has been recognized as a promising strategy for improving the moisture transport properties of fabrics. Biomimetics, of plant branching structures in fabrics, has shown great potential for enhanced one-way liquid transport and evaporation [35, 41, 170].

Although enhanced wicking combined with one-way liquid transport can be advantageous in managing body sweat under low to moderate sweating intensities, under heavy sweating, effective liquid and moisture transmission through clothing are crucial for improving the wearer's wet-thermal comfort. A person's impression of moisture comfort in continuous sweating is heavily impacted by the rate of liquid moisture transferred from the skin to the garment and then the environment [53]. To relieve the sweat load and obtain the comfort sensation of the body, the garment should accelerate the transmission of liquid sweat and vapours from the skin to the environment. While the accumulation of sweat in the fabric should be avoided to sustain the perpetual liquid and moisture transmission function of the fabric. However, if sweat transported from the skin to the fabric, under intense sweating, is not quickly dispersed and drained, its localised accumulation in the fabric, along with increasing wet sensation can influence the rate of one-way liquid transmission and thin film evaporation [171]. On the other hand, the improper spatial distribution of sweat into the entire garment can make it wet thoroughly, heavier, clumsy, and, even odorous thereby increasing the discomfort of the wearer under profuse sweating [62]. Similarly, the quick dry ability of fabric is adversely impacted by the higher accumulation of sweat in garments, creating serious concerns about the post-exercise chilling effect in cold climates [172, 173]. Research revealed that strategies controlling the areal density of the fabrics, mixing hydrophobic fibres with hygroscopic fibres in blends, or combining hydrophobic and hydrophilic yarns together in a fabric, creating some hydrophobic finishing patterns on highly absorbent fabrics can help decrease liquid accumulation and increase drying rates of fabrics. Nevertheless, with the growing hydrophobic portion in fabric, the areas of liquid saturation and rate of sweat transportation can rise quickly [55, 142]. Consequently, another nuisance of sweat dripping on the floor may come to face. The sweat dripped in an inappropriately, where doesn’t contribute to the cooling of the body, can also make the floor slippery causing performance disruption during some indoor games, concerts, or working conditions.

Indeed, a combination of hydrophobic and hydrophilic treatments can favour the patterned distribution and controlled release of superfluous sweat from the fabric, if designed properly. In this regard, mother nature has been very kind in providing creative solutions to the complex challenges, problems, and needs of mankind. Nature-inspired innovation, known as biomimicry, has provided a promising way of getting inspiration from various biological functions of living creatures and emulating them into innovative products and solutions [100, 171, 174-176]. In the human system of blood circulation, capillary beds are networks of fine vascular pathways, which play a central role in the cardiovascular system, facilitating the exchange of gasses, nutrients, hormones, and wastes between the blood and various tissue cells. A network of capillary beds may begin with a large artery carrying blood away from the heart and then branch into numerous tiny capillaries in the middle which then combine into a large vein carrying blood back to the heart [177, 178]. Concisely, the capillary bed consisting of an interconnected vascular network provides a novel system wherein the blood supplied from one end can be collected at the other end after passing through the plurality of fine branches.

Herein, inspired by the capillary bed of the cardiovascular system, a fibrovascular capillary bed (FVCB) network is introduced which was rationally designed to regulate the liquid sweat flux, liquid evaporation, body vapour transmission and collection of sweat dripping from fabric under profuse sweating. Typically, the middle of the chest and the back of the human body are high-intensity sweating zones. Here, the plurality of the branches in the middle of FVCB can prevent localized sweat accumulation into fabric by spreading it into numerous branched paths. While moving down from the middle to the bottom of the body trunk, the majority of fine branches can combine step by step, constituting a large terminal branch, which can provide a proper site for superfluous sweat drainage and collection.

To test the concept, a common moisture management fabric was laser cut into FVCB networks with ingeniously varying the number of branches and its liquid moisture management properties were evaluated using NSS. With this biomimetic system, the laser cut-produced FVCB networks demonstrated excellent potential for sweat regulation into branch path, higher area-specific evaporation, proper drainage and collection of superfluous sweat and improved drying efficiency in a simulated sweating and drying phase on NSS. Thereafter, to realize the practical application of the FVCB network in a moisture management garment, the FVCB network was created in a conventional moisture management fabric using a water-repellent mask of FVCB and spraying a superhydrophobic agent. After curing, as produced fabric demonstrated super hydrophilic characteristics in all the branch paths of its FVCB network while the rest of the areas exhibited superhydrophobic characteristics. The sweat absorbed into fabric was found to spread along FVCB paths while leaving the hydrophobic areas typically dry to facilitate the body vapour transmission. This design philosophy of creating the plurality of isolated hydrophobic regions within a super hydrophilic network of FVCB to regulate the sweat flux, facilitate body vapours transmission, higher area-specific evaporation, faster drying, and proper drainage and collection of sweat from fabric, can pave a novel way to engineer fabrics with the superior potential of liquid and moisture management under profuse sweating.

5.2 Experimental

5.2.1 Design and preparation of FVCB networks

The schematic design of a FVCB network is shown on the right side of Figure 5.1a, which in principle can manage the liquid distribution akin to blood flow in a natural capillary bed, as shown on the left. The FVCB network primarily consists of primary, secondary, and tertiary branches.

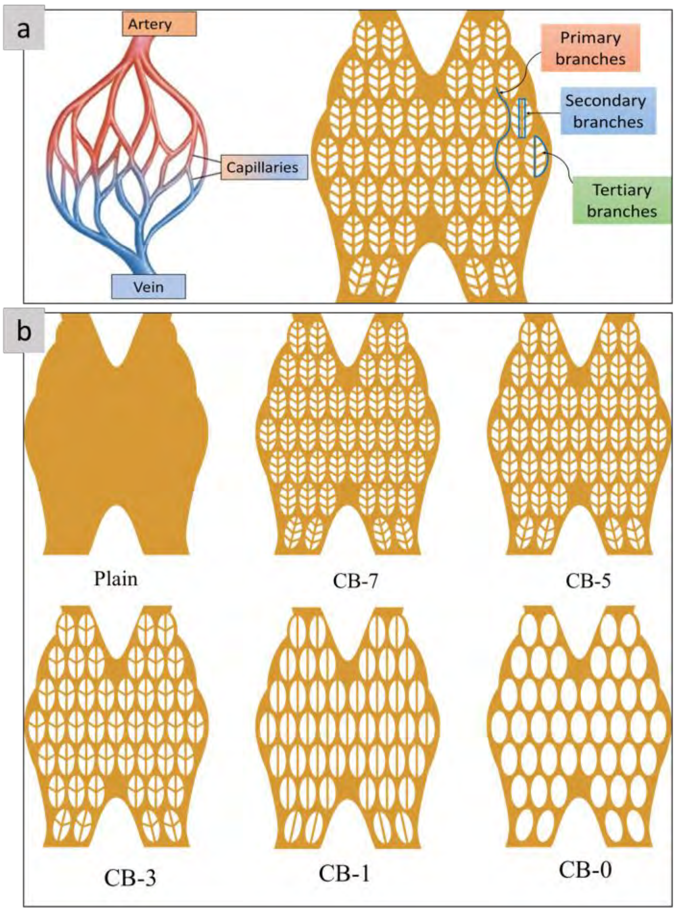

Figure 5.1. Nature-inspired design of laser-cut FVCB patterns. (a) Replication of natural blood flows through a capillary bed in a fabric having primary, secondary and tertiary branches. (b) Multiple variants of FVCB networks.

The primary and secondary branches are created within an elliptical shape. The side-by-side distribution of such elliptical units constituted the whole FVCB network in the fabric. The FVCB networks were designed based on the following criteria: (i) sweat from the skin should be absorbed quickly and spread along branches of the network from high-intensity sweating areas in the middle to the low-intensity sweating area on the periphery of the body; (ii) the FVCB network must enable the fast capillary flow and strong evaporation of liquid; (iii) the FVCB network must allow sweat discharged at the lower end of its sideways branches to be collected; (iv) the other areas except for the interconnected branches of the FVCB network should superhydrophobic without liquid sweat absorption. To unleash the potential of the perspective FVCB network for anticipated outcomes, the representative designs are revealed in Figure 5.1b. The schematic drawings were created in graphic design software, Adobe Illustrator CC 2018. From Figure 5.1b "plain" refer to the conventional fabric, used as a comparative reference, without branches while "CB" represents the FVCB networks and "number" indicates the corresponding number of branches within each elliptical shape. The area covered by each pattern was also determined by the same design software.

A conventional moisture management fabric (material: super hydrophilic polyester, areal density:130 gm^{-2}, absorbency time: less than 1sec,) was taken to produce one plain and five FVCB networks (i.e., CB-7 to CB-0) by a laser cutting technique according to the drawings shown in Figure 5.1b. For each pattern, three replicates were cut from the same fabric. The consistency among sample sizes was verified from the mean dry weight and standard deviations.

The liquid accumulation, dripping and drying properties of each pattern were studied using the novel sweating simulator (NSS) shown in Figure 5.2 and described in Chapter 3 [179]. The distilled water as the simulation of liquid sweat was supplied at a constant rate of 120 gh^{-1} at room temperature. Each test lasted for two hours in total, with phase 1 (P1) consisting of one hour of sweating and phase 2 (P2) consisting of one hour of drying. Three replicates of each pattern were tested to evaluate its repeatability, and the results obtained were plotted using Origin lab 2021. The tests were conducted under controlled environmental conditions at a temperature of 20±1°C and relative humidity of 65±2.5%.

The NSS works on the gravimetric measuring principle comprising a set of three electronic balances measuring real-time rates of liquid supplied, evaporated, and dripped from the fabric. The mass of liquid accumulation (m_{accu}) in the fabric at any instant can be calculated by Equation 5.1:

$$m_{accu} = m_{supp} - (m_{drip} + m_{evap}) \tag{5.1}$$

Where, m_{supp} is the mass of liquid supplied to the fabric, m_{drip} is the mass of liquid dripped from the fabric, and m_{evap} is the mass of liquid evaporated from the fabric.

Figure 5.2. Testing of fabric's liquid accumulation, dripping and evaporation properties on NSS

5.2.2 Fabric preparation for a proof-of-concept moisture management garment

A conventional moisture management fabric (pique knit, areal density 130 gm^{-2}) composed of super hydrophilic polyester yarns (70D/100F) was sourced from Startex Textile Ltd. Hong Kong. The fabric was cut into two pieces with an equal size of 45cm x 55cm, and then washed and dried according to ISO6330. As shown in Figure 5.3, one piece of fabric was treated on its backside to create a FVCB network by applying a capillary bed mask (made of a hydrophobic polypropylene sheet produced by laser cutting) and spraying the exposed area with a hydrophobic spray (ChoPores®). The depth of coating was controlled manually by adjusting the height and pressure of the spray gun based on experience gained from preliminary attempts. As a result of treatment, the area covered by the mask remained super hydrophilic while the area exposed became hydrophobic with a water contact angle of 125°. Consequently, an in-plane differential absorbency was realised in the fabric between treated and untreated areas.

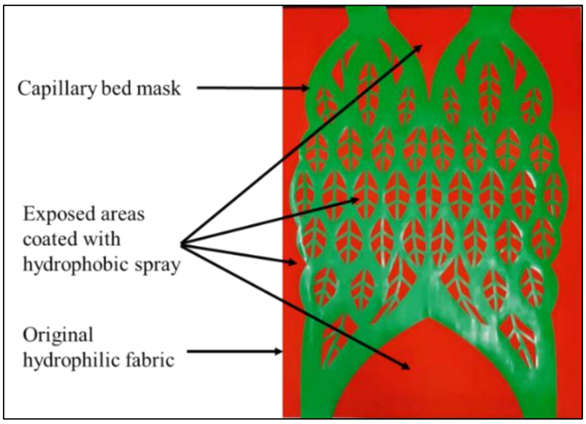

Figure 5.3. Creation of FVCB network on a hydrophilic fabric by applying mask and coating with hydrophobic spray

Both the fabrics, untreated and capillary bed treated, were tested for concurrent and real-time liquid moisture management properties using NSS at ambient conditions of 22± 2% °C temperature and 58±3% relative humidity. Before the experiment, the fabrics were preconditioned for 12 hours under the same environmental conditions. The tests were then conducted under continuous sweating for one hour at a constant sweat rate of about $120gh^{-1}$ followed by another hour of drying. The amount of sweat accumulated, dripped, and evaporated from each fabric was recorded and compared to evaluate its liquid moisture management performance.

5.3 Result and discussion

5.3.1 Liquid accumulation, dripping and evaporation in laser cut FVCB Patterns

Validation of specimen homogeneity

Figure 5.4a displays the dry mass and surface area of laser-cut specimens. The standard deviation in dry mass is indicated by error bars on respective column bars in the chart. The nominal variation indicates that the specimens produced by the laser cutting method are highly consistent in size and surface area. The plotted surface area of the specimen was determined by design software according to the drawing of each specimen. The dry mass and surface area are the largest for the plain specimen and decrease stepwise from CB-7 to CB-0 as the number of secondary and tertiary branches decreases, leaving a greater amount of empty space. A direct and strong positive linear relationship (R^2=0.999) between dry mass and surface area of fabrics is shown in Figure 5.4b, confirming that the mass of the specimen will vary directly according to the controlled surface area of the specimen in drawings. As a result, the mass of patterns can be easily tailored via the change in the surface area of the corresponding pattern design.

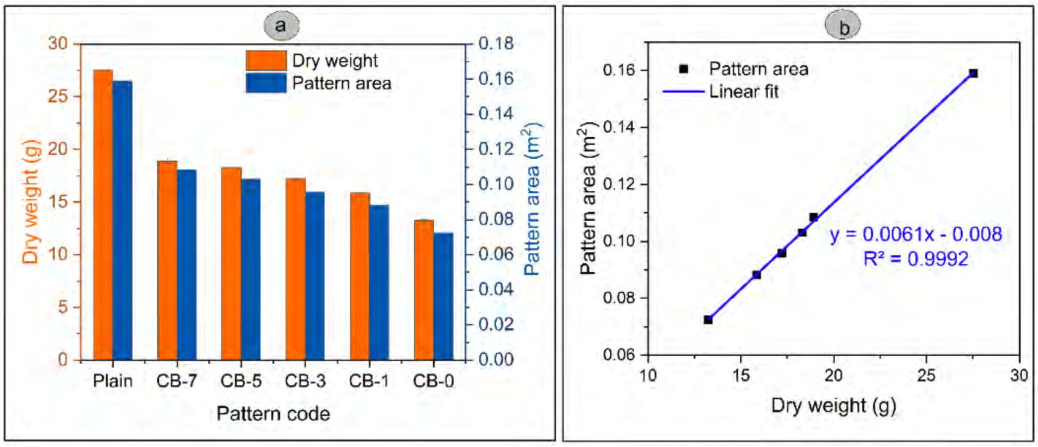

Figure 5.4. The physical properties of fabrics samples. (a) The dry mass and surface area of the pattern fabrics. (b) Relationship between the dry mass and surface area of fabric samples

Liquid accumulation

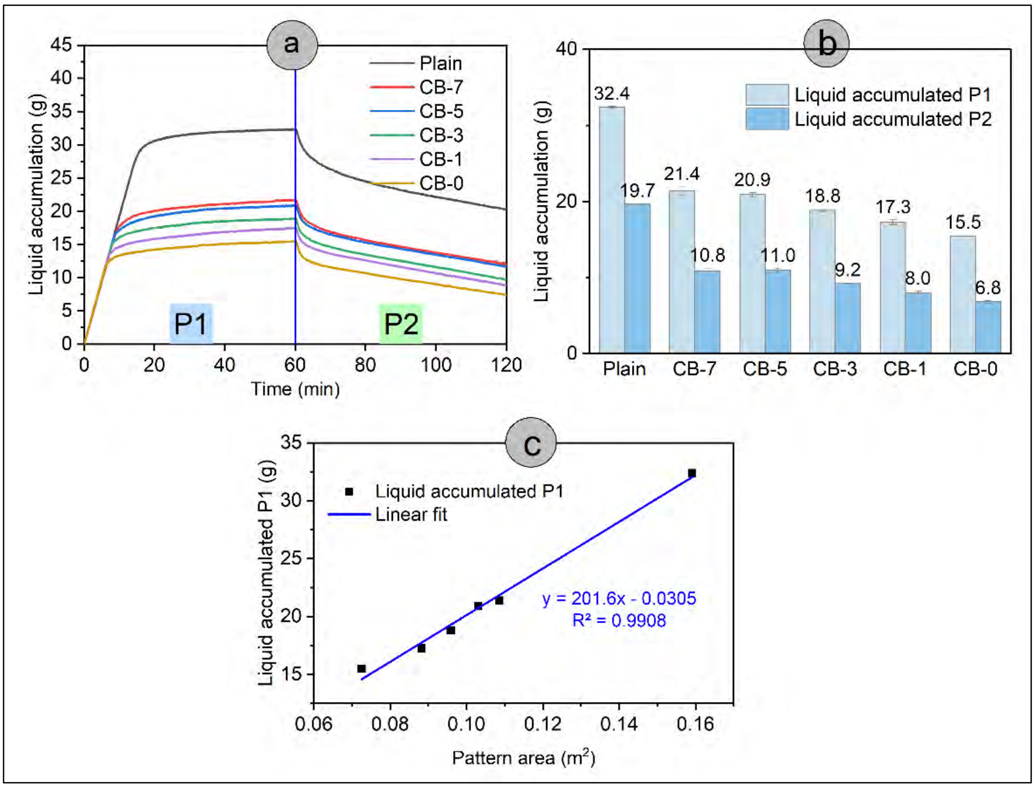

Figure 5.5. Liquid accumulation properties of laser cut FVCB networks. (a) Dynamic liquid accumulation during P1 and P2. (b) Absolute amount of liquid accumulation during P1 and P2. (c) Regression relationship between patterns surface area and maximum liquid accumulation during P1

The liquid accumulation properties of the designed specimen are summarised in Figure 5.5. The real-time liquid accumulation is shown in Figure 5.5a while the average amount of liquid accumulated in each phase of the test is plotted in Figure 5.5b. The real-time liquid accumulation curves indicate the mass change of liquid accumulated in the fabric over time. The constant rate of liquid accumulation during the early period of P1 corresponds to the constant rate of sweating, whereas the subsequent decrease in the rate of accumulation during P1 is caused by the onset of liquid dripping from fabric. Following dripping onset, the liquid accumulation tends to stabilise over time under the fabric's perpetual upward and lateral wicking action around the sweating zone until sweating stops during P1[109, 114, 180]. The FVCB networks with a small number of branches revealed that the liquid spread faster into them, covering the maximum area in a shorter period due to the corresponding small surface area, as indicated by their shortening period of the constant rise of liquid accumulation in Figure 5.5a.

The results of the linear regression between surface area and liquid accumulation as revealed in Figure 5.5c indicates that liquid accumulation changes linearly with surface area. As R^2=0.9908, the change in the surface area of the specimen can explain approximately 99% of the change in liquid accumulation. Hence, the plain fabric achieved the highest liquid accumulation because of its higher surface area for liquid spreading and thus ability to delay dripping during P1. In the other FVCB networks from CB-7 to CB-0, as the total surface area decreased by decreasing the number of secondary and tertiary branches, the liquid accumulation decreased accordingly. The liquid wicked into the fabric is held in place among macro and micro pores formed at the inter-yarn and intra-yarn levels of the fabric, maintaining the consistent wicking and evaporation of liquid during P1.

At the start of P2, in addition to evaporation, an instantaneous fall in the curve was due to the residual dripping of liquid during P2. However, soon after the dripping ended, the slopes of curves became constant indicating the drying occurred at a constant rate of evaporation. By the end of P2, the relative position of the curves indicates that higher the liquid accumulated during P1 more the liquid accumulated during P2. The average amount of liquid accumulated during each phase is shown separately in Figure 5.5b.

The quick-drying ability of specimens mainly relies on the liquid accumulation during P1. At a constant rate of liquid supply, less amount of liquid stored in P1 results in a higher drying efficiency of the fabric during P2. Herein, the drying efficiency is defined as the percentage of the liquid evaporated during P2 to the amount of liquid accumulated during P1 minus the amount of liquid dripped during P2, which is presented in Figure 5.6. Compared to plain fabric, the FVCB networks are found to improve the quick drying ability by 24% to 39%.

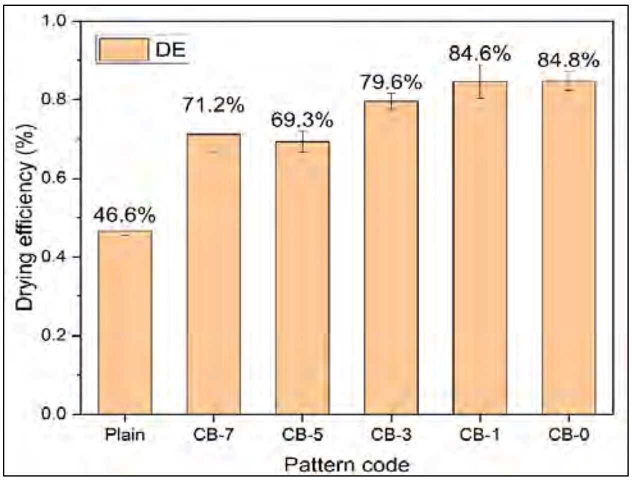

Figure 5.6. Drying efficiency of plain and CBVF networks

Liquid discharge

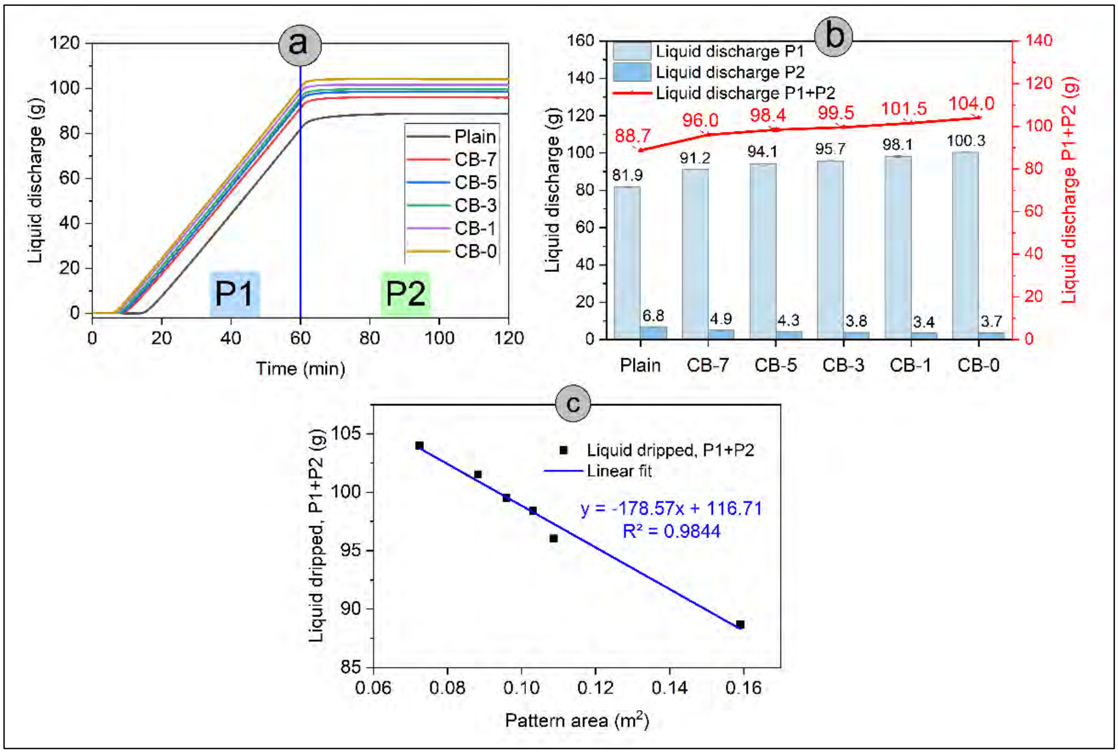

Figure 5.7. Liquid discharge proprieties of laser cut FVCB networks. (a) Dynamic liquid discharge during P1 and P2. (b) Absolute amount of liquid discharged during P1, P2 and P1+P2. (c) Regression relationship between pattern surface area and total amount of liquid dripped during P1 and P2

The liquid discharge by dripping is summarised in Figure 5.7. The real-time curve plotted in Figure 5.7a demonstrates the mass of liquid dripping over time. A constant rate of liquid discharge can be observed in all specimens during P1. However, the prominent late start and lower liquid discharge are clearly visible in plain fabric. Instead, the liquid discharge accelerates in FVCB networks with decreasing number of branching due to the decrease in the corresponding surface area. The quicker start of liquid dripping leads to a higher amount of liquid discharged. The phase-wise and cumulative amount of liquid discharged is presented in Figure 5.7b. The amount of liquid discharged during P1, as well as that during P1+P2, increases slightly with decreasing the surface area of the specimen from CV-7 to CB-0. However, a few amounts of liquid discharged during P2 is followed by the termination of liquid supplied during P1. In contrast, the remarkably large amount of liquid discharge during P1 is attributed to the continuous supply of liquid during P1.

It is noteworthy that, under continuous sweating, the liquid initially spreads on fabric in all directions. Nevertheless, with the growing content of liquid over time, the water saturation in the position just below the sweat area may rise quickly. As a result, the liquid flow rate through the fabric increases in the saturation direction, causing the liquid to move down and spread along the fabric. Upon continuous sweating, though the evaporation may increase with the increasing wet area of fabric, a stable stage may arrive when the liquid reaches the bottom edge. The gravity force of the continuously accumulating liquid at the bottom edge eventually overcomes the liquid surface tension and finally drips off. Once the dripping begins, the ongoing rate of dripping will be primarily governed by the rate of liquid supply, because the liquid accumulation and evaporation have reached their maximum values by the onset of dripping. Nonetheless, at the forefront of liquid movement through the fabric, the intrinsic capillary pressure, the number of capillary branches, corresponding surface area and thickness of fabrics govern the resultant flow rate of the liquid through the fabric.

In the case of liquid spread on a larger area of plain fabric, the liquid may take longer to spread before reaching the bottom edge, leading to a relatively lower amount of liquid discharge. On the contrary, the reduced surface area induced by the decreasing number of capillary branches in FVCB networks has resulted in higher liquid discharge. Accordingly, liquid accumulation will decrease, and the quick-drying properties will be improved. Figure 5.8 compares the apparent spread area and the propensity of liquid dripping between plain and CB-7 fabrics. Compared with the plain specimen, the liquid has reached the pattern bottom and started to drip for CB-7 fabric within the same time interval, which is induced by the continuous branching network and the corresponding lower surface area of CB-7. According to Figure 5.7c, the amount of liquid discharged in both P1+P2 varies inversely with the surface area of the specimen, with R^2=0.9844 indicating a very strong linear relationship.

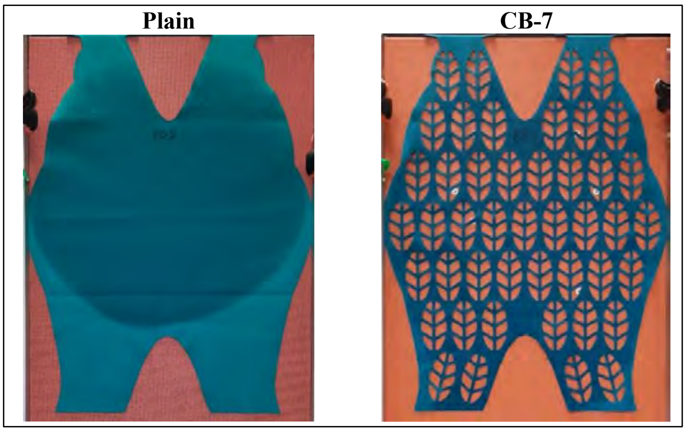

Figure 5.8. Spread of liquid into a plain vs CB-7 specimen after 8 minutes of continuous sweating

Liquid evaporation

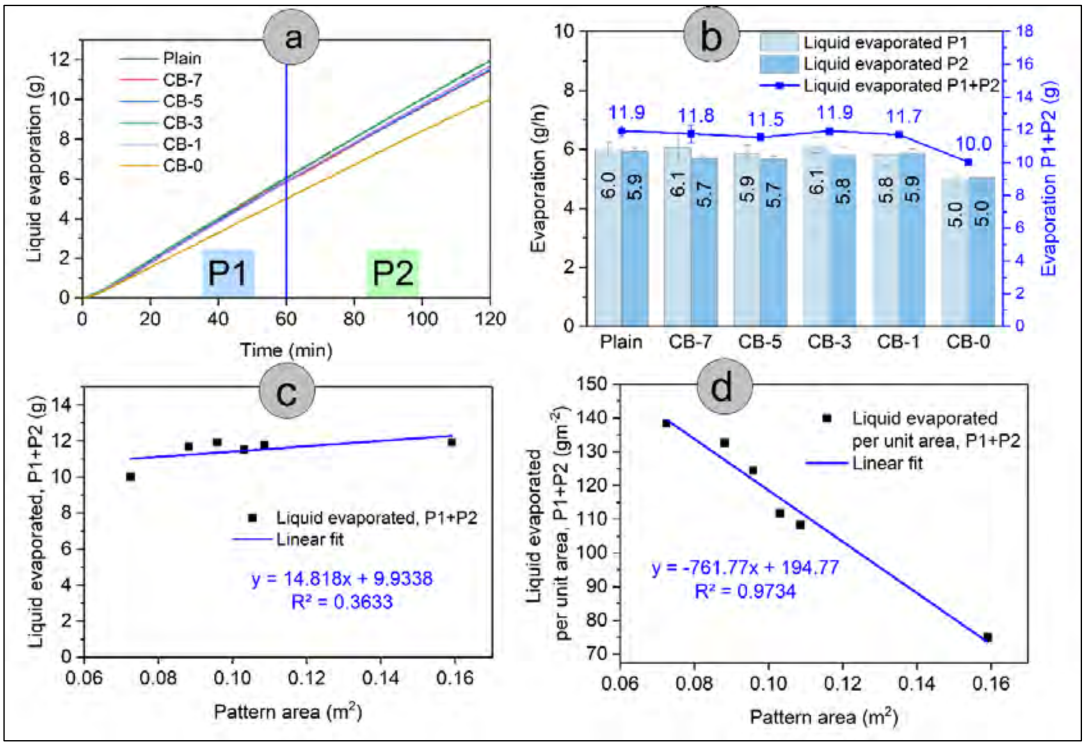

Figure 5.9. Liquid evaporation properties of laser cut FVCB networks. (a) Dynamic liquid evaporation during P1 and P2. (b) Absolute amount of liquid evaporated during P1, P2 and P1+P2. (c) Regression relationship between pattern surface area and absolute liquid evaporated during P1+P2. (d) Regression relationship between pattern surface area and surface-specific liquid evaporated during P1+P2

Figure 5.9 compares the liquid evaporation properties of the specimens. The real-time mass change of liquid evaporated over time is plotted in Figure 5.9a, and the phase-wise and cumulative mass of liquid evaporated are compared in Figure 5.9b, while the linear regression between the total mass of liquid accumulated during P1+P2 and the specimen surface areas is revealed in Figure 5.9c. Figure 5.9a shows that, except for specimen CB-0, the amount of liquid evaporated over time almost rises at the same magnitude among all specimens under testing including the plain one. The CB-0 pattern has no secondary or tertiary branches, whereas the CB-1 pattern has only one secondary branch. The liquid evaporation of CB-1 is greater than that of CB-0 yet comparable to that of all other patterns. As a result, the secondary branch appears to play an important role in increasing the liquid evaporation rate in FVCB networks. From Figure 5.9b, the amount of liquid evaporated during P1 and P2 is similar in all specimens. However, the total amount of liquid evaporated during P1+P2 is slightly lower for CB-0 with the value of 10g, while it varies closely between 11.5g and 11.9g in the other patterns. The value of R^2=0.3633, shown in Figure 5.9c, implies that the specimen area had a very small influence on the amount of liquid evaporation.

Figure 5.9d further depicts the results of the linear regression between surface area and evaporation per unit fabric area (unit: gm^{-2}). The slope of the linear fitting line indicates that the liquid evaporated per unit area of the pattern varies inversely with the surface area of fabric in a linear manner with R^2=0.9734. As a result, the highest liquid evaporation per unit area is 138.4 gm^{-2} in CB-0 over an area of 0.073 m^2 compared to the lowest value of 75 gm^{-2} in the plain fabric over an area of 0.159 m^2. The higher evaporation per unit area of specimen observed particularly in the FVCB networks can be explained by the evaporation edge effect at the boundaries of primary, secondary, and tertiary branches. The coexistence of dry empty spaces at the edges of wet branches potentially creates numerous sites of localised vapour pressure gradient throughout the fabric. In contrast to the 2D planar effect, a plain fabric surfaces the branching creates a 3D planar effect at their hydrophilic edges, as a result, the vapour cans leave at various angles, accelerating the rate of liquid evaporation in FVCB networks [181]. Moreover, no liquid leakage or dripping from the edges of the FVCB network was observed because all the supplied liquid moved along the fibrovascular branches governed by capillary flow. As the edge length increases, more water vapour diffuses into the environment, increasing the amount of liquid evaporation.

5.3.2 Liquid accumulation, dripping and evaporation in surface-treated FVCB fabric-A proof of concept

The proof-of-concept fabric, produced by the surface treatment of a conventional moisture management fabric is shown in Figure 5.10, which compares the liquid spread through the untreated fabric and the FVCB-treated fabric. The liquid spreads thoroughly in the untreated fabric, whereas it preferably flows along the super hydrophilic pattern branches of the FVCB-treated fabric. The sweat flow along branches was regulated by the different liquid absorbency formed in the treated and untreated areas due to the surface wettability gradient. The hydrophobic spray-treated areas appear dry, whereas the super hydrophilic branches appear wet, and water is saturated near the bottom edge. Interestingly, the liquid contained within the branches is directed to drain at specific locations along its terminal branches, allowing the collection of dripping sweat. The masses of liquid accumulated, dripped, and evaporated from both fabrics measured by NSS, are presented in Figure 5.11. Compared with the untreated fabric, the FVCB-treated fabric showed a decrease of 42% in liquid accumulation and an increase of 21% in liquid discharge. As a result, the quick drying ability of fabric will be improved remarkably. On the other hand, the absolute evaporated liquid is slightly reduced, whereas the liquid evaporation per unit wet area is higher in capillary bed-treated fabric.

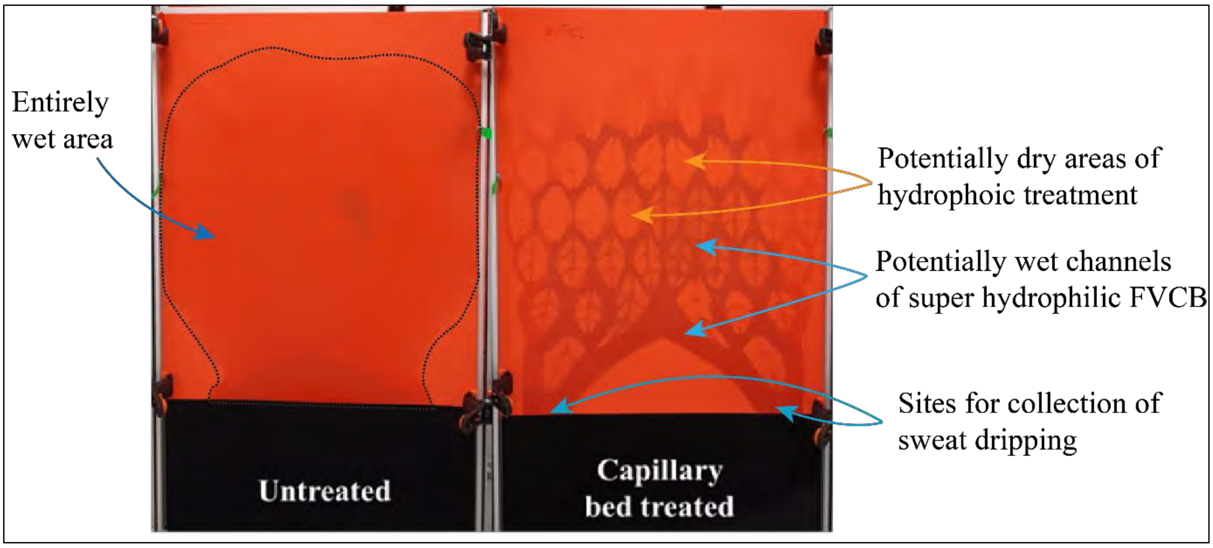

Figure 5.10. The sweat management style of untreated and capillary bed-treated fabrics

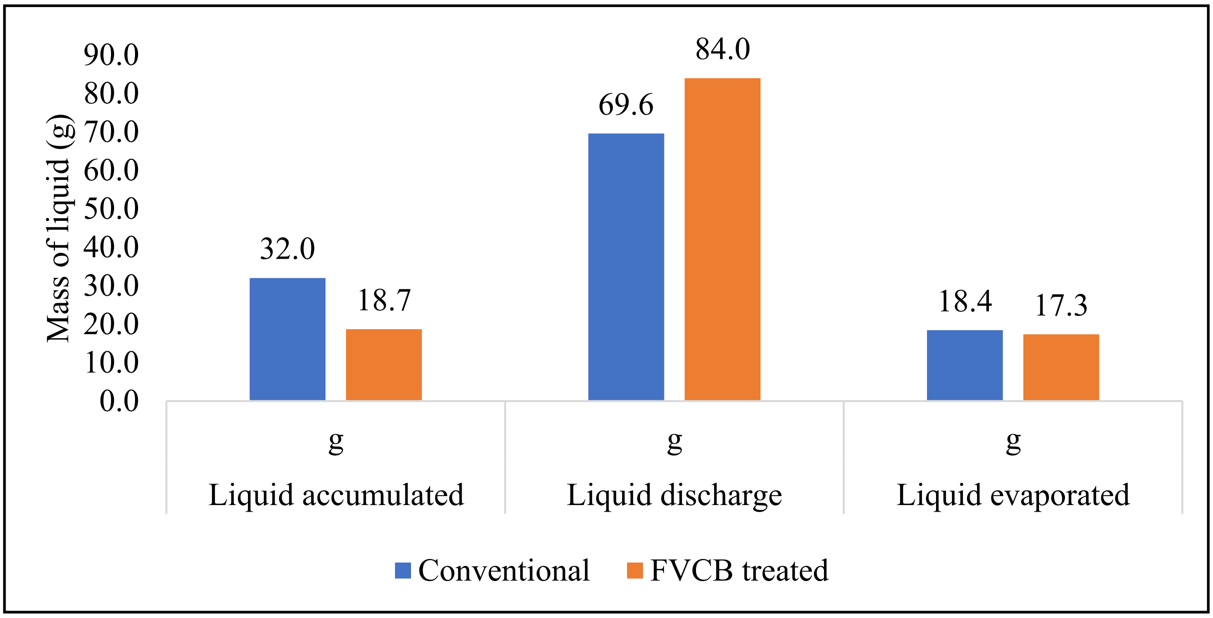

Figure 5.11. Liquid accumulation, dripping and evaporation in conventional vs FVCB-treated fabrics

In a conventional spreading of liquid in a pure hydrophilic fabric, the sweat is distributed spatially and thoroughly in all directions [44, 156, 182]. The increased sweat dispersion and accumulation in fabric, which also increases garment weight, can build wet-thermal stress over the body due to decreased air permeability and moisture vapour transmission. In contrast, a wettability gradient generated between the hydrophobic and hydrophilic areas in the FVCB system could contribute to faster sweat transportation, drainage, evaporation, and drying, as well as weight control of the shirt. Furthermore, unlike pure hydrophilic fabrics, the surface of a FVCB treated fabric will not be totally wet and saturated due to the surface wettability difference. Besides, when there is a lot of sweating, the FVCB network could regulate the liquid and make it drip from the sideways terminal branches at the lower ends, where water bags could be attached to collect it and prevent it from dripping on the floor. Additionally, except for the sweat evaporation from wet channels of the FVCB network, the dry areas in the neighbourhood can be used for vapour moisture diffusion, improving overall moisture management and clothing comfort.

5.4 Conclusions

Inspired by the capillary bed in the cardiovascular system, a new concept of liquid moisture management fabric is developed by introducing the FVCB networks. The FVCB networks were produced by a conventional hydrophilic fabric via laser-cut. The liquid spreading, accumulation, evaporation, dripping, and drying properties of FVCB networks were studied under simulating profuse sweating on a novel sweating simulator. The FVCB network accelerated the spread and flow of absorbed liquid along the branched network. Compared with a plain moisture management fabric, faster evaporation per unit wet area and drained faster per unit area of FVCB networks. In addition, the liquid accumulation is reduced, and drying efficiency is improved accordingly. Besides, the liquid evaporation per unit area is improved by decreasing the branch numbers with a lower corresponding surface area of the FVCB networks. In addition, the FVCB networks created by hydrophobic surface treatment of a conventional moisture management fabric demonstrated a reduction of about 42% in liquid accumulation, an increase of about 20% in liquid discharge, and a slight decrease in liquid evaporation. Nonetheless, the liquid evaporation per unit area increases due to the capillary bed design. The drained sweat could be collected at the end of the sideways branches instead of dripping inappropriately on the floor. The potential benefits of the FVCB-treated fabric were realised with more dry areas than wet channels, including noticeably higher evaporation per unit wet area, collection of sweat dripping and improved fabric drying properties, unanimously improving the overall comfort and moisture management characteristics of garments in profuse sweaty conditions. Consequently, this work on designing and creating FVCB network-based fabrics offers numerous opportunities for developing futuristic moisture management garments for efficient profuse sweat management.

Chapter 6

Conclusions and Suggestions for Future Research

6.1 Conclusions

In this study, liquid and moisture management properties of liquid and moisture management fabrics are investigated using a newly developed "novel sweating simulator" (NSS). Furthermore, a new concept of fibrovascular capillary bed (FVCB) network for liquid and moisture management in activewear is proposed and evaluated. The study comprised three major parts.

In the first part of the study, the basic version of the instrument, NSS, was introduced. In the simulation of a sweating upper back of an individual, the NSS consisted of a flat sweating plane with a sweating zone in the upper middle area. The sweating zone comprised eight sweating outlets distributed carefully with an area of about 750 cm^2. The rate of sweating was adjustable via the precision operation of an installed peristaltic pump. The inclination of the sweating plane was also adjustable to simulate the desired position of a body posture. The liquid moisture management on NSS refers to the measurement of liquid supplied and its distribution into fabric in terms of liquid accumulation, evaporation, and dripping. The NSS employed a gravimetric measuring principle comprising a set of three calibrated electronic balances for concurrent and real-time measurements of fabric rate of liquid accumulation, evaporation, dripping and drying.

To validate the accuracy and reproducibility of NSS measurements, eight different types of knitted moisture management fabrics were tested on NSS at a constant rate of liquid supply of 120 gh^{-1}. Three replicates of each fabric were tested under the controlled environmental condition of 20±1 °C and 65 ± 2.5% relative humidity. The distilled water at room temperature was used to simulate sweat. In this part of the study, the temperature of the sweating plane and sweat were adapted to room temperature. The results of the NSS tests helped to differentiate the fabric's liquid moisture management to a great extent. Some cotton-based fabrics showed higher liquid accumulation, lower liquid discharge and evaporation performance. However, in a pure cotton fabric with a relatively hydrophobic surface, the evaporation rate was low at the beginning but increased afterwards due to gradual increases in sweat absorption and spreading. The evaporation performance of polyester-based weft knit fabrics with different knit designs was found to be similar. However, their ability to store and discharge liquid was discovered to be affected significantly by the constituent fibre type and fabric density. The warp knit mesh type fabrics excelled all other fabrics in terms of evaporation and quick-drying ability. The sweating intensity and slope of the sweating plane were found to have significant effects on fabric liquid moisture management properties. The measurement system accuracy was investigated in terms of weight balance between the collective mass of liquid accumulated, evaporated, and dripped against the known mass of liquid supplied. The measurement accuracy ranged from 98 to 100%, with the majority of tests exceeding 99 %. The mass of liquid evaporated was fairly reproducible, with a maximum coefficient of variation (CV%) of less than 6%.

In the second part of the study, the NSS was further instrumented to control the temperature of the sweat and sweating plane to better simulate a person's sweating skin. The temperature of the sweating plane was regulated using a Proportion-Integral-Derivative (PID) temperature controller and the proper placement of thermocouples temperature sensors on the sweating plane. A thermostatic water bath and a PID temperature-controlled integrated heating element running along the path of the liquid, from the thermostatic water bath to the sweating zone, were used to control the temperature of sweat produced. In addition to temperature control, the NSS capability was further enhanced to measure the liquid flow rates through fabrics simultaneously in three different directions: upward, lateral, and downward, using the thermocouple technique. The eight fabrics were tested again on NSS at the simulated skin and sweat temperature of a sweating person. The results revealed that the measurements from NSS were highly reproducible and accurate. The measurement accuracy was found to range from 98% to 100% with most tests exceeding 99%. The mass of liquid evaporation as determined by NSS was highly reproducible with the maximum CV% of 3.1%. Higher liquid accumulation was observed among weft knit fabrics made of pure cotton (K1), polyester-cotton mix (K2), polyester-Coolmax® (K3) and polyester micro denier fabrics (K6). Lower liquid accumulation and higher liquid dripping were observed in warp knit fabrics composed of pure polyester fibres (K7 and K8). The evaporation rate was comparatively higher among all pure polyester fabrics showing super hydrophilic characteristics. Overall, higher drying rates were observed in pure polyester weft knit fabrics which hold enough liquid to maintain evaporation over an extended period. The drying times of fabrics were found to correlate directly with the amount of liquid retained in the fabrics. The liquid accumulation and evaporation rates of fabrics were discovered to be greatly influenced by the knit types, nature of raw material, fibres, and their composition rather than the areal density and thickness of fabrics.

The rates of liquid flow through fabrics, determined by NSS itself, were found to vary greatly with changing materials, knit construction, and wetting behaviour of fabrics tested. Under continuous sweating, the fabrics K3 (polyester-Coolmax®-bird eye structure), K5 (regular polyester having super hydrophilic finishing treatment-pique knit), and K6 (polyester micro denier-waffle structure) exhibited consistent downflow rates of liquid, showing great potential for excessive sweat management applications. The Pearson correlation results revealed that the liquid evaporation P1 was shown to be significantly positively correlated with LFR only, whilst liquid accumulation P1 was found to be strongly negatively correlated with UFR, LFR, and DFRs. Additionally, there was a strong positive association between the DFRs and the liquid discharge P1.

Against the non-temperature controlled NSS, when measured at temperature controlled NSS, the magnitude of liquid evaporation P1 increased by 5.7 to 8.1 times, amount of liquid accumulation reduced a little while the liquid discharged reduced according to the combined change in liquid evaporation and accumulation. As well, where the inter-fabric differences in liquid evaporation increased, the fabrics' evaporation rankings also changed at the simulated skin and sweat temperature.

Based on testing eight different kinds of moisture management knitted fabrics, it was found that the NSS can distinguish their dynamic liquid and moisture management properties well. It was also found that the liquid flow rates in different directions can be different, but generally are related to the liquid spreading area, which is moderately related to the evaporation rate during the sweating period. Comparing the testing results of NSS and those of MMT, it was found that "Top Max Wetted Radius" and "Top Spreading Speed" measured on MMT, instead of "Bottom Max Wetted Radius" and "Bottom Spreading Speed" as one would expect intuitively, have a stronger relationship with the liquid flow rates and evaporation rates measured on NSS. Furthermore, the "Accumulative one-way transport" and "OMMC" did not have a strong relationship with the evaporation rate and liquid discharge rate measured on NSS.

In the third part of the study, a new concept of a nature-inspired fibrovascular capillary bed (FVCB) network was introduced to develop fabrics with superior performance in liquid sweat management, especially in profuse sweating conditions. Five kinds of FVCB networks with a varying number of branches were produced by laser cutting a conventional moisture management fabric according to the drawings prepared in graphic design software. The liquid spreading, accumulation, evaporation, dripping and drying properties of FVCB networks were studied and compared against the conventional moisture management fabric using NSS. The liquid flow was discovered to move along and spread faster on the FVCB network. As a result, when compared to the conventional moisture management fabric, the liquid supplied was found to evaporate and drain faster in FVCB networks. The liquid accumulation was reduced, and the drying efficiency was improved accordingly. The absolute liquid evaporation though slightly reduced, area-specific liquid evaporation was found to increase substantially in capillary bed design. The sweat drained, instead of dripping inappropriately on the floor, was able to be collected properly by virtue of sweat regulation in an interconnected branching network. The FVCB networks as produced by the hydrophobic surface treatment of a conventional moisture management fabric, demonstrated about a 42% reduction in liquid accumulation, and a 20% increase in liquid discharge, aiding the quick drying characteristics of the fabric. The potential advantages of FVCB-treated fabric were realised in relatively more dry areas among wet channels, noticeably higher evaporation per unit wet area, and improved rapid drying abilities of fabrics.

6.2 Suggestions for future research

Suggestions for future research will be covered in following three parts:

1. New research directions in engineering fabrics for liquid and moisture management apparel
2. Further possible upgrades of NSS
3. Development of FVCB garments

6.2.1 New research directions in engineering fabrics for liquid and moisture management apparel

Based on the concurrent and real-time evaluation of liquid and moisture management properties of fabric using NSS, new research directions are envisaged to explore a variety of factors ranging from fibre, yarns, fabrics, physical and chemical finishing treatments influencing the fabric rate of liquid accumulation, spreading, evaporation, draining and drying under a wide range of controlled environmental conditions. This includes, but not limited to:

i. Investigation of synthetic, regenerated, and natural fibres blends for an optimum blend-ratio to achieve the desired liquid/moisture management properties for use in certain conditions.

ii. While supporting the green practices of sustainability and circularity, Investigation of recycled, reclaimed, and reused fibres and their blends to investigate their liquid and moisture management properties.
iii. Investigation of fabric areal density and thickness for a given kind of fabric having specific fibre and blend composition.
iv. Investigation of a variety of short-staple yarns for a given kind of moisture management fabrics.
v. Investigation of various physical parameters of fibres such as staple length, linear density, fibre cross-section, and surface profile of fibres in a given kind of yarn and its fabrics.
vi. Investigation of numerous kinds of composite yarns composed of both staple and filament fibre on liquid transport, accumulation, and evaporation properties of fabrics
vii. Investigation of hydrophilic and hydrophobic arrangement of yarns in a given type of fabric for desired moisture management properties.
viii. Investigation of various kinds of fabric structures and process settings for optimum construction of desired fabric with improved liquid and moisture management properties.
ix. Investigation of various kinds of fabric finishing patterns on their liquid and moisture management properties.
x. Investigation of the durability of moisture management treatments applied to the fibre or fabric surface by its repetitive testing in NSS against a certain sweating intensity.
xi. Investigation of various wettability gradients between two planes of fabric and its impact on fabric directional liquid transport and evaporation.
xii. Investigation of various bilayer and tri-layer fibrous assemblies on their liquid transmission, accumulation, and evaporation properties.
xiii. Evaluation of adaptable moisture-responsive materials and their functions in controlling the liquid and moisture management abilities of fabrics.
xiv. Investigation of various functional materials embedded in fabrics and their effect on liquid and moisture management behaviour at the regulated skin temperature.

6.2.2 Further developments on NSS and correlation with wearer trials

Further instrumentation on NSS can be envisioned in the following aspects:

i. A chamber can be built around the instrument to locally simulate the in-practice environmental conditions, extending NSS's applicability to real-world applications. Inside the chamber, the temperature, humidity, airflow, and solar radiation can be adjusted to simulate the various environmental conditions under observation.
ii. The instrument can be equipped with a camera and image processing software to study sweat-wicking, spreading, and downward migration under simulated sweating, and wearing conditions.
iii. The design of NSS should be improved to make it compact and composite one unit for easy handling, quick operation, and better space utilization in laboratories.
iv. The use of battery-operated weighing balances, wireless power transfer and wireless data acquisition can be established to minimise the use of cords in order to quickly stabilise the mass readings on the weighing balance, upon loading of the instrument.
v. Additionally, NSS can be equipped with computer-based software for automatic data acquisition, processing, visualisation, analysis, and preparation of results reports.
vi. Similarly, instead of continuous sweating for one hour, the testing of fabrics can also be studied at half-hour sweating intervals to closely simulate the period of typical wearer trials.
vii. The correlation between objective measurements of NSS and comfort evaluation of garments by subject trials also needs to be investigated in future.
viii. In addition, it would be valuable to explore how the data obtained from the NSS could be further utilized to improve or enhance existing methods, such as through the development of a comprehensive model to capture the missing features highlighted by the NSS.

6.2.3 Development of FVCB garments

For capillary bed liquid moisture management fabrics, the study at its preliminary stage has been reported here. However, cutting the pattern and fusing it to the fabric is not ideal for practical application! Hence, further attempts should be made in the following aspects:

i. The pattern can be treated on a bilayer or any moisture management fabric having a higher one-way liquid transport capacity so that the sweat comes out and then move along the FVCB channels at the outer surface of the fabric. In this way, the wearer may feel cool and dry due to lower sweat accumulation on the inner layer of the fabric.

ii. Integrating the FVCB pattern into fabric by using a combination of hydrophobic and hydrophilic yarns through some advance knitting techniques.
iii. The areas next to the FVCB network's branches can be transformed into a mesh-like structure to promote air permeability and release of insensible perspiration, thereby delaying the commencement of liquid sweating.
iv. Further investigations can be made by stitching a garment and conducting human trials for the evaluation of wet sensation and thermal comfort.

References

[1] B. Das, A. Das, V. K. Kothari, and R. Fangueiro, "Mathematical model to predict vertical wicking behaviour. Part II: flow through woven fabric," *The Journal of The Textile Institute,* vol. 102, no. 11, pp. 971-981, 2011.

[2] M. Datta Roy, R. Chattopadhyay, and S. K. Sinha, "Wicking performance of profiled fibre part a: Assessment of yarn," *Journal of The Institution of Engineers (India): Series E,* vol. 98, no. 2, pp. 155-163, 2017.

[3] M. Datta Roy, R. Chattopadhyay, and S. K. Sinha, "Wicking performance of profiled fibre part b: Assessment of fabric," *Journal of The Institution of Engineers (India): Series E,* vol. 99, no. 1, pp. 1-8, 2018.

[4] P. D. Dubrovski and M. Brezocnik, "Porosity and nonwoven fabric vertical wicking rate," *Fibers and Polymers,* vol. 17, no. 5, pp. 801-808, 2016.

[5] Y. K. Kamath, S. B. Hornby, H. D. Weigmann, and M. F. Wilde, "Wicking of Spin Finishes and Related Liquids into Continuous Filament Yarns," *Textile Research Journal,* vol. 64, no. 1, pp. 33-40, 1994.

[6] B. Kumar and A. Das, "Vertical wicking behavior of knitted fabrics," *Fibers and Polymers,* vol. 15, no. 3, pp. 625-631, 2014.

[7] U. J. Patil, C. D. Kane, and P. Ramesh, "Wickability behaviour of single-knit structures," *The Journal of The Textile Institute,* vol. 100, no. 5, pp. 457-465, 2009.

[8] P. Singh, A. Chatterjee, and S. Ghosh, "Vertical wicking tester for monitoring water transportation behavior in fibrous assembly," *Review of Scientific Instruments,* vol. 87, no. 10, pp. 105114 1-6, 2016.

[9] Q. Zhuang, S. C. Harlock, and D. B. Brook, "Longitudinal Wicking of Weft Knitted Fabrics: Part II: Wicking Mechanism of Knitted Fabrics Used in Undergarments for Outdoor Activities," *The Journal of The Textile Institute,* vol. 93, no. 1, pp. 97-107, 2002.

[10] S. Bajaj and S. Bains, "A comparative study on wicking behavior of blended knitted fabrics and their relationship with structural parameters," *Current Advances in Agricultural Sciences (An International Journal),* vol. 10, no. 2, pp. 126-131, 2018.

[11] K. Parveen Banu and S. Lakshmi Manokari, "Wicking behaviour of woven cotton fabrics by horizontal method," *International Journal of Science and Research,* vol. 3, pp. 1147-1151, 2014.

[12] D. Raja, G. Ramakrishnan, V. R. Babu, M. Senthilkumar, and M. B. Sampath, "Comparison of different methods to measure the transverse wicking behaviour of fabrics," *Journal of Industrial Textiles,* vol. 43, no. 3, pp. 366-382, 2012.

[13] C. B. Simile and H. W. Beckham, "Permeability–saturation–capillary pressure relations in textile fabrics from an integrated upward–horizontal–downward wicking test," *The Journal of The Textile Institute,* vol. 103, no. 9, pp. 945-951, 2012.

[14] R. M. Rossi, R. Stämpfli, A. Psikuta, I. Rechsteiner, and P. A. Brühwiler, "Transplanar and in-plane wicking effects in sock materials under pressure," *Textile Research Journal,* vol. 81, no. 15, pp. 1549-1558, 2011.

[15] M. Sarkar, J. Fan, and X. Qian, "Transplanar water transport tester for fabrics," *Measurement Science and Technology,* vol. 18, no. 5, pp. 1465-1471, 2007.

[16] A. Nazir, T. Hussain, F. Ahmad, and S. Faheem, "Effect of Knitting Parameters on Moisture Management and Air Permeability of Interlock Fabrics," *Autex Research Journal,* vol. 14, no. 1, pp. 39-46, 2014.

[17] A. Nazir, T. Hussain, G. Abbas, and A. Ahmed, "Effect of Design and Method of Creating Wicking Channels on Moisture Management and Air Permeability of Cotton Fabrics," *Journal of Natural Fibers,* vol. 12, no. 3, pp. 232-242, 2015.

[18] M. Umair, T. Hussain, K. Shaker, Y. Nawab, M. Maqsood, and M. Jabbar, "Effect of woven fabric structure on the air permeability and moisture management properties," *The Journal of The Textile Institute,* vol. 107, no. 5, pp. 596-605, 2016.

[19] A. Lolaki, M. Shanbeh, and S. Borhani, "Effect of structural parameters of porous yarns and fabric on air permeability and moisture transfer of double-face woven fabrics," *The Journal of The Textile Institute,* vol. 108, no. 6, pp. 992-1000, 2017.

[20] H. Ozdemir, "Permeability and wicking properties of modal and lyocell woven fabrics used for clothing," *Journal of Engineered Fibers and Fabrics,* vol. 12, no. 1, pp. 12-21, 2017.

[21] N. Ahsan, H. Tanveer, A. Faheem, and F. Sajid, "Effect of Knitting Parameters on Moisture Management and Air Permeability of Interlock Fabrics," (in English), *Autex Research Journal,* vol. 14, no. 1, pp. 39-46, 2014.

[22] P. Gurkan Unal and M. E. Üreyen, "Permeability properties of single jersey fabrics made of hollow yarns," *The Journal of The Textile Institute,* vol. 108, no. 11, pp. 1957-1965, 2017.

[23] E. T. Özkan and B. Meriç, "Thermophysiological comfort properties of different knitted fabrics used in cycling clothes," *Textile Research Journal,* vol. 85, no. 1, pp. 62-70, 2014.

[24] O. Troynikov and W. Wardiningsih, "Moisture management properties of wool/ polyester and wool/bamboo knitted fabrics for the sportswear base layer," *Textile Research Journal,* vol. 81, no. 6, pp. 621-631, 2011.

[25] M. M. Hassan and S. J. Leighs, "Quick dry ability of various quick drying polyester and wool fabrics assessed by a novel method," *Drying Technology,* vol. 35, no. 5, pp. 585-592, 2017.

[26] N. Erdumlu and C. Saricam, "Wicking and drying properties of conventional ring- and vortex-spun cotton yarns and fabrics," *The Journal of The Textile Institute,* vol. 104, no. 12, pp. 1284-1291, 2013.

[27] R. Fangueiro, A. Filgueiras, F. Soutinho, and M. Xie, "Wicking Behavior and Drying Capability of Functional Knitted Fabrics," *Textile Research Journal,* vol. 80, no. 15, pp. 1522-1530, 2010.

[28] T. Suganthi, P. Senthilkumar, and V. Dipika, "Thermal comfort properties of a bi-layer knitted fabric structure for volleyball sportswear," *Fibres & Textiles in Eastern Europe,* vol. 25, no. 1 (121), pp. 75-80, 2017.

[29] C. Saricam, "Absorption, wicking and drying characteristics of compression garments," *Journal of Engineered Fibers and Fabrics,* vol. 10, no. 3, pp. 146-154, 2015.

[30] M. Yanılmaz and F. Kalaoğlu, "Investigation of wicking, wetting and drying properties of acrylic knitted fabrics," *Textile Research Journal,* vol. 82, no. 8, pp. 820-831, 2012.

[31] S. Caroline J. and H. George, "Body mapping of sweating patterns in athletes: a sex comparison," *Medicine and Science in Sports and Exercise,* vol. 44, no. 12, pp. 2350–2361, 2012.

[32] Y. Inoue, G. Havenith, W. L. Kenney, J. L. Loomis, and E. R. Buskirk, "Exercise- and methylcholine-induced sweating responses in older and younger men: effect of heat acclimation and aerobic fitness," *International Journal of Biometeorology,* vol. 42, no. 4, pp. 210-216, 1999.

[33] G. Havenith, A. Fogarty, R. Bartlett, C. J. Smith, and V. Ventenat, "Male and female upper body sweat distribution during running measured with technical absorbents," *European Journal of Applied Physiology,* vol. 104, no. 2, pp. 245-255, 2008.

[34] C. J. Smith and G. Havenith, "Body mapping of sweating patterns in male athletes in mild exercise-induced hyperthermia," *European Journal of Applied Physiology,* vol. 111, no. 7, pp. 1391-1404, 2011.

[35] Q. Chen, J. Fan, and C. Sun, "The comfort evaluation of weft knitted plant structured fabrics and garment. II. Sweating manikin and wearer trial test on polo shirt," *Fibers and Polymers,* vol. 16, no. 9, pp. 2077-2085, 2015.

[36] B. Alber-Wallerström and I. Holmér, "Efficiency of sweat evaporation in unacclimatized man working in a hot humid environment," *European Journal of Applied Physiology and Occupational Physiology,* vol. 54, no. 5, pp. 480-487, 1985.

[37] M. Guan, S. Annaheim, J. Li, M. Camenzind, A. Psikuta, and R. M. Rossi, "Apparent evaporative cooling efficiency in clothing with continuous perspiration: A sweating manikin study," *International Journal of Thermal Sciences,* vol. 137, pp. 446-455, 2019.

[38] Y. Shapiro, K. B. Pandolf, and R. F. Goldman, "Predicting sweat loss response to exercise, environment and clothing," (in eng), *European Journal of Applied Physiology and Occupational Physiology,* vol. 48, no. 1, pp. 83-96, 1982.

[39] R. R. Gonzalez *et al.*, "Sweat rate prediction equations for outdoor exercise with transient solar radiation," *Journal of applied physiology,* vol. 112, no. 8, pp. 1300-1310, 2012.

[40] Y. Jhanji, D. Gupta, and V. Kothari, "Liquid transfer properties and drying behavior of plated knitted fabrics with varying fibre types," *Indian Journal of Fibre & Textile Research (IJFTR),* vol. 40, no. 2, pp. 162-169, 2015.

[41] Q. Chen, J. T. Fan, and M. K. Sarkar, "Biomimetics of branching structure in warp knitted fabrics to improve water transport properties for comfort," *Textile Research Journal,* vol. 82, no. 11, pp. 1131-1142, 2012.

[42] B. S. Babu, P. Senthilkumar, and M. Senthilkumar, "Effect of yarn linear density on moisture management characteristics of cotton/polypropylene double layer knitted fabrics," *Industria Textila,* vol. 66, no. 3, pp. 123-130, 2015.

[43] Y. Yang, X. Yu, L. Chen, and P. Zhang, "Effect of knitting structure and yarn composition on thermal comfort properties of bi-layer knitted fabrics," *Textile Research Journal,* vol. 91, no. 1-2, pp. 3-17, 2021.

[44] Q. Chen, D. Shou, B. Fu, R. Zheng, and J. Fan, "Development of Moisture Management Knitted Fabrics Integarated with Non-smooth Concave Surface and Mesh Structure," *Fibers and Polymers,* vol. 23, no. 4, pp. 1142-1149, 2022.

[45] L. B. Baker *et al.*, "Body map of regional vs. whole body sweating rate and sweat electrolyte concentrations in men and women during moderate exercise-heat stress," *Journal of Applied Physiology,* vol. 124, no. 5, pp. 1304-1318, 2018.

[46] C. J. Smith and G. Havenith, "Upper body sweat mapping provides evidence of relative sweat redistribution towards the periphery following hot-dry heat acclimation," *Temperature,* vol. 6, no. 1, pp. 50-65, 2019.

[47] V. Candas, J. P. Libert, and J. J. Vogt, "Human skin wettedness and evaporative efficiency of sweating," *Journal of Applied Physiology,* vol. 46, no. 3, pp. 522-528, 1979.

[48] T. T. Sakoi, Naoto ; Melikov, Arsen Krikor; Kolencíková, Sona, "Cooling clothing utilizing water evaporation," in *Indoor Air 2014 [HP0470] International Society of Indoor Air Quality and Climate*, Hong Kong, 2014.

[49] *Cooling Fabrics Market Global Forecast to 2025.* [Online]. Available: https://www.marketsandmarkets.com/pdfdownloadNew.asp?id=34980818, (Accessed on: December 22, 2022).

[50] G. Song and S. Mandal, Testing and evaluating the thermal comfort of clothing ensembles, in *Performance Testing of Textiles* Elsevier, 2016, pp. 39-64.

[51] G. Song, *Improving Comfort in Clothing*. Elsevier Science, 2011.

[52] *TM 79 Absorbency of Textiles*, AATCC, 2014.

[53] K. P. M. Tang, C. W. Kan, and J. T. Fan, "Evaluation of water absorption and transport property of fabrics," *Textile Progress,* vol. 46, no. 1, pp. 1-132, 2014.

[54] E. Jönsson, "A comparison of absorption methods," Degree of Master in Textile Technology, The Swedish School of Textiles, University of Boras, Report no.2010.7.8, 2011.

[55] K. Ghali, B. Jones, and J. Tracy, "Experimental Techniques for Measuring Parameters Describing Wetting and Wicking in Fabrics," *Textile Research Journal,* vol. 64, no. 2, pp. 106-111, 1994.

[56] P. R. Harnett and P. N. Mehta, "A survey and comparison of laboratory test methods for measuring wicking," *Textile Research Journal,* vol. 54, no. 7, pp. 471-478, 1984.

[57] Y.-L. Hsieh and B. Yu, "Liquid Wetting, Transport, and Retention Properties of Fibrous Assemblies: Part I: Water Wetting Properties of Woven Fabrics and Their Constituent Single Fibers," *Textile Research Journal,* vol. 62, no. 11, pp. 677-685, 1992.

[58] M. Karahan, "Experimental Investigation of the Effect of Fabric Construction on Dynamic Water Absorbtion in Terry Fabrics," *Fibres & Textiles in Eastern Europe,* vol. 3, no. 62, pp. 74-80, 2007.

[59] C. J. Hong and J. B. Kim, "A study of comfort performance in cotton and polyester blended fabrics. I. Vertical wicking behavior," *Fibers and Polymers,* vol. 8, no. 2, pp. 218-224, 2007.

[60] M. Lei, Y. Li, Y. Liu, Y. Ma, L. Cheng, and Y. Hu, "Effect of Weaving Structures on the Water Wicking–Evaporating Behavior of Woven Fabrics," *Polymers,* vol. 12, no. 2, p. 422, 2020.

[61] K. P. M. Tang, C. w. Kan, and J. t. Fan, "Comparison of test methods for measuring water absorption and transport test methods of fabrics," *Measurement,* vol. 97, pp. 126-137, 2017.

[62] K. P. M. Tang, C. W. Kan, and J. T. Fan, "Assessing and predicting the subjective wetness sensation of textiles: subjective and objective evaluation," *Textile Research Journal,* vol. 85, no. 8, pp. 838-849, 2015.

[63] D. Raja, V. R. Babu, M. Senthilkumar, G. Ramakrishnan, and N. Kannan, "A dynamic sweat transfer tester for analyzing transverse sweat transfer properties of multi-weave structure fabrics," *Journal of Industrial Textiles,* vol. 44, no. 2, pp. 211-231, 2014.

[64] B. S. Andrew TEAL, Iain Taylor, John Pratt, Neil Pryke, Helen Jones, "System and method for testing wetting of fabric samples," WO Patent WO2020161455A1, 2020.

[65] *WickView - James Heal.* [Online]. Available: https://www.jamesheal.com/instrument/wickview, 2023, (Accessed on: 17 May 2023).

[66] J. Hu, Y. Li, K.-W. Yeung, A. S. W. Wong, and W. Xu, "Moisture management tester: A method to characterize fabric liquid moisture management properties," *Textile Research Journal,* vol. 75, no. 1, pp. 57-62, 2005.

[67] H. S. Kim, S. Michielsen, and E. Denhartog, "New wicking measurement system to mimic human sweating phenomena with continuous microfluidic flow," *Journal of Materials Science,* vol. 55, no. 18, pp. 7816-7832, 2020.

[68] K. P. M. Tang, Y. S. Wu, K. H. Chau, C. W. Kan, and J. T. Fan, "Characterizing the transplanar and in-plane water transport of textiles with gravimetric and image analysis technique: Spontaneous Uptake Water Transport Tester," *Scientific Reports,* vol. 5, no. 1, p. 9689, 2015.

[69] K. P. M. Tang, K. H. Chau, C. W. Kan, and J. T. Fan, "Characterizing the transplanar and in-plane water transport properties of fabrics under different sweat rate: Forced Flow Water Transport Tester," *Scientific Reports,* vol. 5, p. 17012, 2015.

[70] T. Zimmerli and Weder, "Protection and Comfort@ A Sweating Torso for the Simultaneous Measurement of Protective and Comfort Properties of PPE," *ASTM SPECIAL TECHNICAL PUBLICATION,* vol. 1273, pp. 271-282, 1997.

[71] *ISO 18640-1:2018/AMD 1:2019 Protective clothing for firefighters — Physiological impact — Part 1:Measurement of coupled heat and moisture transfer with the sweating torso*, 2019.

[72] S. Annaheim, L.-c. Wang, A. Psikuta, P. Morrissey Matthew, A. Camenzind Martin, and M. Rossi René, "A new method to assess the influence of textiles properties on human thermophysiology. Part I: Thermal resistance," *International Journal of Clothing Science and Technology,* vol. 27, no. 2, pp. 272-282, 2015.

[73] M. Raccuglia, C. Heyde, A. Lloyd, S. Hodder, and G. Havenith, "Spatial and temporal migration of sweat: from skin to clothing," *European Journal of Applied Physiology,* vol. 118, no. 10, pp. 2155-2169, 2018.

[74] I. Holmer, "Heated manikins as a tool for evaluating clothing," *The Annals of Occupational Hygiene,* vol. 39, no. 6, pp. 809-818, 1995.

[75] I. Holmer, "Thermal manikin history and applications," *European Journal of Applied Physiology,* vol. 92, no. 6, pp. 614-618, 2004.

[76] T. Peters and W. Fay, "Composite yarns and moisture management fabrics made therefrom," Patent US20030182922A1, 2003.

[77] M. Katz, "Synthetic fiber fabrics with enhanced hydrophilicity and comfort," United States Patent US5888914A, 1999.

[78] Y. Jhanji, D. Gupta, and V. K. Kothari, "Moisture management properties of plated knit structures with varying fiber types," *The Journal of The Textile Institute,* vol. 106, no. 6, pp. 663-673, 2015.

[79] R. A. M. Iii and J. B. Cravotta, "Knitted fabric construction with improved moisture management," Patent WO2004079074A3, Sep 16, 2004.

[80] G. Supuren, N. Oglakcioglu, N. Ozdil, and A. Marmarali, "Moisture management and thermal absorptivity properties of double-face knitted fabrics," *Textile Research Journal,* vol. 81, no. 13, pp. 1320-1330, 2011.

[81] J. Foshee, "Knitted fabric with dual layer construction," Patent US20050282455A1, 2005.

[82] Rebecca P. Hurd and S. L. Sokolowski, "Moisture Management Support Garment With A Denier Differential Mechanism," United States Patent US20120178343A1, 2012.

[83] R. Kasdan and S. Kornblum, "Synthetic knit fabric having superior wicking and moisture management properties," United States Patent US6427493B1, 2002.

[84] M. Rock, E. P. Dionne, C. Haryslak, W. K. Lie, and G. Vainer, "Plaited double-knit fabric with moisture management and improved thermal insulation," United States Patent US7217456B1, May 15, 2007.

[85] J. Fan, Y.-c. Szeto, and M. K. Sarkar, "Fabric simulating the plant structure for moisture management," United States Patent US8486847B2, 2013.

[86] C. Qing, J. Fan, M. Sarkar, and J. Gaoming, "Biomimetics of Plant Structure in Knitted Fabrics to Improve the Liquid Water Transport Properties," *Textile Research Journal,* vol. 80, no. 6, pp. 568-576, 2010.

[87] C. Qing, F. Jin Tu, S. Manas Kumar, and K. Bal, "Plant-based biomimetic branching structures in knitted fabrics for improved comfort-related properties," *Textile Research Journal,* vol. 81, no. 10, pp. 1039-1048, 2011.

[88] C. Incorporated. *Wicking windows™ moisture management technology for cotton.* [Online]. Available: https://www.cottoninc.com/wp-content/uploads/2017/12/TRI-3020-Wicking-Windows-Moisture-Management-Technology-for-Cotton.pdf, 2006, (Accessed on: March 04, 2021).

[89] T. Kawase, T. Fujii, and M. Minagawa, "Repellency of Textile Assemblies: Part I: Apparent Contact Angle of Wax-Coated Monofilament Mesh Screen," *Textile Research Journal,* vol. 57, no. 4, pp. 185-191, 1987.

[90] *TransDRY® Technology.* [Online]. Available: https://www.cottonworks.com/topics/fabric-technology/performance-technologies/transdry-technology/, (Accessed on: March 03, 2021).

[91] P. S. Brown and B. Bhushan, "Bioinspired materials for water supply and management: water collection, water purification and separation of water from oil," *Philosophical Transactions of the Royal Society A: Mathematical, Physical and Engineering Sciences,* vol. 374, no. 2073, p. 20160135, 2016.

[92] C. Pang, C. Lee, H. E. Jeong, and K. Y. Suh, Skin and dry adhesion, in *Living Machines: A Handbook of Research in Biomimetic and Biohybrid Systems*, 2018, pp. 200-207.

[93] S.-Y. Teh, R. Lin, L.-H. Hung, and A. P. Lee, "Droplet microfluidics," *Lab on a Chip,* 10.1039/B715524G vol. 8, no. 2, pp. 198-220, 2008.

[94] Y.-Q. Liu *et al.*, "Laser-structured Janus wire mesh for efficient oil–water separation," *Nanoscale,* 10.1039/C7NR06110B vol. 9, no. 45, pp. 17933-17938, 2017.

[95] Y. Sun and Z. Guo, "Recent advances of bioinspired functional materials with specific wettability: from nature and beyond nature," *Nanoscale Horizons,* 10.1039/C8NH00223A vol. 4, no. 1, pp. 52-76, 2019.

[96] J. Ju, H. Bai, Y. Zheng, T. Zhao, R. Fang, and L. Jiang, "A multi-structural and multi-functional integrated fog collection system in cactus," *Nature Communications,* vol. 3, no. 1, p. 1247, 2012.

[97] H. Chen *et al.*, "Continuous directional water transport on the peristome surface of Nepenthes alata," *Nature,* vol. 532, no. 7597, pp. 85-89, 2016.

[98] É. Lorenceau and D. QuÉRÉ, "Drops on a conical wire," *Journal of Fluid Mechanics,* vol. 510, pp. 29-45, 2004.

[99] Y. Si and Z. Dong, "Bioinspired Smart Liquid Directional Transport Control," *Langmuir,* vol. 36, no. 3, pp. 667-681, 2020.

[100] L. Lao, D. Shou, Y. S. Wu, and J. T. Fan, "“Skin-like” fabric for personal moisture management," *Science Advances,* vol. 6, no. 14, 2020.

[101] D. Miao, Z. Huang, X. Wang, J. Yu, and B. Ding, "Continuous, Spontaneous, and Directional Water Transport in the Trilayered Fibrous Membranes for Functional Moisture Wicking Textiles," *Small,* vol. 14, no. 32, p. 1801527, 2018.

[102] K. A. McCulloh, J. S. Sperry, and F. R. Adler, "Water transport in plants obeys Murray's law," *Nature,* vol. 421, no. 6926, pp. 939-942, 2003.

[103] T. D. Wheeler and A. D. Stroock, "The transpiration of water at negative pressures in a synthetic tree," *Nature,* vol. 455, no. 7210, pp. 208-212, 2008.

[104] X. Wang, Z. Huang, D. Miao, J. Zhao, J. Yu, and B. Ding, "Biomimetic Fibrous Murray Membranes with Ultrafast Water Transport and Evaporation for Smart Moisture-Wicking Fabrics," *ACS Nano,* vol. 13, no. 2, pp. 1060-1070, 2019.

[105] B. Dai *et al.*, "Bioinspired Janus Textile with Conical Micropores for Human Body Moisture and Thermal Management," *Advanced Materials,* vol. 31, no. 41, p. 1904113, 2019.

[106] Y. Peng *et al.*, "Integrated cooling (i-Cool) textile of heat conduction and sweat transportation for personal perspiration management," *Nature Communications,* vol. 12, no. 1, 2021.

[107] R. Hu *et al.*, "Bilayer Nanoporous Polyethylene Membrane with Anisotropic Wettability for Rapid Water Transportation/Evaporation and Radiative Cooling," *ACS Applied Materials & Interfaces,* vol. 14, no. 7, pp. 9833-9843, 2022.

[108] G. Bedek, F. Salaün, Z. Martinkovska, E. Devaux, and D. Dupont, "Evaluation of thermal and moisture management properties on knitted fabrics and comparison with a physiological model in warm conditions," *Applied Ergonomics,* vol. 42, no. 6, pp. 792-800, 2011.

[109] A. Patnaik, R. S. Rengasamy, V. K. Kothari, and A. Ghosh, "Wetting and Wicking in Fibrous Materials," *Textile Progress,* vol. 38, no. 1, pp. 1-105, 2006.

[110] B. Miller and D. B. Clark, "Liquid Transport Through Fabrics; Wetting and Steady-State Flow Part I: A New Experimental Approach," *Textile Research Journal,* vol. 48, no. 3, pp. 150-155, 1978.

[111] R. J. Good, "Contact angle, wetting, and adhesion: a critical review," *Journal of Adhesion Science and Technology,* vol. 6, no. 12, pp. 1269-1302, 1992.

[112] S. Feier-Iova, "The behaviour of water drops on insulating surfaces stressed by electric field," Technische Universität, 2009.

[113] A. W. Adamson and A. P. Gast, *Physical chemistry of surfaces*. Interscience publishers New York, 1967.

[114] Y. L. Hsieh, "Liquid Transport in Fabric Structures," *Textile Research Journal,* vol. 65, no. 5, pp. 299-307, 1995.

[115] N. Mao and S. J. Russell, "Directional Permeability in Homogeneous Nonwoven Structures Part I: The Relationship between Directional Permeability and Fibre Orientation," *The Journal of The Textile Institute,* vol. 91, no. 2, pp. 235-243, 2000.

[116] B. Miller, "Critical evaluation of upward wicking tests," *International Nonwovens Journal,* vol. 9, no. 1, pp. 35-40, 2000.

[117] *TM 195 Liquid Moisture Management Properties of Textile Fabrics*, AATCC, 2017.

[118] *TM 198 Horizontal wicking of Textiles*, AATCC, 2018.

[119] *BS 4554:1970. Method of Test for Wettability of Textile Fabrics*.

[120] D. Raja, S. PriyaLatha, and M. Senthilkumar, "Novel device to measure multi-directional wicking of elastic knitted fabric for active sportswear," *Indian Journal of Fibre & Textile Research (IJFTR),* vol. 44, no. 2, pp. 173-179, 2019.

[121] K. P. M. Tang, C.-w. Kan, and J. Fan, "Comparison of test methods for measuring water absorption and transport test methods of fabrics," *Measurement,* vol. 97, pp. 126-137, 2017.

[122] K. Chau, K. M. Tang, and C. Kan, "Constant temperature drying rate tester: Real-time water evaporation measurement of fabrics," *IEEE Transactions on Instrumentation and Measurement,* vol. 67, no. 11, pp. 2635-2648, 2018.

[123] F. N. Craig, "Evaporative cooling of men in wet clothing," *Journal of Applied Physiology,* vol. 33, no. 3, pp. 331-336, 1972.

[124] F. N. Craig and J. T. Moffitt, "Efficiency of evaporative cooling from wet clothing," *Journal of Applied Physiology,* vol. 36, no. 3, pp. 313-316, 1974.

[125] D. Celcar, H. Meinander, and J. Geršak, "A study of the influence of different clothing materials on heat and moisture transmission through clothing materials, evaluated using a sweating cylinder," *International Journal of Clothing Science and Technology,* vol. 20, no. 2, pp. 119-130, 2008.

[126] Jintu Fan and Y.-s. Chen, "Thermal manikin," United States Patent US 6,543,657 B2, Apr. 8, 2003.

[127] F. Wang, "Measurements of clothing evaporative resistance using a sweating thermal manikin: an overview," *Industrial Health,* vol. 55, no. 6, pp. 473-484, 2017.

[128] A. Psikuta, M. Richards, and D. Fiala, "Single-sector thermophysiological human simulator," *Physiological Measurement,* vol. 29, no. 2, pp. 181-192, 2008.

[129] "ISO 6330:2021. Textiles — Domestic washing and drying procedures for textile testing."

[130] W. H. Hulme, *The Theory of Garment-Pattern Making - A Textbook for Clothing Designers, Teachers of Clothing Technology, and Senior Students*. Kennelly Press, 2011.

[131] A. Warrener, R. Tamai, and D. E. Lieberman, "The effect of trunk flexion angle on lower limb mechanics during running," *Human Movement Science,* vol. 78, 2021.

[132] A. Warrener, R. Tamai, and D. E. Lieberman, "The effect of trunk flexion angle on lower limb mechanics during running," *Human Movement Science,* vol. 78, p. 102817, 2021.

[133] H.-L. Teng and C. M. Powers, "Influence of Trunk Posture on Lower Extremity Energetics during Running," *Medicine & Science in Sports & Exercise,* vol. 47, no. 3, 2015.

[134] Y.-L. Chen and M.-L. Yu, "A preliminary field study of optimal trunk flexion by subjective discomfort in recreational cyclists," *Journal of the Chinese Institute of Industrial Engineers,* vol. 29, no. 8, pp. 526-533, 2012.

[135] H. G. Atasağun, A. Okur, T. Akkan, and L. Ö. Akkan, "A test apparatus to measure vertical wicking of fabrics – a case study on shirting fabrics," *The Journal of The Textile Institute,* vol. 107, no. 12, pp. 1483-1489, 2016.

[136] M. B. Sampath, S. Mani, and G. Nalankilli, "Effect of filament fineness on comfort characteristics of moisture management finished polyester knitted fabrics," *Journal of Industrial Textiles,* vol. 41, no. 2, pp. 160-173, 2011.

[137] B. Das, A. Das, V. Kothari, R. Fanguiero, and M. Araújo, "Moisture transmission through textiles. Part I: Processes involved in moisture transmission and the factors at play," *AUTEX Research Journal,* vol. 7, no. 2, pp. 100-110, 2007.

[138] R. M. Crow and R. J. Osczevski, "The interaction of water with fabrics," *Textile Research Journal,* vol. 68, no. 4, pp. 280-288, 1998.

[139] A. Calvimontes. Moisture absorption and drying dynamics of cotton fabrics [Online]. Available: https://www.researchgate.net/publication/278603044_Moisture_absorption_and_drying_dynamics_of_cotton_fabrics

[140] B.-g. Yao, Y. Li, J.-y. Hu, Y.-l. Kwok, and K.-w. Yeung, "An improved test method for characterizing the dynamic liquid moisture transfer in porous polymeric materials," *Polymer Testing,* vol. 25, no. 5, pp. 677-689, 2006.

[141] M. S. Novaković, J. Milanović, D. Grujić, and S. Stanković, "Liquid transfer properties of textile fabrics as a function of moisture content," *Hemijska industrija,* vol. 74, no. 2, pp. 118-131, 2020.

[142] T. L. Owens, J. Leisen, V. Breedveld, and H. W. Beckham, "Validation of the integrated upward–horizontal–downward wicking test for providing intensive properties of textile fabrics," *Journal of the Textile Institute,* vol. 103, no. 9, pp. 952-959, 2012.

[143] K.-H. Chau, K.-P. M. Tang, N.-F. Lam, and C.-W. Kan, "Constant Power Drying Rate Tester: Measurement of Water Evaporation from Textiles with Heat," *Fibers and Polymers,* vol. 19, no. 10, pp. 2208-2217, 2018.

[144] *Vertical wicking of Textiles*, AATCC 197, 2018.

[145] D. Bhatia and U. Malhotra, "Thermophysiological wear comfort of clothing: an overview," *J. Text. Sci. Eng,* vol. 6, no. 2, pp. 1-8, 2016.

[146] Z. Ma, D. Zhao, C. She, Y. Yang, and R. Yang, "Personal thermal management techniques for thermal comfort and building energy saving," *Materials Today Physics,* vol. 20, p. 100465, 2021.

[147] M. Mokhtari Yazdi and M. Sheikhzadeh, "Personal cooling garments: a review," *The Journal of The Textile Institute,* vol. 105, no. 12, pp. 1231-1250, 2014.

[148] L. Peng, B. Su, A. Yu, and X. Jiang, "Review of clothing for thermal management with advanced materials," *Cellulose,* vol. 26, no. 11, pp. 6415-6448, 2019.

[149] J. Qian *et al.*, "Effect of Knitting Structure and Polyethylene Content on Thermal-wet Comfort and Cooling Properties of Polyethylene/polyester Fabrics," *Fibers and Polymers,* vol. 23, no. 11, pp. 3297-3308, 2022.

[150] M. S. Anas, H. Awais, S. T. Ali Hamdani, K. Shaker, Z. Azam, and Y. Nawab, "Investigating the Thermo-Physiological Comfort Properties of Weft-Knitted Smart Structures Having a Negative Poisson's Ratio," *Advances in Materials Science and Engineering,* vol. 2022, pp. 1-14, 2022.

[151] Y. Yang, Z. Weijing, and P. Zhang, "Evaluation method for the hygroscopic and cooling function of knitted fabrics," *Textile Research Journal,* vol. 89, no. 23-24, pp. 5024-5040, 2019.

[152] H. M. K. Ullah, J. Lejeune, A. Cayla, M. Monceaux, C. Campagne, and É. Devaux, "A review of noteworthy/major innovations in wearable clothing for thermal and moisture management from material to fabric structure," *Textile Research Journal,* vol. 92, no. 17-18, pp. 3351-3386, 2021.

[153] A. S. Farooq and P. Zhang, "Fundamentals, materials and strategies for personal thermal management by next-generation textiles," *Composites Part A: Applied Science and Manufacturing,* vol. 142, p. 106249, 2021.

[154] U. Sajjad *et al.*, "Personal thermal management - A review on strategies, progress, and prospects," *International Communications in Heat and Mass Transfer,* vol. 130, p. 105739, 2022.

[155] L. Stygienė, S. Krauledas, A. Abraitienė, S. Varnaitė-Žuravliova, and K. Dubinskaitė, "Thermal Comfort and Electrostatic Properties of Socks Containing Fibers with Bio-Ceramic, Silver and Carbon Additives," *Materials,* vol. 15, no. 8, p. 2908, 2022.

[156] Y. Yang, L. Xin, Y. Xin, Z. Peihua, and W. Xungai, "Thermal comfort properties of cool-touch nylon and common nylon knitted fabrics with different fibre fineness and cross-section," *Industria Textila,* vol. 72, no. 2, pp. 217-224, 2021.

[157] Y. Yang, X. Yu, X. Wang, Y. Sun, P. Zhang, and X. Liu, "Effect of jade nanoparticle content and twist of cool-touch polyester filaments on comfort performance of knitted fabrics," *Textile Research Journal,* vol. 90, no. 21-22, pp. 2385-2398, 2020.

[158] H. A. Kim, "Physical properties of ring, compact, and air vortex yarns made of PTT/wool/modal and wearing comfort of their knitted fabrics for high emotional garments," *The Journal of The Textile Institute,* vol. 108, no. 9, pp. 1647-1656, 2017.

[159] J. M. Souza, S. Sampaio, W. C. Silva, S. G. de Lima, A. Zille, and R. Fangueiro, "Characterization of functional single jersey knitted fabrics using non-conventional yarns for sportswear," *Textile Research Journal,* vol. 88, no. 3, pp. 275-292, 2016.

[160] N. Sharma, P. Kumar, D. Bhatia, and S. K. Sinha, "Moisture Management Behaviour of Knitted Fabric from Structurally Modified Ring and Vortex Spun Yarn," *Journal of The Institution of Engineers (India): Series E,* vol. 97, no. 2, pp. 123-129, 2016.

[161] D. Raja, V. Ramesh Babu, G. Ramakrishnan, and M. Senthilkumar, "Effect of cyclic stress on the transverse wicking behaviour of cotton/lycra knitted fabrics," *The Journal of The Textile Institute,* vol. 104, no. 5, pp. 502-510, 2013.

[162] M. Senthilkumar and N. Anbumani, "Dynamics of Elastic Knitted Fabrics for Sports Wear," *Journal of Industrial Textiles,* vol. 41, no. 1, pp. 13-24, 2011.

[163] M. Ozturk, B. Nergis, and C. Candan, "A study of wicking properties of cotton-acrylic yarns and knitted fabrics," *Textile Research Journal,* vol. 81, pp. 324-328, 2011.

[164] T. Suganthi and P. Senthilkumar, "Comfort properties of double face knitted fabrics for tennis sportswear," *Indian Journal of Fibre & Textile Research (IJFTR),* vol. 43, no. 1, pp. 9-19, 2018.

[165] T. Suganthi and P. Senthilkumar, "Thermal comfort characteristics of bi-layer knitted fabrics for sportswear," *International Journal of Fashion Design, Technology and Education,* vol. 11, no. 2, pp. 210-222, 2018.

[166] F. Wang, X. Zhou, and S. Wang, "Development processes and property measurements of moisture absorption and quick dry fabrics," *Fibres & Textiles in Eastern Europe,* vol. 17, no. 2, pp. 46-49, 2009.

[167] B. Senthil Kumar, M. Ramesh Kumar, M. Parthiban, and T. Ramachandran, "Effect of Pique and Honeycomb Structures on Moisture Management Properties of Eri Silk Knitted Fabrics," *Journal of Natural Fibers,* pp. 1-10, 2019.

[168] E. Öner and A. Okur, "The effect of different knitted fabrics' structures on the moisture transport properties," *The Journal of The Textile Institute,* vol. 104, no. 11, pp. 1164-1177, 2013.

[169] S. Benltoufa, F. Fayala, and S. BenNasrallah, "Capillary Rise in Macro and Micro Pores of Jersey Knitting Structure," *Journal of Engineered Fibers and Fabrics,* vol. 3, no. 3, p. 155892500800300305, 2008.

[170] Q. Chen, J. Fan, and C. Sun, "The comfort evaluation of weft knitted plant structured fabrics and garment. I. Objective evaluation of weft knitted plant structured fabrics," *Fibers and Polymers,* vol. 16, no. 8, pp. 1788-1795, 2015.

[171] Y. Bu *et al.*, "A bioinspired 3D solar evaporator with balanced water supply and evaporation for highly efficient photothermal steam generation," *Journal of Materials Chemistry A,* 10.1039/D1TA09288J vol. 10, no. 6, pp. 2856-2866, 2022.

[172] V. T. Bartels, Physiological comfort of sportswear, in *Textiles in Sport*, R. Shishoo, Ed. Woodhead Publishing, 2005, pp. 177-203.

[173] T. P. Gavin, "Clothing and Thermoregulation During Exercise," *Sports Medicine,* vol. 33, no. 13, pp. 941-947, 2003.

[174] Y. Gao, Q. Sun, Y. Chen, X. Zhou, C. Wei, and L. Lyu, "A highly efficient bio-inspired 3D solar-driven evaporator with advanced heat management and salt fouling resistance design," *Chemical Engineering Journal,* p. 140500, 2022.

[175] X. He, C. Fan, T. Xu, and X. Zhang, "Biospired Janus Silk E-Textiles with Wet–Thermal Comfort for Highly Efficient Biofluid Monitoring," *Nano Letters,* vol. 21, no. 20, pp. 8880-8887, 2021.

[176] J. Fan, M. Sarkar, and Q. Chen, "Biomimetics of tree-shaped branching structure in textile fabrics," *International Journal of Design & Nature and Ecodynamics,* vol. 5, no. 3, pp. 221-229, 2010.

[177] Y. C. Fung, "Blood flow in the capillary bed," *Journal of Biomechanics,* vol. 2, no. 4, pp. 353-372, 1969.

[178] *Capillary Bed Network, Function & Diagram | What is a Capillary Bed? - Video & Lesson Transcript | Study.com.* [Online]. Available: https://study.com/learn/lesson/capillary-bed-network-function-diagram.html, 2022, (Accessed on: March 15, 2022).

[179] S. Amir and J. Fan, "Concurrent and real-time measurement of fabric liquid moisture management properties using a novel sweating simulator," *Textile Research Journal,* p. 00405175221124337, 2022.

[180] T. Kawase, S. Sekoguchi, T. Fuj, and M. Minagawa, "Spreading of Liquids in Textile Assemblies: Part I: Capillary Spreading of Liquids," *Textile Research Journal,* vol. 56, no. 7, pp. 409-414, 1986.

[181] S. Feng and Z. Xu, "Edges facilitate water evaporation through nanoporous graphene," *Nanotechnology,* vol. 30, no. 16, p. 165401, 2019.

[182] F. Wang, S. Annaheim, M. Morrissey, and R. M. Rossi, "Real evaporative cooling efficiency of one-layer tight-fitting sportswear in a hot environment," *Scandinavian Journal of Medicine & Science in Sports,* vol. 24, no. 3, pp. e129-e139, 2014.